UNIVERSIDADE FEDERAL DE OURO PRETO

ESCOLA DE MINAS

DEPARTAMENTO DE GEOLOGIA

TRABALHO DE CONCLUSÃO DE CURSO

Petrographic and geochemical attributes of the basalts from Stolpen, Saxony, Germany

Gabriel Oliveira Sepulveda

MONOGRAFIA nº 224

Ouro Preto, Maio de 2017

Petrographic and geochemical attributes of the basalts from Stolpen, Saxony, Germany

FUNDAÇÃO UNIVERSIDADE FEDERAL DE OURO PRETO

Reitora

Profª. Drª. Cláudia Aparecida Marliére de Lima

Vice-Reitor

Prof. Dr. Hermínio Arias Nalini Júnior

Pró-Reitor de Graduação

Prof. Drª. Tânia Rossi Garbin

ESCOLA DE MINAS

Diretor

Prof. Dr. Issamu Endo

Vice-Diretor

Prof. Dr. José Geraldo Arantes de Azevedo Brito

DEPARTAMENTO DE GEOLOGIA

Chefe

Prof. Dr. Luís Antônio Rosa Seixas

TRABALHO DE CONCLUSÃO DE CURSO

Nº 224

Petrographic and geochemical attributes of the basalts from Stolpen, Saxony, Germany

Gabriel Oliveira Sepulveda

Orientadora (Supervisor)

Gláucia Nascimento Queiroga

Co-Orientador(Co-supervisor)

Manuel Lapp

Monografia do Trabalho de Conclusão de Curso apresentada ao Departamento de Geologia da Escola de Minas da Universidade Federal de Ouro Preto como requisito parcial à obtenção do Título de Engenheiro Geólogo em cumprimento ao disposto nas normas da Universidade Federal de Ouro Preto.

OURO PRETO

2017

Universidade Federal de Ouro Preto – http://www.ufop.br

Escola de Minas - http://www.em.ufop.br

Departamento de Geologia - http://www.degeo.ufop.br/

Campus Morro do Cruzeiro s/n - Bauxita

35.400-000 Ouro Preto, Minas Gerais

Tel. (31) 3559-1600, Fax: (31) 3559-1606

Catalogação elaborada pela Biblioteca Prof. Luciano Jacques de Moraes do Sistema de Bibliotecas e Informação

SISBIN - Universidade Federal de Ouro Preto

S479p

Sepulveda, Gabriel.

Petrographic and geochemical attributes of the basalts from Stolpen, Saxony, Germany [manuscrito] / Gabriel Sepulveda. - 2017.

126f.; il. color.; grafs; tabs; mapas.

Orientadora: Prof. Dra. Glaucia Queiroga
Coorientador: Prof Dr. Manuel Lapp

Monografia (Graduação) - Universidade Federal de Ouro Preto. Escola de Minas. Departamento de Geologia.

1. Petrografia. 2. Geoquímica 3. Basalto. I. Queiroga, Glaucia. II. Lapp, Manuel III. Universidade Federal de Ouro Preto. IV. Título

CDU: 552.323

Catalogação: ficha@sisbin.ufop.br

Ficha de Aprovação

TRABALHO DE CONCLUSÃO DE CURSO

TÍTULO: Petrographic and Geochimical Attributes of the Basalts from Stolpen, Saxony, Germany

AUTOR: GABRIEL OLIVEIRA SEPULVEDA

ORIENTADORA: Profa. Glaucia Queiroga Nascimento

Aprovada em: 16 de maio de 2017

BANCA EXAMINADORA:

Profa. Glaucia Queiroga Nascimento Glaucia N. Queiroga DEGEO/UFOP

Prof. Edgar Batista Medeiros Jr. Edgar Batista de Medeiros Júnior DEGEO/UFOP

Profa. Maria Eugênia Silva Souza Maria Eugênia S. Souza DEGEO/UFOP

Ouro Preto, 16/05/2017

Joga na tela e confia.

Agradecimentos

Agradeço aos meus pais por me concederem a oportunidade. Ao DEGEO e à UFOP pelo ensino de qualidade.

Agradeço ao Laboratório de Microanálises do DEGEO/EM - Laboratório integrante da RMIc, Rede de Microscopia e Microanálises de Minas Gerais - FAPEMIG, pelos dados químicos gerados.

Ao IAEST, DAAD e LfULG pelo apoio durante a experiência de intercâmbio.

Agradeço aos meus amigos do PET Geologia e à tutora Adivane pela ajuda sempre que necessário.

À Gláucia Queiroga e Manuel Lapp pela paciência e atenção durante a confecção deste trabalho.

Summary

Illustration Index

Table list

Abstract

The Lusatia Volcanic Field is an important igneous province of the Central European Volcanic Province. Within this context there is Stolpen town, eastern Saxony, Germany, where important column basalts outcrop. During field works in this area basalt boulders that have not been previously described in the literature, presenting similar macroscopic features to the Stolpen columnar basalt such as aphanitic texture, blue-greyish color, with high hardness and density, were found. These boulders were the aim of this study, through mapping and sampling, followed by petrographic and mineral chemistry analysis, together with the Stolpen basalts in order to compare both rocks. The Stolpen basalt presents glomeroporphyritic and amygdaloidal textures, with subhedral phenocrystals of clinopyroxene that fill the amygdales and olivine, and a thin matrix of plagioclase laths and opaque minerals. Both phenocrystals present zoning: olivine with increasing of FeO and decreasing of MgO contents and pyroxen showing an enrichment in FeO/SiO_2 and impoverishment in MgO/Al_2O_2 contents from cores toward the rims. NaO contents in plagioclase crystals increase to the rims, a typical igneous feature. Olivine is dominated by the forsterite component and the pyroxene is Ca-rich member (diopside or Ca-augite). Plagioclase is classified as albite and labradorite. The boulders present subophitic texture, with phenocrystals of olivine and clinopyroxene, carbonate replacing plagioclase and matrix composed of plagioclase and opaque minerals. Olivine presents an increasement of FeO and decrement of MgO from cores toward the rims, pyroxene is quite homogeneous and plagioclase has zoning with enrichment in NaO to the rims. Olivine is dominantly forsterite, pyroxene is classified as augite and plagioclase as labradorite. Thermometry analyses, based on clinopyroxene and feldspar compositions, defined the crystallization temperature of pyroxen in 650° C for the core and < 500° C for the rims in the Stolpen samples and the homogeneous pyroxene crystals from the boulders provide crystallization temperatures of between 900 to 1250° C. In plagioclase, the thermometry determined temperatures of 755° C for the Na-rich plagioclase and 1150° C for Na-Ca plagioclase in the Stolpen samples and between 1130° C to 1150° C for Ca-Na-rich plagioclase of the boulders. The different crystallization temperatures for core and rims in plagioclase associated with the crystals zoning could be linked to the Bowen Reaction Series.

Keywords: Germany, Lusatia Volcanic Field, Stolpen basalt, boulders, petrography, mineral chemistry, termometry

Resumo

O Campo Vulcânico de Lusatia (Lusatia Volcanic Field) faz parte da Província Vulcânica Central Europeia. Nesse contexto, está a cidade de Stolpen, leste da Saxônia, Alemanha, onde afloram basaltos colunares de grande importância histórica para a geologia. Durante trabalhos de campo realizados próximos a Stolpen foram encontrados blocos de basalto que não estavam descritos previamente na literatura. Os blocos, por apresentarem características macroscópicas (afaníticos, coloração cinza-azulada, alta dureza e densidade) muito similares àquelas do famoso afloramento de Stolpen, foram alvo deste estudo, através de mapeamento e amostragem, seguido de análises petrográficas e de química mineral. As análises foram realizadas em conjunto com o basalto de Stolpen para fins de comparação. Os basaltos de Stolpen possuem uma textura glomeroporfirítica e estrutura amigdaloidal, com fenocristais subédricos de clinopiroxênio, que preenche as amigdalas, olivina e fina matriz composta por ripas plagioclásio e minerais opacos. Ambos os fenocristais possuem zonamento composicional: a olivina com enriquecimento de FeO e empobrecimento de MgO e o piroxênio com aumento de FeO/SiO_2 e redução de MgO/Al_2O_3 do centro pra borda. O plagioclásio apresenta aumento do conteúdo de NaO para as bordas, feição tipicamente ígnea. A olivina é dominada pelo componente forsterita e o piroxênio é rico em cálcio (diopsídio ou Ca-augita). O plagioclásio é classificado como albita e labradorita. Os blocos apresentam textura subofítica, com fenocristais de olivina e clinopiroxênio, carbonato substituindo plagioclásio e matriz composta por plagioclásio e minerais opacos. A olivina apresenta aumento de FeO e redução de MgO do núcleo para a borda, o piroxênio é homogêneo e o plagioclásio apresenta zonamento, com aumento do conteúdo de NaO para as bordas. A olivina é dominantemente forsterita, o piroxênio classifica-se como augita e o plagioclásico como labradorita. Através da termometria realizada, com base na química mineral de clinopiroxênio e feldspato, foram definidas temperaturas de cristalização do piroxênio em 650° C para o núcleo e < 500° C para a borda nas amostras de Stolpen e para os cristais de piroxênio homogêneos dos blocos as temperaturas estão entre 900 a 1250° C. Já para o plagioclásio definiram-se temperaturas de 755° C para o Na-plagioclásio e 1150° C para o Ca-Na plagioclásio nas amostras de Stolpen e entre 1130° C a 1150° C para o Ca-Na plagioclásio dos blocos. As diferentes temperaturas de cristalização de núcleo e borda dos plagioclásios, junto do zonamento químico dos demais cristais, podem ser associados a Série de Bowen.

Palavras-chave: Alemanha, Campo Vulcânico de Lusatia, basaltos de Stolpen, blocos, petrografia, química mineral, termometria

CHAPTER 1
INTRODUCTION

1.1 PRESENTATION

The bachelor thesis (called here as Trabalho de Conclusão de Curso; TCC) is part of the curriculum of the Geological Engineer Course of the Universidade Federal de Ouro Preto (UFOP). This work presents the data from the thesis, which was made through eight-weeks internship started in August of 2015, mapping basalt boulders in and around the Stolpen town, Saxony, Federal State of Germany, and making a petrographic and geochemical characterization of the bodies between June/2016 and April/2017 in Ouro Preto, Minas Gerais, Brazil.

This monograph is supervised by Prof. Dra. Gláucia Queiroga, from the Universidade Federal de Ouro Preto, and by Dr. Manuel Lapp, geologist from the Landesamt für Umwelt, Landwirtschaft und Geologie (LfULG, State Geological Survey, Saxony). Field support is due to the LfULG, Germany, and laboratorial support is due to the Microanalysis Laboratory from UFOP, a member of the Microscopy and Microanalysis Network of Minas Gerais State/Brazil/FAPEMIG.

1.2 NATURE OF THE WORK

The region of interest belongs to the ***Lusatia Volcanic Field***, part of the Central European Volcanic Province (Büchner *et al.* 2015). Through some field trips in the northeastern part of the Stolpen region, in order to make a detailed geological mapping campaign, basalt boulders were found by the co-supervisor of this monograph – geologist Manuel Lapp. These basalt boulders had not been previously described in the literature and had similar macroscopic characteristics to the "Stolpen Basalt" – a famous outcrop of columnar basalt joints that rises in the Stolpen region. After the boulders sampling and thin sections preparation, the samples were petrographically described. In Brazil, petrological analyses as soon as mineral chemistry were made in order to provide a comparison between the boulders and the "Stolpen Basalt", characterizing main similarities and differences.

1.3 OBJECTIVES

The main goals of this monography are:

1) To realize a detailed petrographic description of the boulders and the Stolpen basalt;
2) To obtain mineral chemical data of the main minerals (phenocrysts and matrix constituints) by electron microprobe (EMPA);
3) To realize a thermometric study using feldspars and clinopyroxene thermometry and,
4) To compare petrografically the Stolpen basalt and the adjacent stones.

1.4 LOCATION

The area with the occurrence of the boulders is located in the Stolpen region, east of Germany, near to the boundary with Czech Republic and Poland (Figure 1).

Stolpen is situated approximately 40 km east of Dresden in the Federal State of Saxony (Figure 1).

Figure 1 - Location of the studied area (red quadrangle). Source: Google Maps.

1.5 METHODS

This work can be subdivided into **five** stages, systematically carried out: literature review, fieldwork and sampling, description of the thin sections, electron microprobe analyses and drafting of the final monograph. Table 1 provides the schedule of the activities.

Table 1- Table with the schedule of the activities

Schedule	**Month**					
Activities	**1**	**2**	**3**	**4**	**5**	**6**
Literature review	x	x	x	x	x	x
Polished thin sections description	x	x	x	x	x	x
Mineral chemistry by electron microprobe						x
Compilation of the litochemistry data						x
Processing of the obtained data						x
	7	**8**	**9**	**10**	**11**	**12**
Literature review	x	x	x	x	x	x
Polished thin sections description	x	x				
Compilation of the litochemistry data	x	x	x			
Processing of the obtained data	x	x	x	x		
Drafting of the final monograph and oral presentation			x	x	x	x

1.5.1 Literature review

The project begins with a review of the local and regional geology, mainly based on the works of Koch (1972; review about the Stolpen Basalt), Tietz & Büchner (2015; main features of the Lusatia Volcanic Field) and Kozdrój *et al.* 2001 (2001; comments on the Geological Map of the Lausitz-Jizera-Karkonosze area), in order to understand the geological framework and to compare the boulders and Stolpen basalts.

A review about mafic rocks, including definition, main textures and examples, was also made and presented in Chapter 3. The main works considered here were Le Bas *et al*. (1986; chemical classification of volcanic rocks), MacKenzie *et al.* (1982) and Philpotts (1989) for the texture of

igneous rocks, Press *et al.* (2006; review about igneous rocks), Sgarbi (2007; texture and structure of igneous rock) and Sigurdsson *et al*. (2015; petrogenesis of igneous rocks).

1.5.2 Geological mapping and sampling

The mapping stage was done during the internship in Germany (August-September, 2015). This step consisted in identify the boulders on the field, mark in GPS and measure them, and collect samples (Figure 2) for the petrographic and chemical analyses (Table 2).

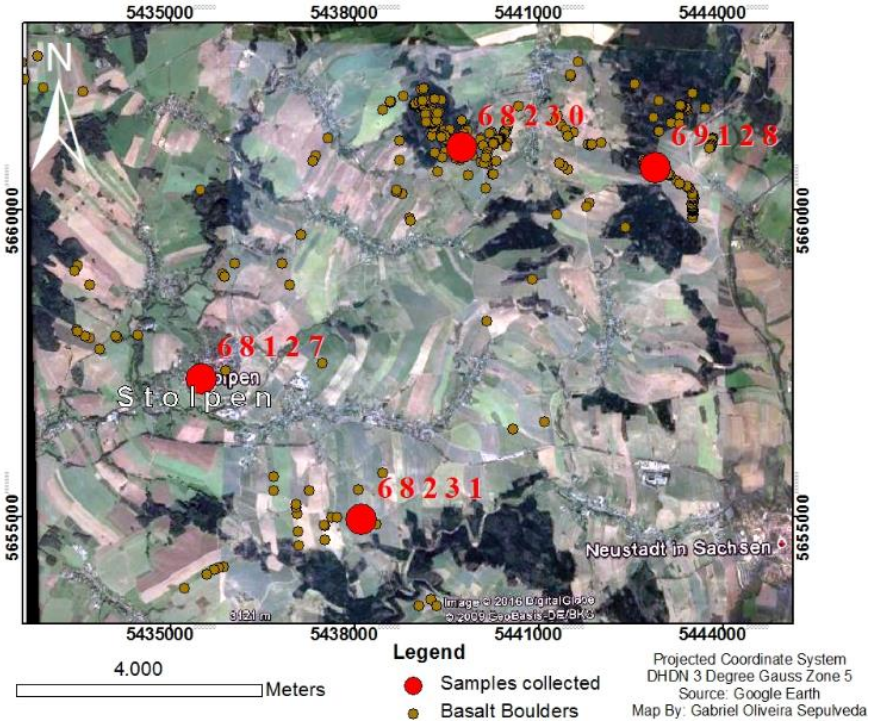

Figure 2– Distribution of basalt boulders around Stolpen.

Table 2 - Table showing the samples and the respective performed analysis

Sample	Gauss-Krüger Coordinates	Lithotype	Analysis		
			Thin Section	Mineral Chemistry	Geochemistry
68227	5435506/5657245	Columnar basalt	X	X	X
68230	5439748/5661014	Basalt	X	X	
68231	5438112/5654953	Basalt	X	X	X
69128	5442905/5660690	Basalt	X	X	

1.5.3. Petrographic Description

Samples from four different sampling spots in the Stolpen region (Table 2) were take into account for the petrographic description of the hand specimens and their microscopic textures. In the microscopic descriptions the main and accessory mineralogical composition and the main igneous microstructures were considered. The descriptions were made in a petrographic microscopic, model ZEISS. The photomicrographs were obtained in the same microscope coupled to an AxioCam Erc5s camera. The mineral abbreviations used in the photomicrographs and throughout the text followed the international standardization proposed by Whitney & Evans (2010).

1.5.4. Mineral chemistry

The microanalyses of olivine, clinopyroxene and plagioclase were performed with an electron microprobe JEOL JXA-8230 at the Microanalysis Laboratory of the Universidade Federal de Ouro Preto. The electron beam was set at 15 kV, 20 nA, 2-5 µm and the common matrix ZAF corrections were applied. Counting times on the peaks/background were 10/5 s for all elements (Na, Si, Al, Mg, Fe, Cr, Ti, Ca, Ni, K, Mn), except for Ba (30/15 s). Olivine and clinopyroxene were analyzed along transgranular profiles. Plagioclase was characterized by few analyses from cores and rims. Table 3 sumarizes the main features of the analysis, as the analyzed elements and correspondent standards.

Table 3 - Overview of the major element set-up for olivine, clinopyroxene and plagioclase.

Elements	Energetic Line	Spectrometer	Crystal	Standard
Na	Kα	1	TAPH	Anorthoclase
Si	Kα	2	TAP	Quartz
Al	Kα	2	TAP	Corundum
Mg	Kα	2	TAP	Olivine
Ba	Lα	3	PETH	Barite
Fe	Kα	3	LIFH	Almandine
Cu	Kα	3	LIFH	G-Augite
Ti	Kα	3	LIFH	Ilmenite
Ca	Kα	4	PETJ	Cu-Augite
Ni	Kα	4	LIF	Glass-Rhyolitic IR-X
K	Kα	5	PETL	Microcline
Mn	Kα	5	LIFL	Ilmenite

Notes: TAP - Thallium acid phthalate crystal; PET - Pentaerythritol crystal; LIF – Lithium fluoride crystal.

The mineral formulas were calculated based on 4 oxygens for olivine, 6 for pyroxene and 8 for plagioclase crystals (Deer *et al.* 1992). The total iron content obtained by the microprobe was considered as FeO. The binary and ternary digrams used to characterize the main minerals were obtained by Excel and Origin 6.1 programs, respectively.

Chemical maps of olivine and clinopyroxene were also obtained by the microprobe in order to illustrate the mineral zonations. Operating conditions were 15-kV acceleration, 20-nA beam current, and 20-ms dwell time per spot (stage mode). All the elements considered here (Si, Al, Fe, Mg, Mn, Ca, Ti) were analyzed by wavelength dispersion spectroscopy (WDS). Maps show quantitative element distributions.

1.6 PHYSIOGRAPHIC ASPECTS

This topic is based on the work of Central Intelligence Agence (2013).

Stolpen region is inserted in the continental Eastern European climate, dominated by humid westernly winds. Germany gets an average of 789 mm of precipitation per year. In the east, winters can be very cold and summers tend to be warm: can exceed -10 °C and 30 °C, respectively.

This region of Germany has agriculture dominating with some forests at less fertile slopes. The land is fertile and intensively used since about 1000 years. The land is hilly with hills up to 387 m and deepest locations about 200 m. Most of the land is between 260 and 300 m. Stolpen castle is 357 m.

The main rivers in this region of Saxony are the Polenz River in the southeast and the Wesenitz River in the west/northwestthat flows to the Elbe River, which goes to the North Sea near Hamburg.

The vegetation in Germany includes those common to the Central Europe. Beeches, oaks and other deciduous trees constitute one third of the forests; conifers are increasing as result of reforestation.

1.7 STRUCTURE OF THE WORK

The Bachelor thesis is composed by **seven** chapters, as summarized below:

Chapter 1 presents the introduction, emphasizing the location of the basalts, the nature of the research and the methodology.

Chapter 2 brings a synthesis about the geological framework of the area were the stones were collected, based on bibliographic revision. It presents the tectonic context, with stratigraphic and structural aspects of the ***Lusatia Volcanic Field***.

Chapter 3 presents a revision based on a bibliographic compilation about mafic rocks and their main features.

Chapter 4 shows the petrographic characterization of the columnar basalt and the boulder samples collected during the geological mapping.

Chapter 5 is dedicated to the mineral chemistry characterization of the main phases (phenocrysts and matrix).

Chapter 6 presents the discussions and main conclusions.

The last Chapter brings the references.

CHAPTER 2
GEOLOGICAL FRAMEWORK

2.1 THE LUSATIAN VOLCANIC FIELD

The ***Lusatian Volcanic Field*** (LVF) is located in the tri-border region of Poland, Czech Republic and Germany and is spread over several paleo-tectonic units (Figure 3). The Cenozoic volcanic rocks at the LVF are part of the Central European Volcanic Province (CEVP) and form a link between the sub-province of Silesia in Poland and volcanic fields of the Ohře rift zone in North Bohemian (Tietz *et al.* 2011a). The LVF spread over volcanic formations from the Bohemian mass (consists of crystalline rocks, mainly of granites and gneisses), the Saxon Switzerland (plataform sediments from minor Upper Permian to mostly Upper Cretaceous), the Upper Lusatia (volcanic and sedimentary rocks from Paleozoic-Cabrian), the Lusatian Mountains and the Zittau Mountains (early Paleozoic igneous rocks) (Kozdrój *et al.* 2001). The boundary of the LVF to the southwest is indistinct, because there are smooth transitions to the České Středohoři Volcanic Field (Cajz *et al.* 1996 *in* Kozdrój*et al.* 2001). To the north and westward there are no volcanic structures known at the surface. The eastern limit of the LVF is defined by the decreasing number of vents.

The central portion of the ***Lusatian Volcanic Field*** lies within the Lusatia Block, an area of continuous uplift since late Cretaceous (Voigt 2009 *in* Büchner 2015); it consists of the Variscan Görlitz Sycline Zone (granites massifs) in the north and the Cadomian Lusatia Anticline Zone (LAZ) in the south (Katzung & Ehmke 1993 *in* Büchner 2015). Both basement units are separated by the Intra-Lusatia fault. The Lusatia Block is bound in the south by the Lusatia Thrust and in the north by the main Lusatia Fault. The LAZ represents the northern part of the Bohemian Massif and consists of Cadomian granodiorites of early Cambrian age (Lusatia biotite-granodiorite and two mica granodiorite), early Ordovician granites (Rumburk granite) and small stocks of Variscan granites (Stolpen and Königshain) within Neoproterozoic greywackes. These rocks continue eastward to the western margin of the West Sudetic Block consisting in Paleozoic gneisses of the Jizera Metamorphic Complex and Variscan granites in the Karkanosze Mountains. Paleozoic sediments, volcanic rocks and schists occur within the Görlitz Sycline Zone. The Elbe Zone, as second tectonic unit, is located to the south of the Lusatia Overthrust and is part of the North Bohemian Cretaceous Basin, where the late Cretaceous limestones and sandstones represent the cover rocks in the LAZ. The eastern portion of the LVF is located in the Czech Jizerské Mountains and Polish Góry Kaczawkie Mountains (Krentz 2001 *in* Kozdrój*et al.* 2001).

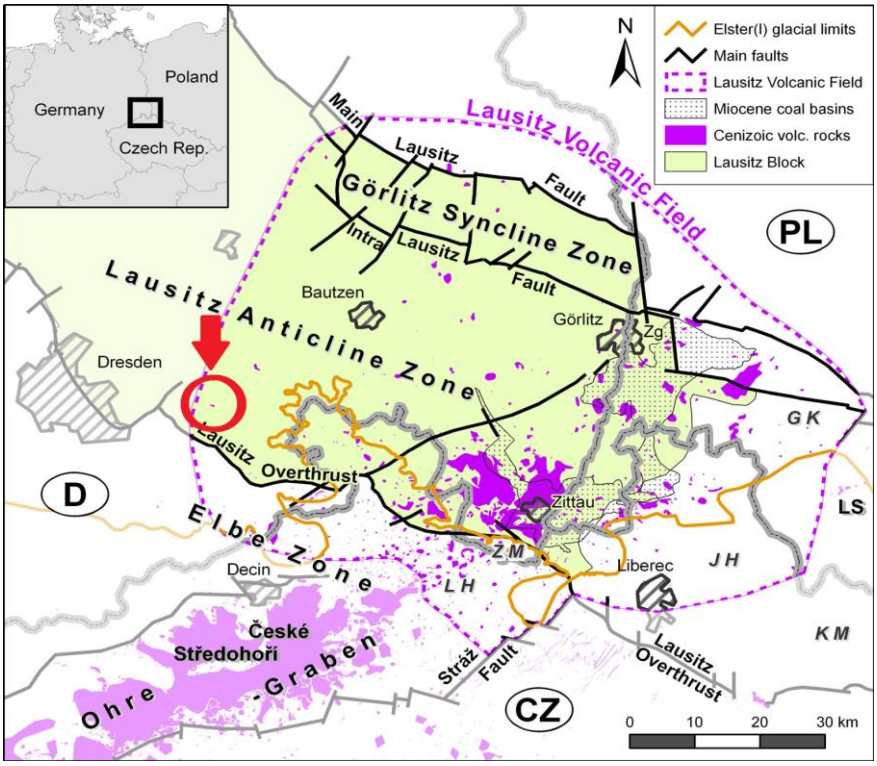

Figure 3– Lusatia (Lausitz) Volcanic Field with its regional tectonic framework and the studied area (red circle). GK Góry Kaczawskie, JH Jizerke hory, KM Krkonoše Mountains, LH Lužické hory, LS Lower Silesia Volcanic Field, Zg Zgorzelec, ZM Zittau Mountains (Based on Büchner *et al.* 2015).

2.2 STRATIGRAPHY

Figure 4 represents the geological map of the ***Lusatia Volcanic Field***. The stratigraphic description made below took into account the age of the sequences, being made from the bottom to the top.

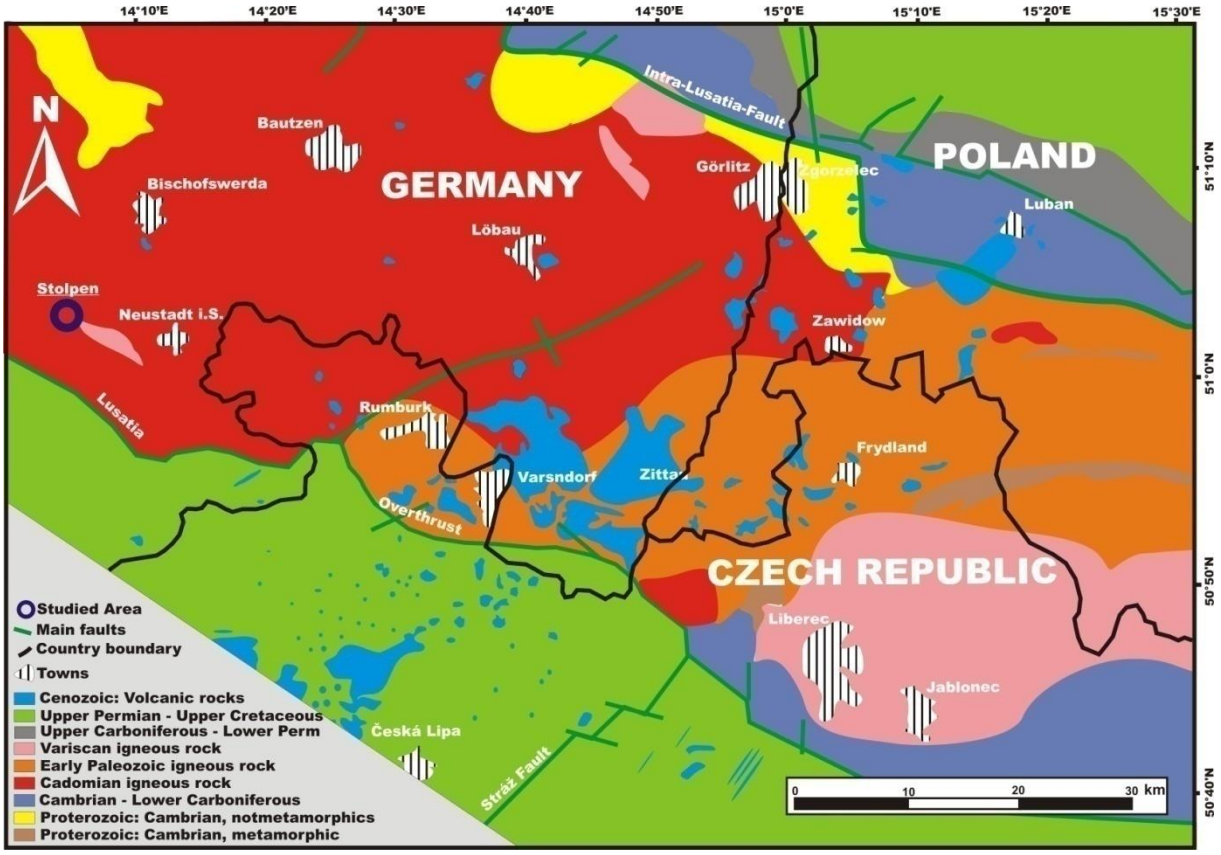

Figure 4– Geological map of the **Lusatia Volcanic Field**, with the studied area highlighted in the black circle. Adapted from Büchner *et al.* (2015).

2.2.1 Proterozoic-lower Carboniferous

The Lusatia region is an equivalent of the SE-NW trending coherent Lusatia Anticlinal, comprising two main units: the Lusatian Greywackes in the NW part and the Lusatian Granodiorite Massif in the SE part (Kozdrój*et al.* 2001).

The Lusatian Greywackes cover an area still about 40 x 50 km, predominantly in the NW part of the Lusatian Anticlinal. Within the Lusatian Greywackes the Lausitz Main Group consists of a succession of anchimetamorphic greywackes and intercalation of greywackes and slates of a thickness reaching around more than several thousand meters. In all outcrops, they show the same lithofacial character of hemipelagic turbidites with claystones (1-15 modal volume %), mudstones and fine-grained greywackes (50-85%), middle to coarse-grained greywackes (5-10%) and calc-silicate layers (Kemnitz &Budzinski 1994, Kemnitz 1998 *in* Kozdrój*et al.* 2001). Detritus as well as geochemical composition suggests that these sediments were derived from a sub-divided magmatic arc and that deposition took place on an active continental margin (Kemnitz & Budzinski1991 *in* Kozdrój *et al.* 2001).

The Lusatian Granodiorite Massif (Cadomian) is composed by biotite-rich granodiorites clearly intrusive as evidenced by broad contact aureole in the greywackes. The characteristic components are numerous veins and dykes, acid, intermediate and basic ("lamporphyric") in composition, predominantly with 5 m width. The Lusatia magmatites can be subdivided into two mica granodiorites with partial transition to biotite granodiorite; biotite granodiorites with typical magmatic structures and granites with large orthoclase and "blue" quartz.

Early Paleozoic rocks can be generally subdivided into two parts: northern, represented by Jizera Metamorphic Complex and SE part comprising the South and East Karkonosze Metamorphic Complexes. In LVF the Jizera Metamorphic Complex occurs in the eastern prolongation of the Lusatian Thurst and consists of deformation/metamorphism of undeformed igneous rocks (Jizera granites) to gneisses (Kozdrój *et al.* 2001).

The Variscan rocks are represented by the Karkonosze Granite Massif and Stolpen Königshain. The Karkonosze granites intruded in the center of a large asymmetric dome composed of the above-described low to medium grade metamorphic rocks. The Karkonosze pluton may be characterized by muscovite-biotite monzogranites, medium grained; muscovite-biotite monzogranites and granites of diferent textures; and hornblende-biotite granodiorites (Kozdrój *et al.*2001).

2.2.2 Upper Carboniferous – Lower Permian

In the Lusatia area, the Upper Carboniferous to Lower Permian sequence reaches almost 800m in thickness. These sediments consist of grey conglomerates, sandstones, rhyolites and rhyodacites of Wesphalian to Stephanian age. Terrestrial red conglomerates and sandstones devoid of fossils as well rhyolitic volcanic rocks are distributed along the Lusatian Main Fault (Kozdrój *et al.* 2001).

2.2.3 Upper Permian – Upper Cretaceous

In the south of the LVF the Permian Upper series consists in four salinar cyclotherms, with sedimentary succession beginning with the 0.1 to 1 m thick, marly to pelitic and bituminous copper shale followed by partly ore-bearing marl. These are covered by anhydrite and salts, followed by more anhydrite. This last cyclotherm attained a thickness of up top 400 m. There are other incomplete cyclotherms. The entire profile of the cyclotherms succession in Lusatian attains a thickness of about 500 m (Franz *et al.* 1997, Hennig *et al.* 1974, Gottesman 1968, Berber *et al.* 1983, Schubert *et al.* 2000 in Kozdrój *et al.* 2001).

The Jurassic sediments ocurr along the Lusatian Fault zone and are represented by steeply inclined and tectonically strongly disturbed sandstones, claystones, limestones and dolomites.

The Upper Cretaceous sediments deposited in the northeast of Děčín, in the southeast of the LVF, are a sandstone sequence, up to 500m in thickness. (Kozdrój *et al.* 2001)

2.2.4 Terciary Volcanic Rocks

The stones studied in this work are part of this unit. The volcanic rocks in the LVF are distributed all over the region (Figure 4) and basalts and phonolites are approximately equally represented. Several basaltics diatremes were newly discovered in this area close to the Lusatian Thurst. The youngest volcanic rocks are presented close to the Lusatian Thurst Fault and consist of olivine basaltic lavas (nepheline basanites), with age around 6-4 Ma (Kozdrój *et al.* 2001).

CHAPTER 3
KNOWLEDGE REVISION - MAFIC ROCKS

The objective of this chapter is present a revision about mafic rocks, describing their variety of types, characteristics, kinds of occurrence and geotectonic context, in order to bring a theoretical knowledge for correlations along the later chapters.

The igneous rock can be basically distinguished by composition and texture (Figure 5). The chemistry composition allows to separate the rocks in different types based in their content in silica (Sigurdsson *et al.*, 2015).

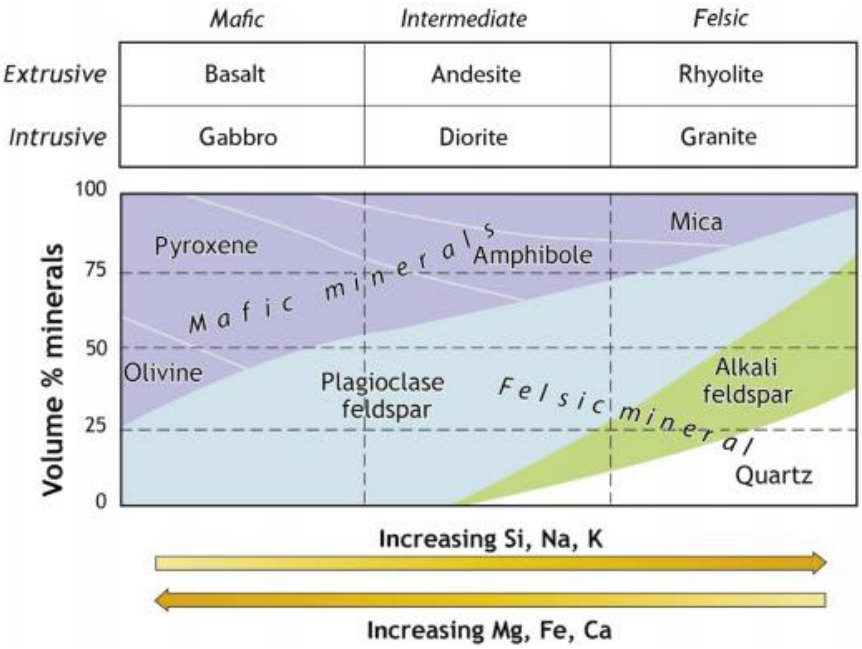

Figure 5 – Mineralogy and compositional characteristics of the most common igneous rock types. Adapted from Sigurdsson *et al.*(2015).

Mafic rocks is a term to describe igneous rocks specifically dense, dark and predominantly composed by mafic minerals, like pyroxenes, olivine and calcic plagioclase. Mafic rocks have lower content of felsic elements and low silica (45-52 wt%) as classified by Streckeisen (1978) through lozenge diagrams with four mainly components (Figures 6 and 7).

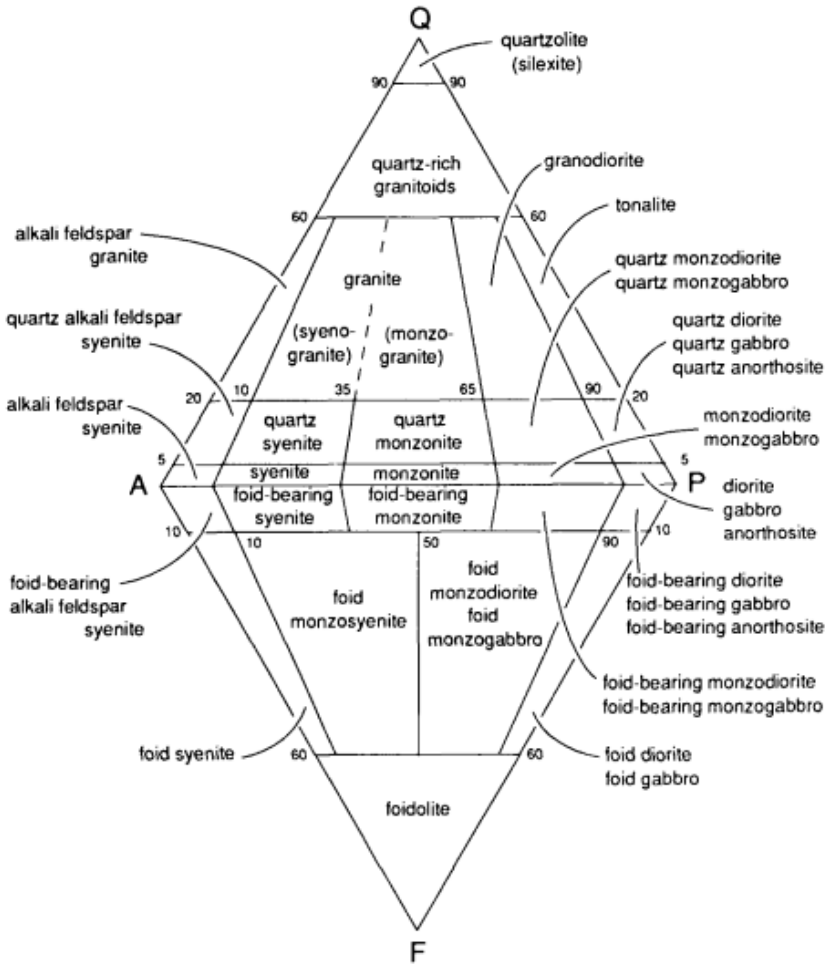

Figure 6- Classification and nomenclature of the plutonic igneous rocks according to their felsic modal contents when mafic is less than 90%. Q = quartz; A = alkali feldspar; P = plagioclase; F = feldspathoid (foid). From Strecksein (1976).

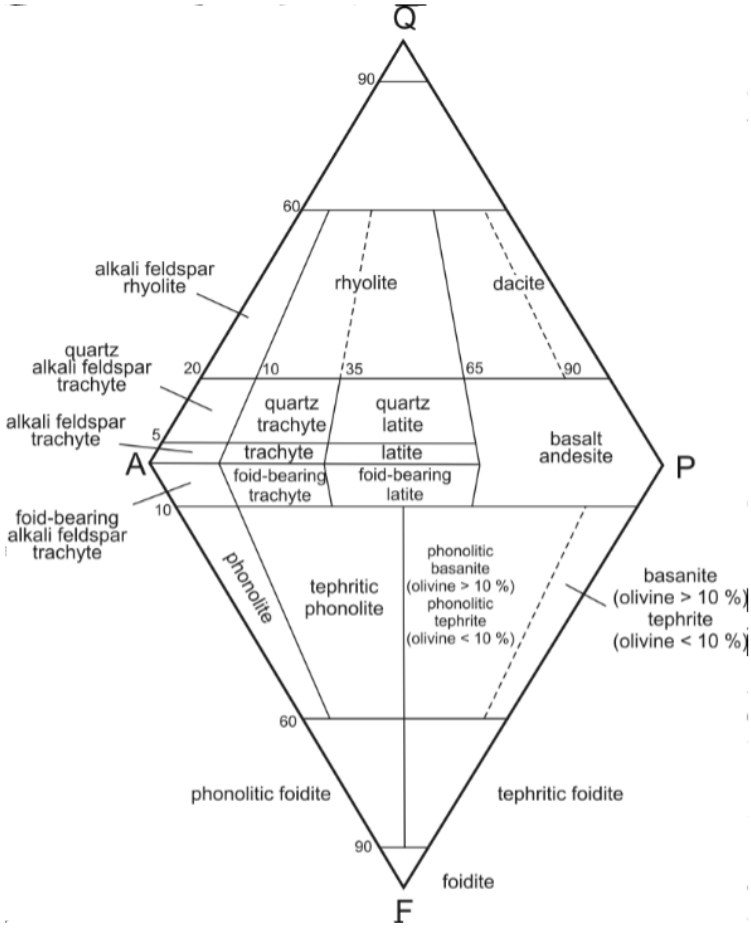

Figure 7- Classification and nomenclature of the volcanic igneous rocks according to their felsic modal contents when mafic is less than 90%. Q = quartz; A = alkali feldspar; P = plagioclase; F = feldspathoid (foid). From Streckeisen (1978).

The basalt, one of the main mafic rock, is the most abundant rock of the crust and is present in the whole seabed (Press *et al.* 2006). In the continents, there is large and thick basalt flows constituting big plateaus – for example the Columbia Plateau in Washington State, USA.

3.1 MAIN TEXTURES AND STRUCTURES OF MAFIC ROCKS

According to Philpotts (1989), ***texture*** refers to the way in wich individual grains relate to grains immediately surronding them. **Structure** represents the features that can be identified at the scale of an outcrop, as flow structure for example. Table 4 shows the main textures and structures of the igneous rocks. These features will be detailed described in the following topics, mainly based on the works of MacKenzie *et al.*(1982), Philpotts (1989) and Sgarbi (2007).

Table 4– Main textures and structures of the igneous rocks. Compiled from Philpotts (1989) and Sgarbi (2007).

TEXTURES	
Degree of Crystallinity	Holohyaline (totally glassy)
	Hypocrystalline (glass and crystals)
	Holocrystalline (totally crystalline)
Grain Size	Aphanitic
	Phaneritic Fine (< 1mm) Medium (1-5mm) Coarse (5 mm – 1cm) Very coarse (> 1cm) * Equigranular and inequigranular textures
Grain Shapes	Euhedral
	Subhedral
	Anhedral
Textures of Glassy or Fine-Grained Rocks	
Flow Textures	
Intergrowth Textures	
Reaction Texture	
STRUCTURES	
Structures in Volcanic Rocks (*pillow*, vesicles, amygdales for example)	
Structures in Plutonic Rocks (flowage differentiation, orbicules, miarolitic cavities etc)	

3.1.1. Textures

3.1.1.1. Degree of Crystallinity

Texture of an igneous rock is normally defined by the shape, size of crystals and their spacial accomodation. The cristallinity is an important property of igneous rocks based on the presence of glass and it can therefore serve as an indication to cooling rate and composition. The crystallinity of a rock can vary from *holohyaline* (totally glassy) (Figure 8B), through *hypohyaline* or *hypocrystaline* (glass and crystals) (Figure 8C and 8D), to *holocrystalline* (totally crystalline) (Figure 8A).

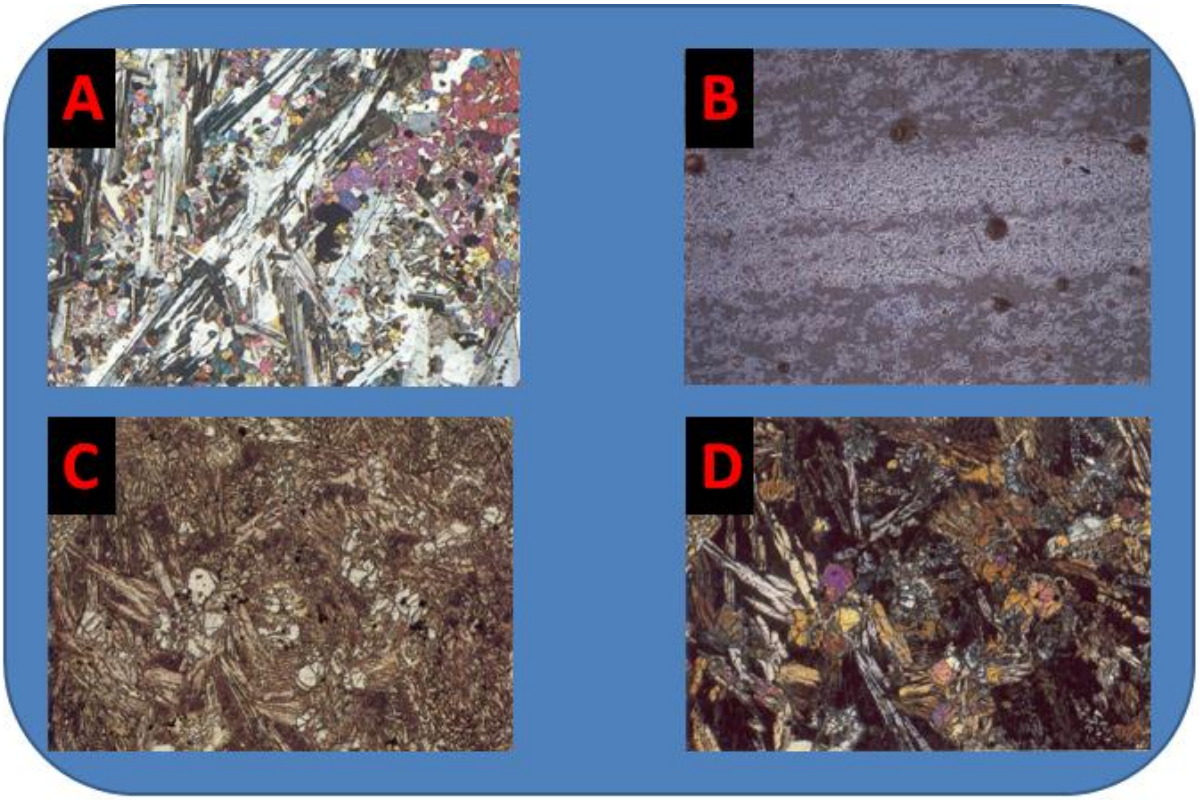

Figure 8 – A) Holocrystalline anhortositic gabbro. Magnification 7x, XPL B) Glassy pitchstone. Magnification 12x, PPL C) Hypocrystalline basalt. Magnification 35x, PPL D) Hypocrystalline basalt. Magnification 35x, XPL. Adapted from MacKenzie *et al.* (1982).

3.1.1.2 Grain Size

The grain sizes of an igneous rock is determined by the rate of cooling magma whereby fast cooling results in small grains and slow cooling in coarse grains. The grains are divided into fine (< 1 mm), medium (1-5 mm), coarse (5-10 mm) and very coarse (> 1 cm) as presented in Table 4. The crystals sizes define if it is possible to discern the grains macroscopically or not. If a rock have crystals of the essential minerals visible without a microscope, the rock is *phaneritic* (Figure 9A). If a rock is so fine-grained that individual crystals cannot be discerned macroscopically, it is said to be *aphanitic* (Figure 9B). If the rock is exceptionally coarse-grained, it is described as *pegmatitic*.

Rocks with crystals of similar size are described as *equigranular*. A rock containing grains of distinctly different sizes with relative large crystals (phenocrysts) surrounded by finer-grained material known as groundmass is said to be *porphyritic*. If the phenocrysts are cluster and grow together it is described as *glomeroporphyritic* (Figure 9C and 9D).

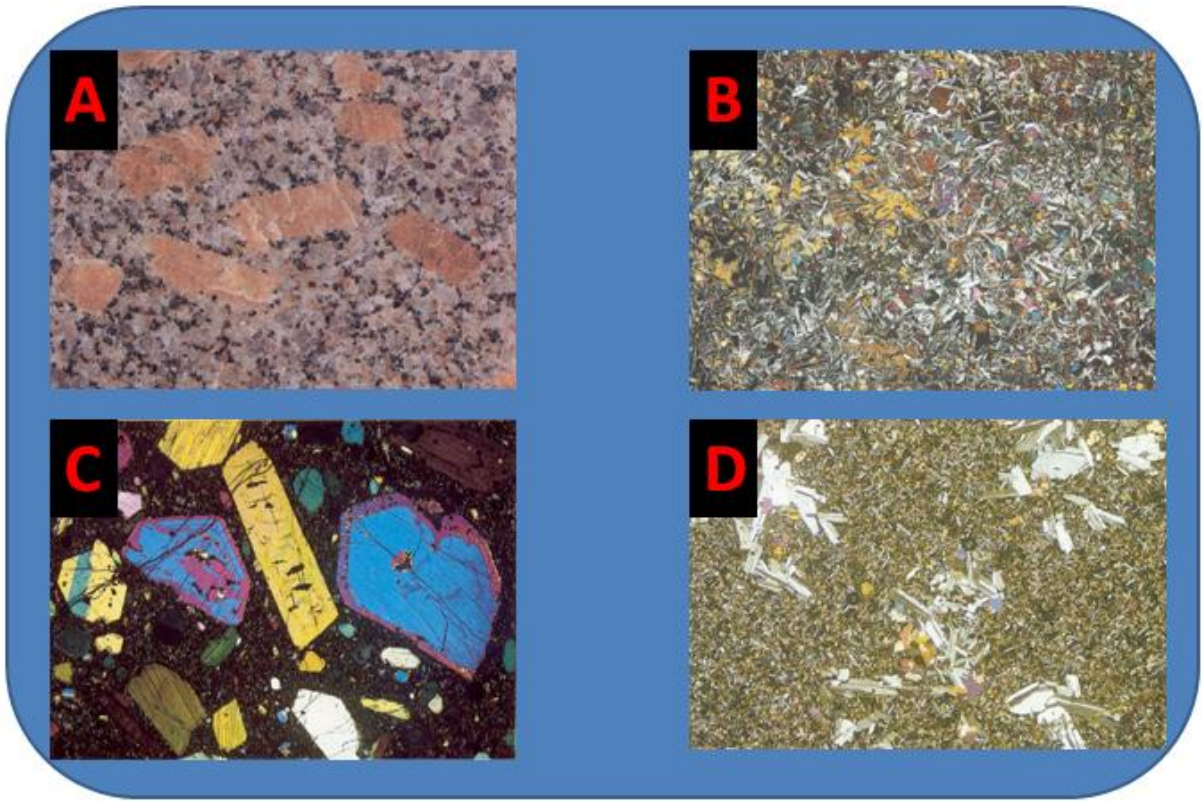

Figure 9 – A) Phaneritic granite. Magnification 1x, PPL B) A) Microcrystalline olivine basalt. Magnification 11x, PPL C) Augite-olivine-leucite-phyric. Magnification 11x, XPL D) Glomeroporphyritic tholeiitic basalt. Magnification x11, XPL. Adapted from MacKenzie *et al.*(1982).

3.1.1.3. Grain Shapes

The mineral crystals of an igneous rock can be classified by perfection rate of crystal faces. Grains with developed crystal faces are said to be *euhedral* (Figure 10 A); if they have a few crystal faces, they are *subhedral* (Figure 10B and 10C); and if they have none, they are *anhedral* (Figure 10D). Whether a grain develops imposed by surrounding crystals depends to a large extent on the stage at which the mineral crystallizes. So, the determination of grain shape can provide information on the sequence of crystallization.

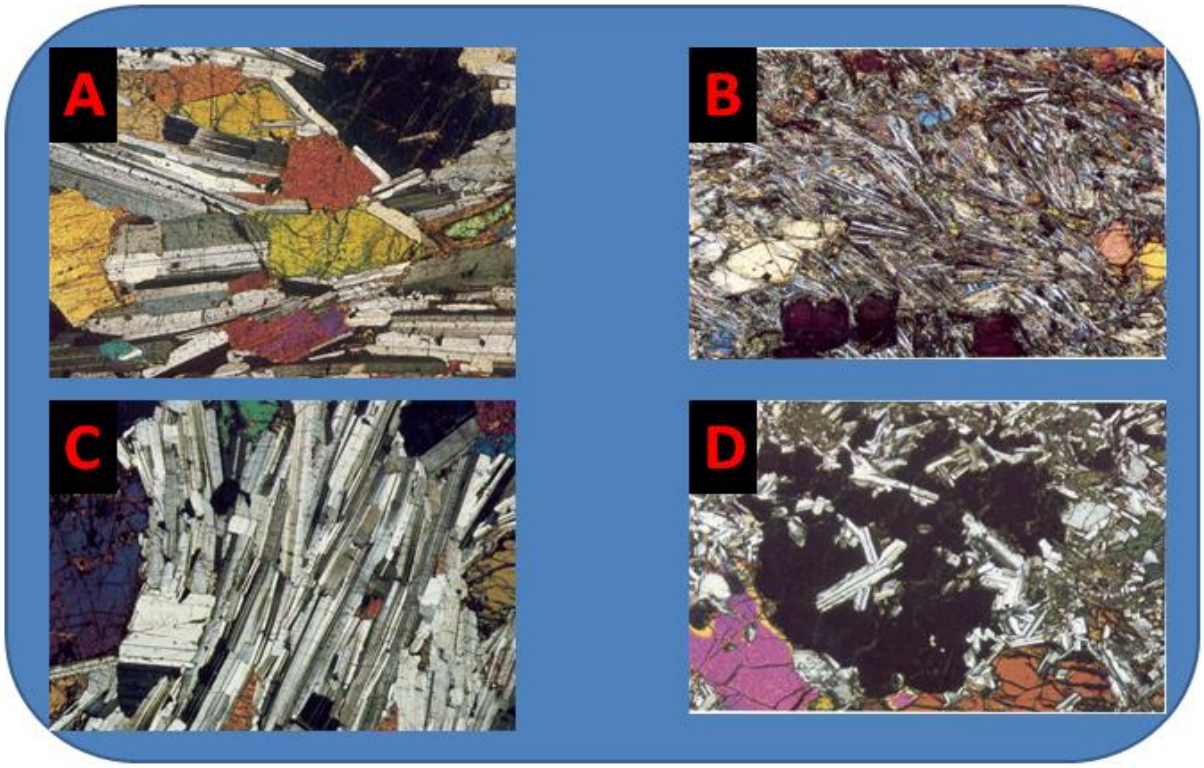

Figure 10 – A) Euhedral crystals in olivine gabro. Magnification 15x, XPL B) Subhedral crystals in variolitic olivine dolerite, with plagioclase needles. Magnification 27x, XPL C) Subhedral crystals in trachytoid gabro. Magnification 12x, XPL D) Anhedral crystals in alkali olivine dolerite. Magnification x26, XPL. Adapted from MacKenzie *et al*. (1982).

3.1.1.4. Glassy or Fine-Grained Rocks

Rapidly cooled magmas can form glass. The crystals that grow in glass are quite unlike those formed by normal growth from a liquid. Individually discernible crystals are not formed, and even under the microscope a birefringent fibrous meshwork is all that is visible. This type of crystallization is known as *devitrification*. Fibers commonly grow perpendicular to cracks in the glass or radiate outward from phenocrysts to produce spherical bodies known as *spherulites* (Figure 11). Many devitrified glasses also have a striking network of curved and concentric fractures referred to as perlitic cracks.

Small crystals that have grown in rapidly cooled magma, but prior to complete solidification, are known as *microlites*. Because their grouwth is rapid and difussion in silicate melts is slow, they grow with *dendritic* habit and are characterized by *skeletal* forms (Figure 11) with considerable open space.

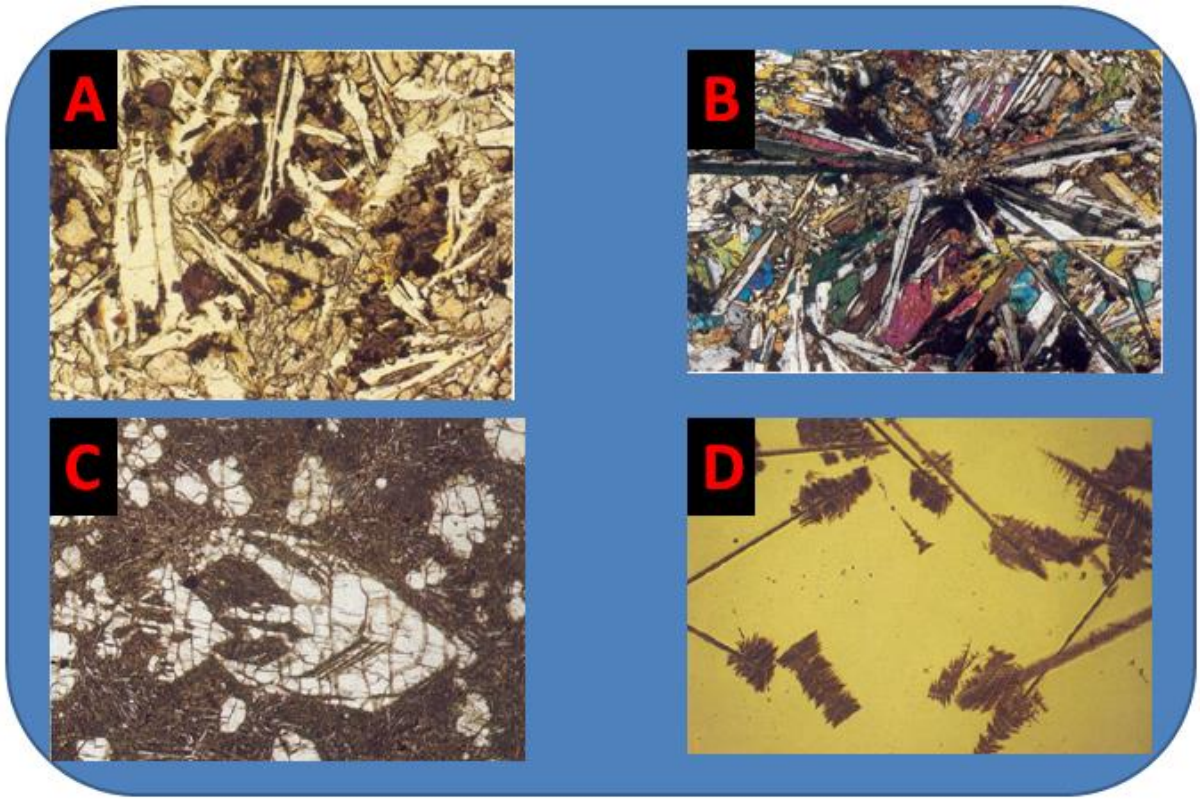

Figure 11 – A) Tholeiitic basalt with intersertal texture. Magnification 65x, PPL B) Plagioclase spherulite in dolerite. Magnification 32x, XPL C) Skeletal olivine in picritic basalt. Magnification 15x, PPL D) Dendritic olivine in basalt. Magnification 40x, PPL. Adapted from MacKenzie *et al.* (1982).

The sheaves, which nucleate at the rapidly cooled tops of flows, radiate downward, and produce a texture resembling inverted tufts of grass; this texture is consequently given the name *spinifex* (Figure 12A and 12B).

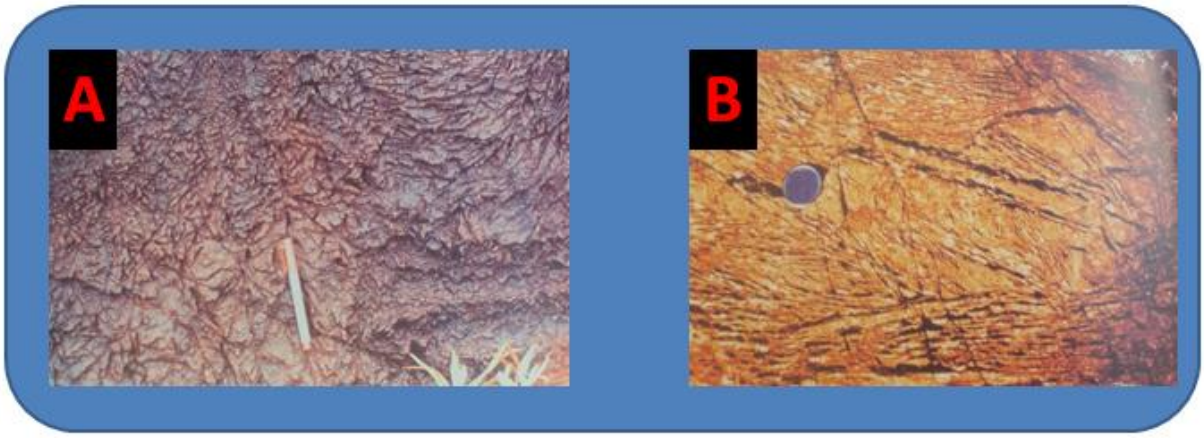

Figure 12 – A) Spinifex texture in komatiite. B) Spinifex texture. Adapted from Sgarbi (2007).

Variolite or *ocelli* (Figure 13A and 13B) is related to spherical bodies of felsic material that occurs in mafic dykes.

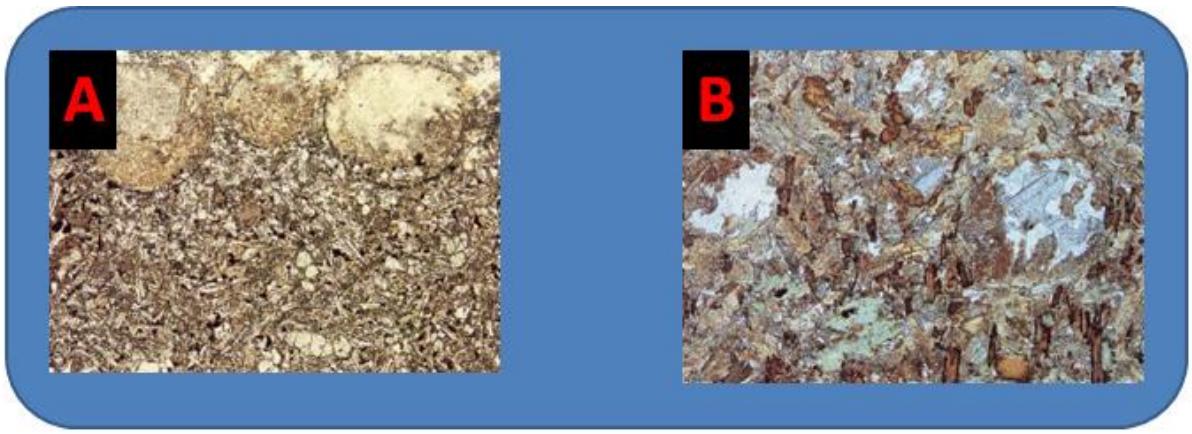

Figure 13 – A) Ocellar texture in olivine dolerite. Magnification 12x, PPL B) Two ocelli occupied by calcite in lamprophyre. Magnification 16x, PPL. Adapted from MacKenzie *et al.* (1982).

3.1.1.5. Flow Textures

Flow textures are produced by the preferencial orientation of grains, elongated or tabular, which creates an alignment of crystals. It's commonly result of magmatic flows. This is particularly true of platy feldspar laths, which produce *trachytic* texture (Figure 14A and 14B). A similar texture involving the more blocky feldspar laths in plutonic rocks is referred to as *trachytoidal*.

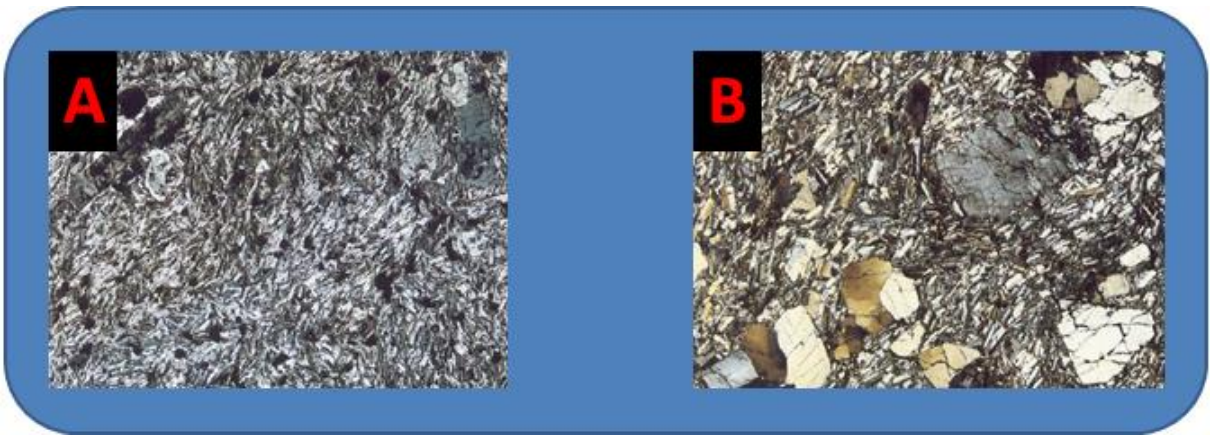

Figure 14– A) Trachytic texture in trachyte. Magnification 16x, XPL B) Trachytic texture in trachyte. Magnification 15x, XPL Adapted from MacKenzie *et al.* (1982).

3.1.1.6. Intergrowth Texture

The minerals in an igneous rock may have crystallized simultaneously or sequentially, or a mineral may have formed at the expense of another. A number of important textures provide evidence for each of these cases.

A *poikilitic* texture (Figure 15A) describes a occurrence of mineral crystals randomly enclosed within larger crystals of another mineral.

Ophitic texture is a term used to basaltic rocks and is related to the poikilitic where randomly oriented laths of plagioclase are enclosed in larger crystals of pyroxene or olivine. Where the olivine or pyroxene are smaller and thus cannot enclose many plagioclase laths, the term used is *subophitic* (Figure 15B).

The ratio of the numbers of plagioclase crystals to olivine or pyroxene crystals can make a precise difference between these terms. If the ratio is greater than one or equal to one, it is subofitic. If the ratio falls below one, the rock has a *intergranular* texture (Figure 15C). The change from intergranular through subophitic to ophitic is a result from slower cooling and slower nucleation rates. If the cooling rate is very fast, the interstices between the plagioclase laths may be quenched to a glass to form an *intersertal* texture (Figure 15D).

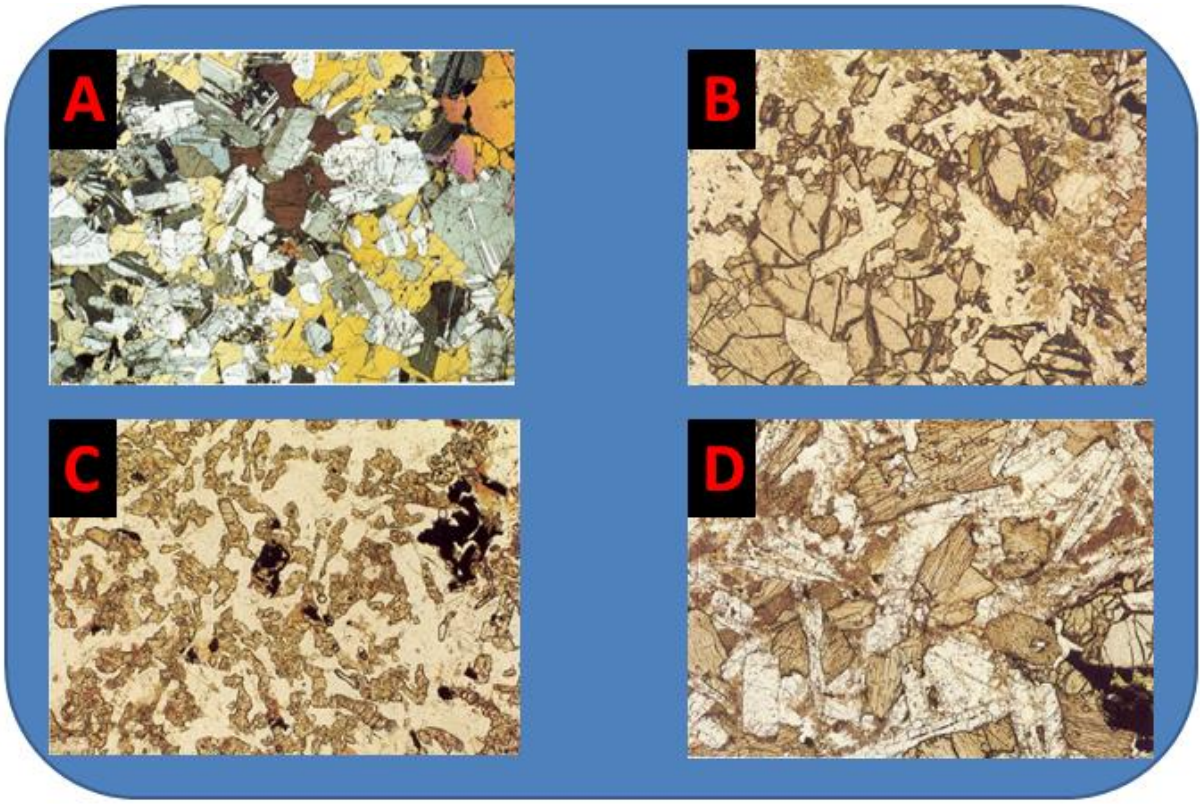

Figure 15 – A) Gabbro with poikilitic texture. Magnification 65x, PPL B) Subophitic olivine dolerite. Magnification 26x, PPL C) Intergranular dolerite. Magnification 60x, PPL D) Intersertal texture in alkali dolerite. Magnification 23x, PPL. Adapted from MacKenzie *et al.* (1982).

The regular intergrowth between two minerals, like quartz and feldspar, one as host and another on his surface is referred as *graphic*texture (Figure 16A and 16B). In rapidly cooled granitic magma a similar texture is developed, but it is less regular and is finer-grained. This is referred to as *granophyric* (Figure 16C). or *micrographic* texture. A still less regular worm-like intergrowth texture of quartz in oligoclase that extends into potassium feldspar crystals known as *myrmekite* (Figure 16D). Although some mymerkite may be of igneous origin and related to the granophyric texture.

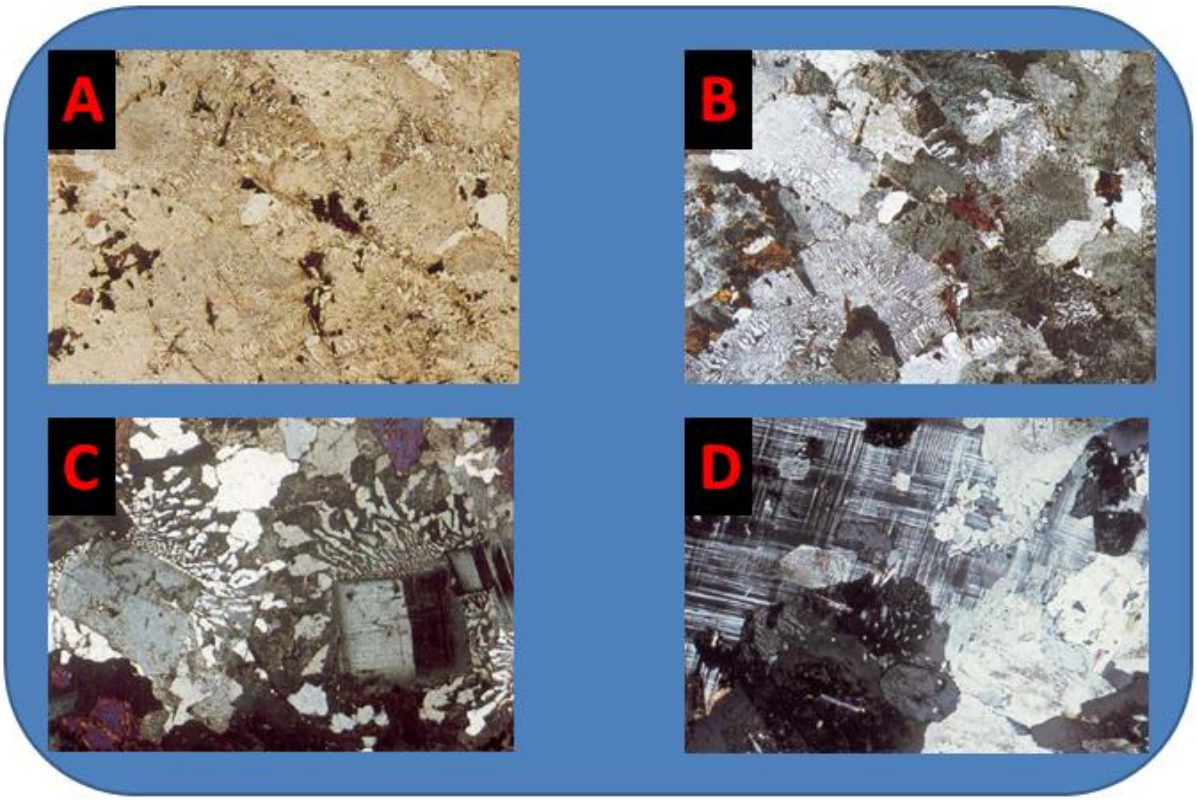

Figure 16 – A) and B) Micrographic and granophyric textures in microgranite. Magnification 20x, PPL and XPL C) Granophyric texture in microgranite. Magnification 37x, XPL D) Mymerkitic texture in granite. Magnification 30x, PPL. Adapted from MacKenzie *et al.* (1982).

The exsolution made by the separation of sodium and potassium feldspar develops a *perthitic* texture (Figure 17A), in which lamellae of albite occur in a potassium-feldspar host crystal. The term *antiperthite* (Figure 17B) has been used where the lamellae are of potassium feldspar and the host is plagioclase.

Figure 17 – A) Microperthitic texture in granite. Magnification 34x, XPL B) Antiperthitic texture in tonalitic gnaise. Magnification 20x, XPL. Adapted from MacKenzie *et al.* (1982).

3.1.1.7. Reaction Texture

Reaction textures are special intergrowths where the distribution of grains is presented as result of a reaction. Reactions may occur between crystals and magma to produce *coronas* (Figure 18A), where a crystal of one mineral is surrounded by a rim of one or more crystals of another mineral.

Minerals belonging to continuous reaction series exhibit evidence of reaction by forming zoned crystals (Figure 18B and 18C). The normal sequence of crystallization in granites can result in early-formed plagioclase being rimmed by alkali feldspar. In granites with a *rapakivi* texture (Figure 18D), early-crystallizating potassium feldspar is mantled by oligoclase.

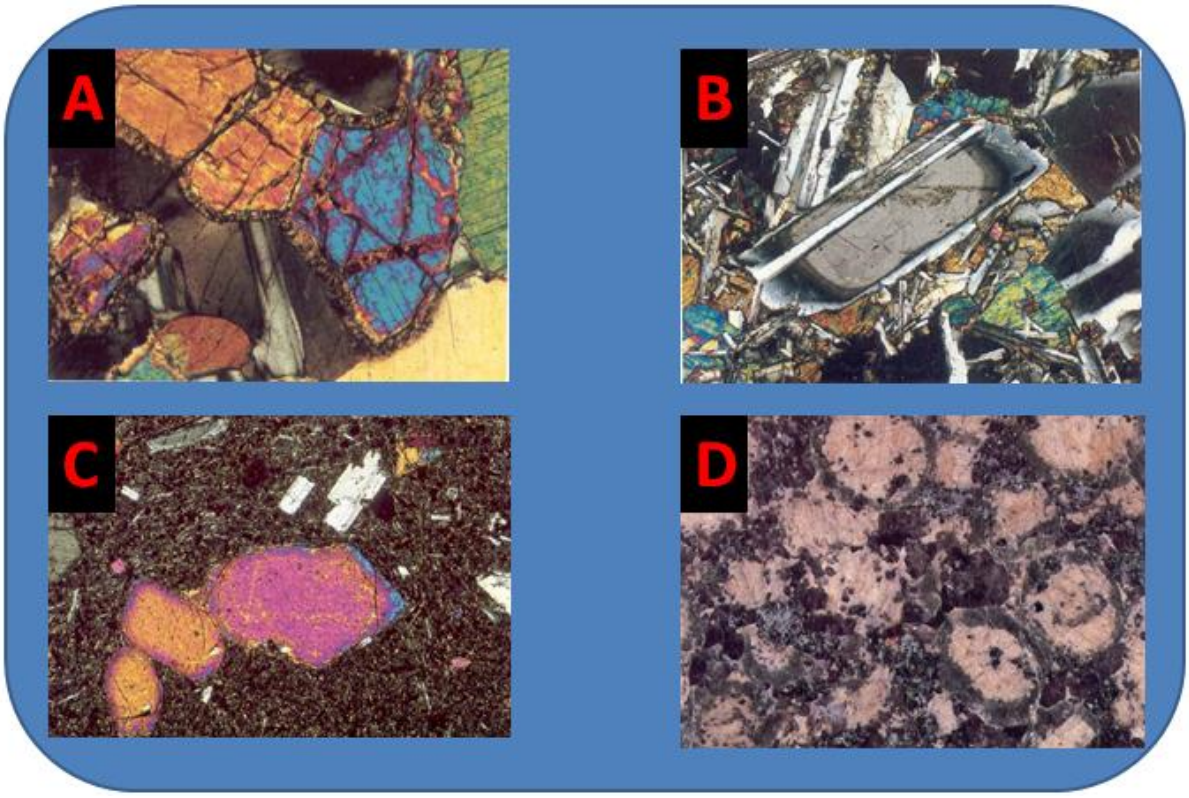

Figure 18– A) Olivine gabbro with corona texture. Magnification 100x, XPL B) Zoned plagioclase in dolerite. Magnification 43x, XPL C) Olivine zoned in basanite. Magnification 43x, XPL D) Rapakivi texture in granite. Magnification 2x, PPL. Adapted from MacKenzie *et al.* (1982).

3.1.2 Structures

Structures in igneous rock are discontinuities presented by the rock and all texture variations. Normally the structures only can be described in rocks bigger than a hand sample and their characteristics have a close relationship with the physic conditions during the crystallization time.

3.1.2.1 Structures in Volcanic Rocks

Aggregates of round mass of solid material, similar to pillows, occur in basic volcanic rocks described as *pillow lava* (Figure 19A and 19B). They are formed by fast cooling of extremily fluid lava in contact with water.

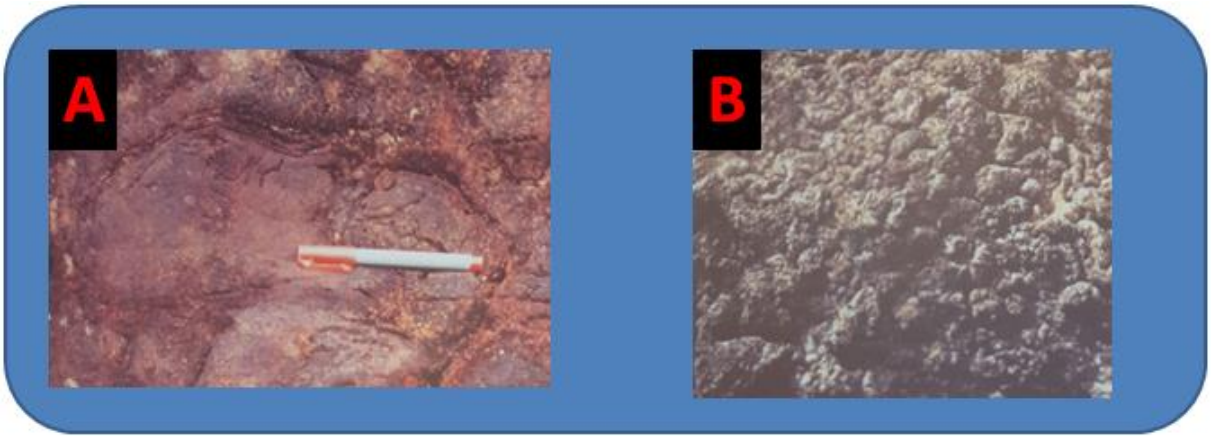

Figure 19– A) Basalts with pillow lava B) Pillow lava. Adapted from Sgarbi (2007).

One of the most common structure in volcanic rocks are “pores” made by the gas escape of lava. These cavities are called *vesicles*, and rocks containing these are said to be *vesicular* (Figure 20A). The size of vesicles is commonly measured in millimeters.

Vesicles may become filled or partially filled with low-temperature secondary minerals, such as zeolites, quartz, carbonates or chalcedony, to form what are referred to as *amygdales*. Rocks that contain amygdales are said to be *amygloidal* (Figure 20B).

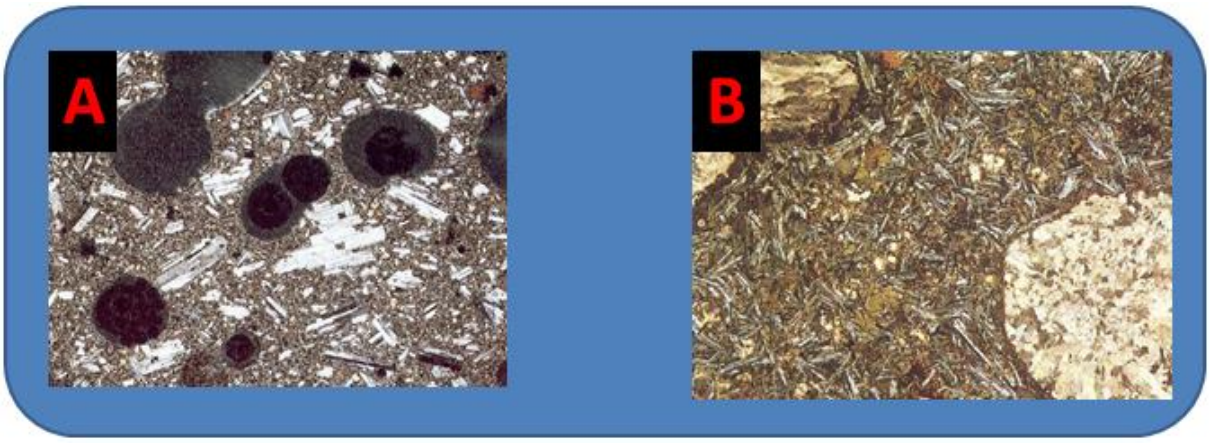

Figure 20 – A) Vesicular feldspar-phyric basalt. Magnification 7x, PPL B) Amygloidal basalt, vesicules filled with calcite. Magnification 11x, XPL. Adapted from MacKenzie *et al.* (1982).

3.1.2.2 Structures in Plutonic Rocks

The most common structure in plutonic igneous rocks is *layering* (Figure 21A). Layers may result from variations in the abundance or grain size of minerals or from elongate minerals being orientated perpendicular or parallel to the layering. Layering can be interpreted as resulting from gravitate settling of minerals from magma and exhibit grading where the larger and denser minerals are concentrated towards the base and the finer and lesse dense towards to the top of a layer. Layering can also be formed by the flow of magma. All or any combination of these various forms of layering may be present in a layered rock and tend to repeat themselves being referred as *rhythmic layering*.

The alternating of felsic and mafic layers concentrically arranged about some nucleus, which may be a phenocryst or fragment of foreign material, is described as orbicules. Rocks that contain orbicules as said with an *orbicular structure* (Figure 21B).

A different type of layering, known as *crescumulate*, consists of crystals of olivine and plagioclase that grow upward from the floor of a magma chamber. A associated structure can be found in many granitic pegmatites where crystals of alkali feldspar, mica, or tourmaline may nucleate on the wall and grow into the pegmatite perpendicular to the contact. The resulting arrangement of crystals is commonly referred to as a *comb structure* (Figure 21C).

Gases dissolved in plutonic magma must be either incorporated into hydrous or other volatile-bearing minerals or be exsolved during crystallizantion. With slow cooling and solidification the volatiles may be completely expelled from the main igneous body to form pegmatites or hydrothermal veins in the surrounding rock. In some near surface plutonic rocks, the dissolved gases that are not incorporated into minerals or exsolved during the crystallization may become trapped and form crystal-lined pore know as *miarolitic* cavities (Figure 21D).

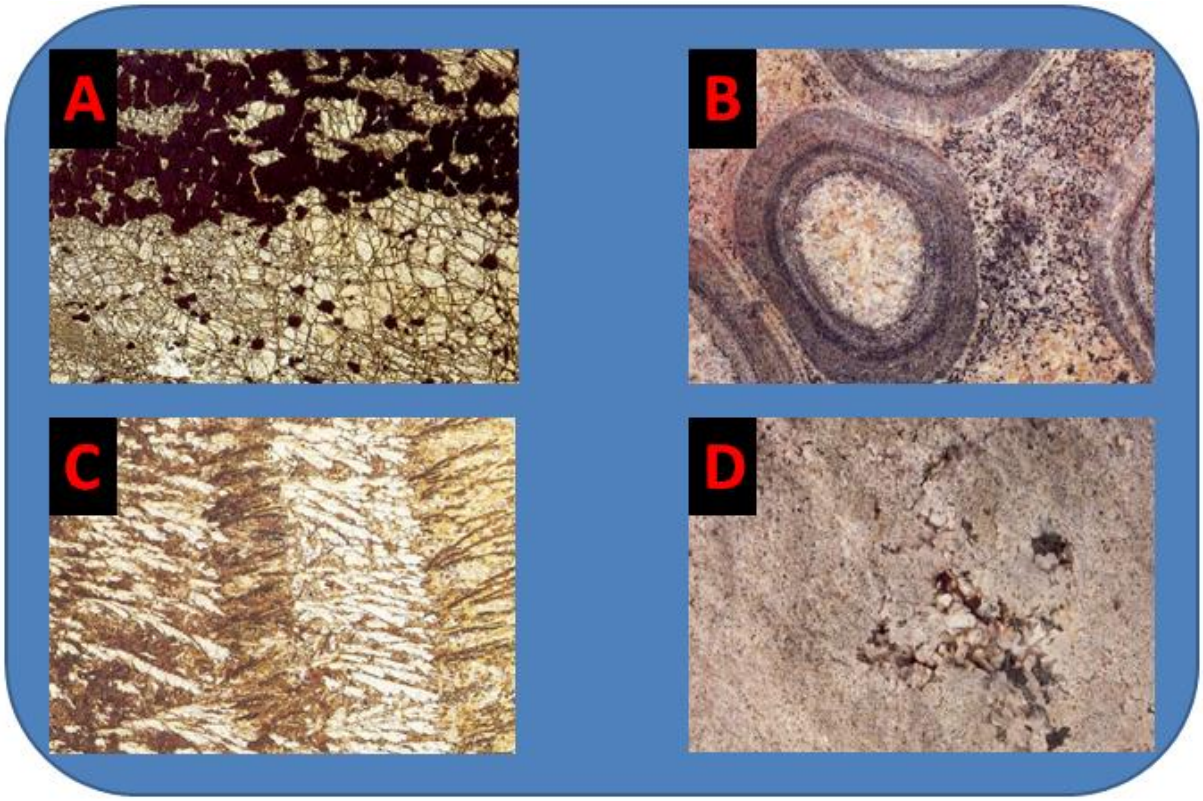

Figure 21 – A) Olivine and chrome-spinel layering. Magnification 11x, PPL B) Orbicular monzodiorite 1x, XPL C) Comb layers in dolerite dyke. Magnification 8x, PPL D) Miarolitic texture in granite. Magnification 1,5x, PPL.Adapted from MacKenzie *et al.* (1982).

3.2 MAIN MAFIC ROCKS

3.2.1 Basalts

This family of rocks include all basic lavas, from glassy to holocrystalline aphanitic (Sgarbi 2007). In the most generalized definition these are fine-grained mafic rocks with essential augite, labradorite to bytownite and opaque minerals (titanomagnetite; illmenite). They may be subdivided into tholeeitic basalts (subalkaline basalts) and alkali olivine basalts on the basis of the presence or absence of accessory olivine, quartz and low-Ca pyroxenes (piogenite or orthopyroxene). Phenocrysts or microphenocrysts of all essential and accessory minerals (except quartz) may be present (MacKenzie *et al.* 1982).

3.2.1.1 Tholeiitic basalt

Tholeiitic basalts contain both augite and low-Ca pyroxene. Olivine is either absence or present only in small amounts (less than 5% by volume) as phenocrysts only, never in the groundmass. The groundmass commonly contains varying amounts of interstitial brown glass, or devitrified glass (intersertal texture); in more slowly cooled rocks the place of the glass is taken by granophyric intergrowths of quartz and alkali feldspar. The remainder of the groundmass usually has an intergranular or subophitic texture (Figure 22A). Macroscopically presents aphanitic texture (Figure 22B).

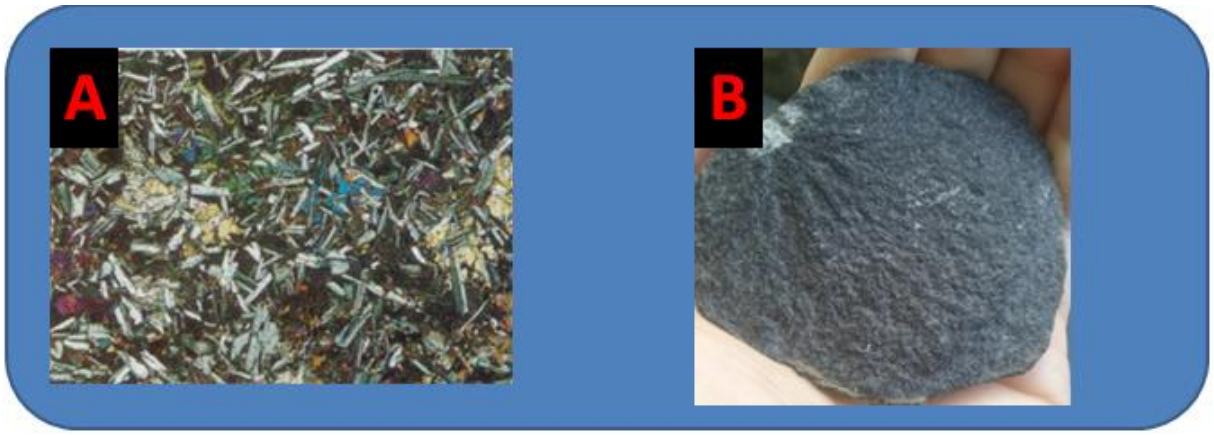

Figure 22– A) Tholeiitic basalt. Magnification 11x, XPL. Adapted from MacKenzie *et al.* (1982). B) Basalt sample with aphanitic texture.

3.2.1.2 Alkali olivine basalts

Alkali olivine basalts contain no low-Ca pyroxene, but plentiful olivine, both as phenocrysts (if present) and in the groundmass (Figure 23B). The augite is often somewhat purplish-grey in color due to high Ti content. Less than 10% of the feldspar is of alkali type. The groundmass texture is usually intergranular of subophitic and glass is very rare, though accessory interstices and as rims on plagioclase (Figure 23A).

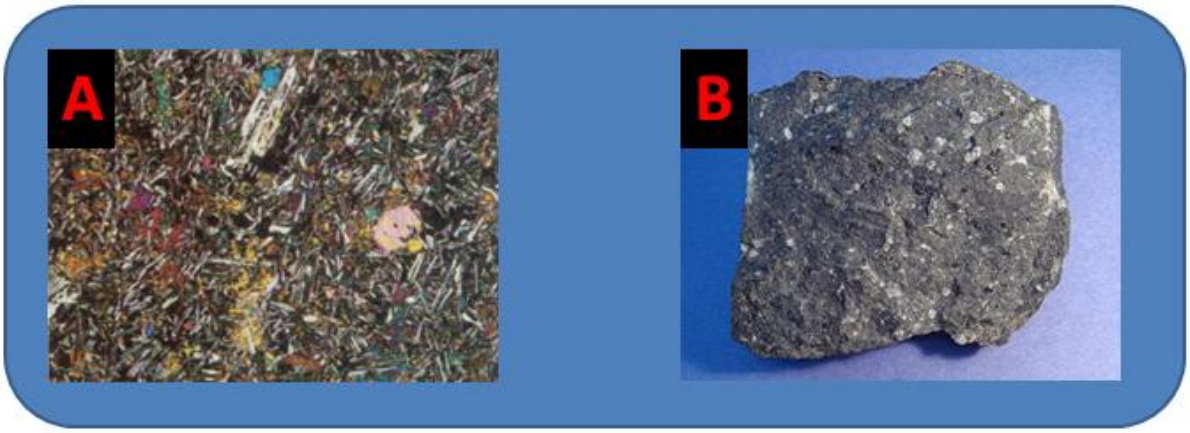

Figure 23 – A) Alkali olivine basalt. Magnification 11x, XPL. Adapted from MacKenzie *et al.* (1982). B) Alkali olivine basalt sample. Avaible in: http://www.petrologyslides.com/mantlegeo2

3.2.2 Diabase (Dolerite)

Medium-grained, dark-grey basic rock (Figure 24B) consisting essentially of labradorite, augite and ore minerals (Figure 24A). In North America the term *diabase*is used in preference to *dolerite*, which is used in the rest of the world. Like basalts and gabbros, there are tholeiitic and alkali varieties which can be identified from the presence or absence of low-Ca pyroxenes, nepheline, analcite, quartz and the absence or presence and amount of olivine.

Figure 24 – A) A subophitic tholeiitic diabase, Magnification 21x, XPL. Adapted from MacKenzie *et al.* (1982). B) Diabase sample. Avaible in: https://commons.wikimedia.org/wiki/File:Polished_Diabase.jpg

3.2.3 Gabbro

A coarse-grained, dark-grey to black rock (Figure 25B) consisting essentially of plagioclase and one or more mafic minerals, which the proportion of the mafic minerals is equal or wider than the plagioclase. The commom mafic minerals are augite, hornblend, biotite and olivine (Figure 25A).

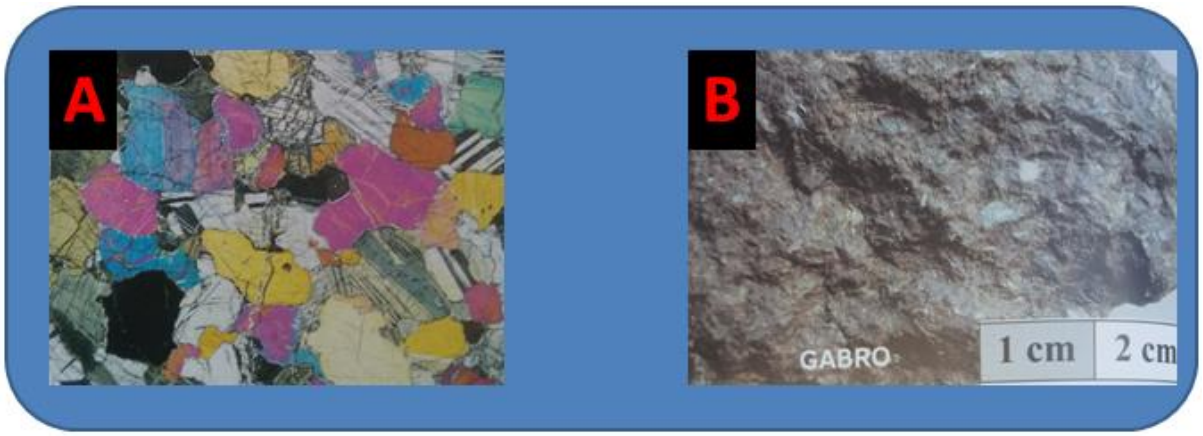

Figure 25 – A) Granular olivine gabbro. Magnification 11x, XPL. Adapted from MacKenzie *et al.* (1982). B) Gabbro sample. Adapted from Sgarbi (2007).

3.3 PETROGENESIS

This topic is based on the work of Sigurdsson *et al.* (2015) and in all references therein.

Igneous rock are classified according to their bulk composition, conventionally expressed in terms of major, minor and trace elements. Conventional analyses of igneous rocks appears in Table 5 which lists a variety of igneous rocks from different locations.

Magma is the term used to describe mobile and largely molten mixtures of liquid and solid material that also include an inventory of dissolved gases, such as water, carbon dioxide and other more exotic components.

The magma erupted on the Earth's surface is generated by partial melting of rocks at depth. The generation of melts and the crystallization and the movement of those melts is the primary mechanism whereby planet Earth has evolved into a core, mantle and crust. At the present time melting is limited to the top 200 km of the earth, within the crust and upper mantle. Because this melts are generally less dense than the rocks from which they are derived, they tend to rise foward the surface.

Table 5 – Major and trace element omposition of representative igneous rock. MORB: mid-ocean ridge basalt; OIB: ocean island basalt. Adapted from Sigurdson *et al*. (2015).

	Peridotite	Tholeiitic Basalt MORB	Alkali Basalt OIB	Andesite	Metaluminous Granite	Peraluminous Granite	Peralkaline Granite
Major and Minor Elements (wt.%)							
SiO_2	44.2	48.77	47.52	59.89	67.89	69.08	70.87
TiO_2	0.13	1.15	3.29	0.95	0.45	0.55	0.1
Al_2O_3	2.05	15.9	15.95	17.07	14.49	14.3	14.78
Fe_2O_3	0.75	1.33	3.16	3.31	1.27	0.73	2.64
FeO	7.54	8.62	8.91	3	2.57	3.23	
MnO	0.13	0.17	0.19	0.12	0.08	0.06	0.06
MgO	42.21	9.67	5.18	3.25	1.75	1.82	0.1
CaO	1.92	11.16	8.96	5.67	3.78	2.49	0.34
Na_2O	0.27	2.43	3.56	3.95	2.95	2.2	6.47
K_2O	0.06	0.08	1.29	2.47	3.05	3.63	4.19
P_2O_5	0.03	0.09	0.64	0.31	0.11	0.13	0.02
H_2O^+		0.3	1.16				0.33
F (ppm)		210	1150				
Total	99.29	99.67	99.81	99.99	98.39	98.22	99.9
Trace Elements (ppm)							
V	70	262	350	125	74	72	9
Cr	3200	528	421	484	27	46	5
Ni	2300	214	153	38.6	9	17	3
Rb	0.64	0.56	31	75.4	132	180	148
Sr	21	90	660	886	253	139	1.8
Y	5	28	29	12	27	32	188
Zr	11	74	280	240	143	170	772
Nb	0.7	2.3	48	15	9	11	100
Ba	7	6.3	350	886	520	480	
La	0.7	2.5	37	38	29	31	59.6
Ce	1.8	7.5	80	67	62.9	69	152
Nd	1.4	7.3	39	32	23.4	25	93.7
Sm	0.44	2.63	10	5.82	4.25	4.89	25.4
Eu	0.17	1.02	3	1.57	2.23	1.74	1.99
Gd	0.6	3.68	7.62	4.73	4.16	4.35	27.8
Tb	0.11	0.67	1.05	0.66	0.59	0.64	4.8
Yb	0.49	3.05	2.16	1.64	1.81	2.25	16.3
Lu	0.07	0.46	0.3	0.25	0.27	0.34	2.46
Ta	0.04	0.13	2.7	0.88	0.42	0.56	6.68
Hf	0.31	2.05	7.8	5	4.1	5.5	26.3
Th	0.08	0.12	4	6.5	16	19	17.8
U	0.02	0.05	1.02	1.89	3	3	4.59

3.3.1 Basaltic Magmas

The basaltic magmas can be divided into four different types: Mid-ocean Ridge Basalts (MORB), Ocean Islands Basalts (OIB), Subduction-related Basalts and Continental Basalts.

3.3.1.1 Mid-ocean Ridge Basalts

Basalts dominate the ocean floor, forming the igneous oceanic crust which is generated at constructive plate margins. Magma is produced in result to the separation of two plates, allowing the mantle to rise to occupy the space made available by the divergent plate motion. In so doing, the mantle melts as a result of adiabatic decompression (Sigurdsson *et al.* 2015).

Adiabatic decompression is one of the major mechanisms of melt generation within the Earth and occurs when hot mantle (peridotite) rises from depth (high pressure) to shallower levels (lower pressures). As the mantle rises adiabatically it cools normally at rate of 0.5° for every km of upward movement. Given that the gradient of the peridotite solidus is greater than the adiabatic gradient, a parcel of mantle originally below the solidus at high pressure can rise through the mantle into a region where the ambient conditions are above the solidus, and it consequently melts. In Figure 26 a parcel of mantle lies on the geotherm at point C. If the overlying crust is stretched and thinned, then the parcel of mantle rises along an adiabatic thermal gradient to point D, at a lower pressure, but with a minimal drop in temperature. Point D is above the solidus at that pressure and so the mantle melts. The vector A-B shows the trajectory of a similar parcel of mantle at higher initial temperature. Descompression melting of this parcel starts at a greater depth and has the potential to produce a greater volume of melt (Figure 26).

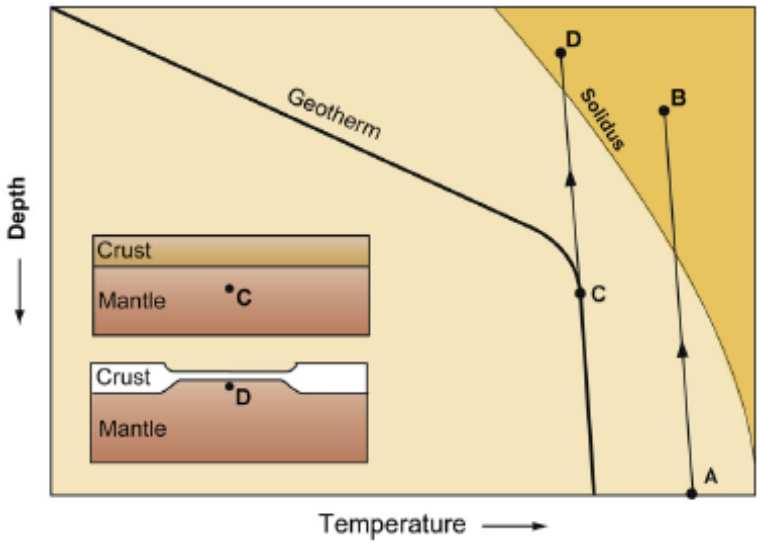

Figure 26– The principles of descompression melting. From Sigurdsson *et al.*(2015).

This mantle composition is predominantly peridotite, a rock which is made up of olivine, clino- and orthopyroxene and an aluminous phase, either garnet at high pressures or spinel at low pressures. Therefore, melts of peridotite are richer in the components of spinel, clinopyroxene and garnet than their peridotite source and, consequently, richer in CaO and Al_2O_3, also have higher SiO_2 and lower MgO contents than peridotite. These melts are known as basalts.

Melting beneath ocean ridges produces a basalt that contains around 50% SiO_2, but poor in K_2O and Na_2O known as *tholeiitic* basalt. Once emplaced within the crust, the basalt cools and starts to crystallize. The melts differ in composition from their source region, so the material that first crystallizes from a basalt also has a different composition from the basaltic liquid, it is the MgO olivine. Olivine is denser than basaltic melt and they are easily separated by crystal settling due to gravity.

This separation leaves the basalt liquid poorer in MgO and relatively enriched in CaO, Al_2O_3, Na_2O, and K_2O. The second mineral crystallizes with these elements and that mineral is plagioclase feldspar and it too separates from the melt, depleting the latter in CaO and Al_2O_3. If the minerals once formed are separated rapidly then this process is described as *fractional crystallization* and is illustrated in Figure 27. This process is one of the most important processes in modifying the composition of magmas and is the cause of much diversity in the compositions of igneous rock (Sigurdsson *et al.* 2015).

The effects of fractional crystallization on ocean floor basalts (MORB) are illustrated in Figure 27. The diagram shows how Na_2O increases as fractional processes, consistent with the removal of Na-poor and Mg-rich phases such an olivine.

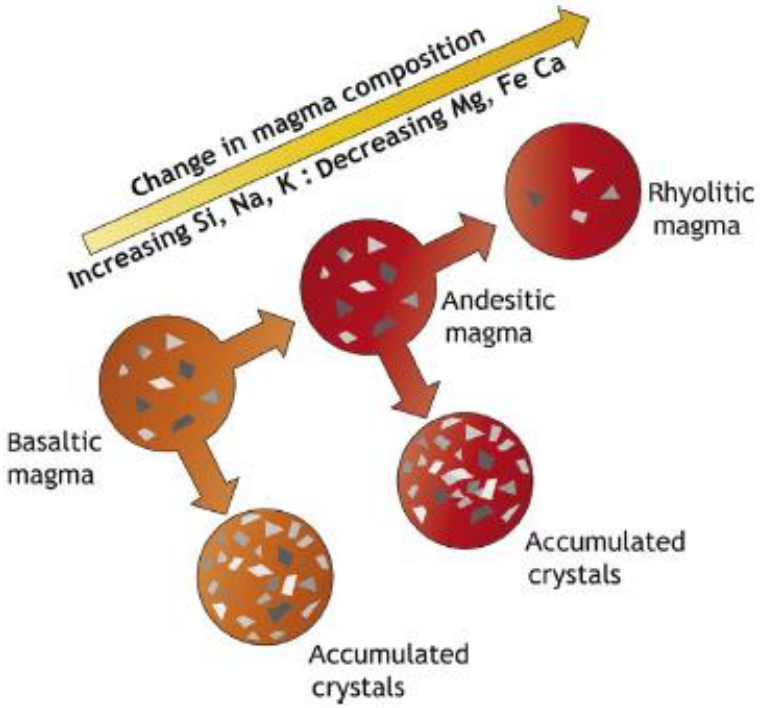

Figure 27 – Evolution of magma by fractional crystallization as a result of cooling and the removal of crystals from the gradually solidifying melt. From Sigurdson *et al.*(2015).

The Figure 28 presents that the basalts from three separate trends and do not converge on a single Na_2O content at a high MgO abundance. This discrepancy strongly suggests that each area has a distinct primitive magma composition which in turn relates differences in the pressure and temperature and the composition of the underlying mantle source or a combination of two.

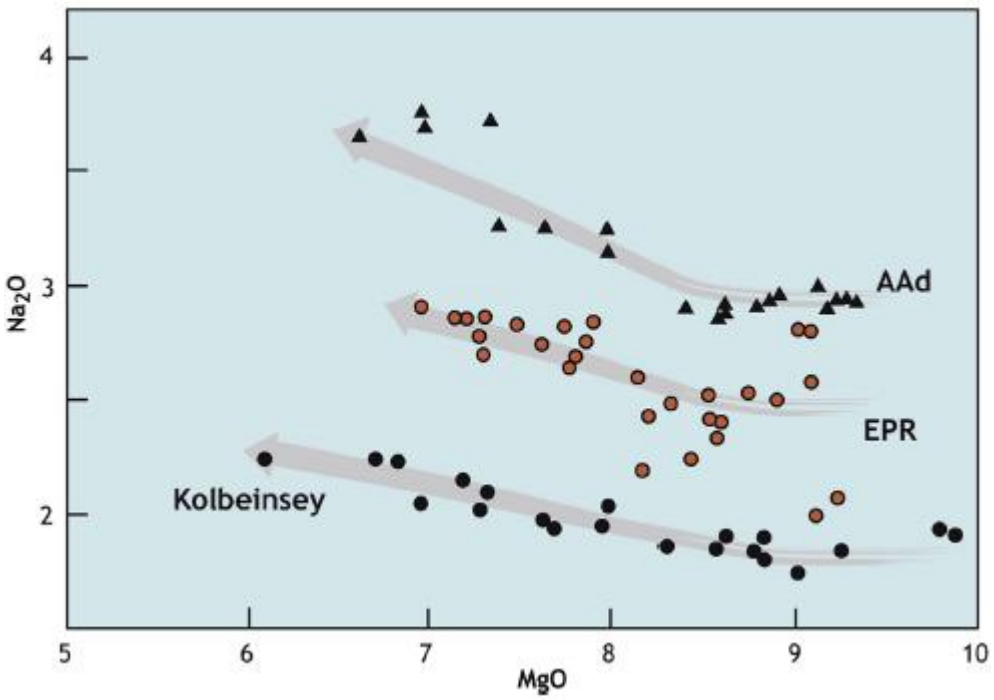

Figure 28 - Variation of sodium with magnesium (expressed as wt.% oxides) in basalts from three segments of the mid ocean ridge system. Kolbeinsey Ridge = extension of the mid-Atlantic ridge, north of Iceland; EPR = East Pacific Rise; AAD = lavas from the Australia-Antarctic discordance, a segment of ridge south of Australia in the Southern Ocean Each region shows an increase in sodium as magnesium decreases, but the trends start at different sodium contents at high magnesium abundances. Adapted from Klein & Langmuir (1987).

3.3.1.2 Ocean Island Basalts (OIB)

An important location where basalts are found is the ocean islands, such as Hawaii. The compositions of basalts in these islands are distinct from MORB, as showed in Table 5. The OIB tends to have a wider range of SiO_2 and greater alkali contents than MORB, suggesting higher pressures and lower degrees of melting, also tend to be more magnesium-rich.

Many ocean islands are located on thick ocean lithosphere. For example, Hawaii is located on 80-100 Ma old lithosphere that is about 80 km thick. They are also situated on uplifted areas of oceanic crust. The presence of basaltic volcanism at the surface implies the presence of hot mantle and these so-called hot spots appear relatively stationary to plate movements. The Hawaiian chain of islands and seamounts stretch along all the way to Midway Island and represents a continuous hot spot basaltic volcanism around 50 Ma.

The combination of these observations has led to the development of the mantle plume hypothesis to explain intraplate volcanism, such as Hawaii. Mantle plumes can occur beneath continents as well as the ocean basins. They are an integral part of convective overturn of the Earth's mantle and have their origins at great depth, possibly at the core-mantle boundary and if the overlying lithosphere is thin enough and the plume is hot enough, then as the plume approaches the base of the lithosphere it can undergo decompressing melting (Watson & McKenzie 1991 in Sigurdson *et al.* 2015).

3.3.1.3 Subduction-Related Basalts

Basalts are produced above active subduction zones where the cold oceanic lithosphere move downward back into the mantle. The subduction oceanic lithosphere carries with it acumulation of deep sea sediments and altered oceanic crust. These rocks release their water as the slab descends into the mantle and warms up. Water has a dramatic effect on the liquidus temperature of the mantle lowering it, thus the mantle can produce melts significantly lower temperatures in the presence of H_2O and the magmas so generated will be very water-rich and this affects their physical and chemical characteristics.

Basaltic magma produced in island arc settings tend to be tholeiitic and the name island arc basalts (IAB) is to distinguish them from MORB due their higher H_2O, K_2O and Al_2O_3 contents. Their higher water contents have a dramatic effect on the crystallization sequence. First, water expands the phase field of olivine at the expense of plagioclase and clinopyroxene. Second, the reduction in the liquidus temperature of plagioclase means that when it does appear on the liquidus it has a much more calcic composition (more anorthite-rich) and so has lower silica content than plagioclase that crystallizes from MORB. Finally, while water lowers the temperature at which silicate minerals crystallize, it has a reduced effect on the temperature of oxide crystallization. Thus, a typical crystallization sequence in an IAB is: olivine, calcic plagioclase and magnetite, all of which heave low SiO_2, resulting in a much more rapid increase in SiO_2 in the fractionating magma. Thus, island arc lavas tend to develop from basalts through low-K andesites to dacites and rhyolites (Sigurdson *et al.* 2015).

In regions where subduction takes place beneath a continental margin, such as Andes, the basaltic magma may become trapped in the overlying continental crust. In these regions, the continental crust can be very thick, with tens of kilometers, and provides ample opportunity for the magma to accumulate in magma chambers and undergo fractional crystallization and interaction with the silica-rich granitic crust. Basaltic magma is denser than continental crust and so can only rise to a level of neutral floatability, frequently at the junction of layers with contrasting density, such as the Moho or at tectonic boundaries. Here it accumulates and undergo fractional crystallization in the same way as arc tholeiites until magma density is such that it becomes floatable once more and continues its passage towards the surface. This critical density is reached after a significant amount of magnetite and olivine fractionation has reduced the iron and magnesium and increased the alkali and silica content of the magma such that it has become an andesite.

The intrusion of significant amounts of basaltic magma into the continental crust can lead to melting and remobilization of the crust. Melts of crustal rocks tend to have a granitic (or rhyolitic) composition and these can mix with the basaltic magma making a hybrid rock that also has a widely andesitic composition. Thus, andesites may originate through magma mixing and contamination of basaltic magma as well as closed system fractional crystallization

3.3.1.4 Continental Basalts

Contemporary and Phanerozoic continental basaltic volcanism is invariably associated with tectonic extension, because continental lithosphere is frequently more than 100 km thick and beneath Archean cratons can be as much as 200 km thick. When continents are stretched over the site of a mantle plume, as in some rift zones, and particularly during continental break-up, basaltic magmas are generated and erupted at the surface. Modern day rift zones include the east African Rift system, the Rhine graben in Europe, the Baikal Rift in Siberia and the Rio Grande rift in the USA. All of them are characterized by alkali basalts, nephelinites and basanites and evolved derivate (phonolite and trachyte). This is because the amount of extension across such rift zones is small and so only small melt fraction alkali-rich magmas are produced from the mantle plume, similar to OIB. Continental flood basalts provinces (or large igneous provinces) contain large volumes ($>10^6$ km^3) of tholeiitic basalts that appear to have erupted geologically rapidly (1 – 2 Myr) (Sigurdson *et al.* 2015).

Examples include Paraná basalts of Brazil, the Karoo lavas of South Africa and Deccan traps of India. They represent large scale magmatic and volcanic events and are associated with continental break-up and development of a new ocean, and some occur at the end of hot-spot traces in the oceans and can be linked to the presence of a mantle plume. Such large volume of magma clearly requires the presence of anomalously hot mantle as in a plume and an association between large igneous province and the initiation of a mantle plume is often invoked.

CHAPTER 4

PETROGRAPHY OF THE STOLPEN BASALTS AND BASALT BOULDERS

This chapter presents the petrographic description of the Stolpen basalts and basalt boulders. In this description we analyzed mainly the mineral assemblage and microstructure, including degree of crystallinity, grain size and grain shapes. The abbreviations for names of rock-forming minerals in the photomicrographies and tables are used according to Whitney & Evans (2010).

4.1 MACROSCOPIC AND MICROSCOPIC DESCRIPTIONS

The rocks studied here were divided into two different types, the Stolpen basalts and the basalt boulders, as described below.

4.1.1 Stolpen basalts

The Stolpen basalt is mainly distributed below the Castle of Stolpen, localized in the center of Stolpen town, with an area around 9.000 m^2(Figure 29).

Figure 29– Basalt joints outcrop below the Stolpen Castle.

The Stolpen basalts are bluish to greyish (Figure 30A), columnar (Figure 30B), aphanitic and present high hardness and high density.

Figure 30 –Main macroscopic features of the Stolpen basalt.

Under transmitted light, the basalts present glomeroporphyritic and intergranular texture and amygdaloidal structure, with subhedral phenocrysts of olivine and clinopyroxene, and a very thin matrix of feldspar. Most of the feldspar crystals show a tabular euhedral shape (Figure 31).

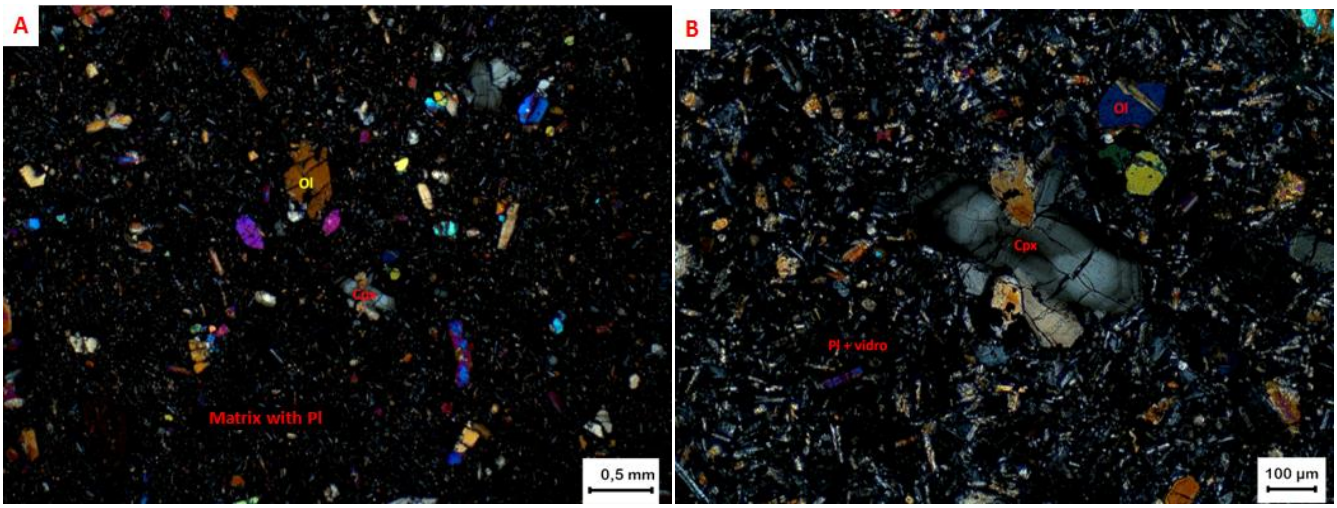

Figure 31– Photomicrographies of the Stolpen basalt (sample 68231). A) Phenocrysts of olivine and clinopyroxene and thin matrix of feldspar. Magnification 2.5x, XPL B) Glomeroporphiric texture with phenocrysts of clinopyroxene and olivine and thin matrix of feldspar. Magnification 10x, XPL.

Olivine is fractured, presenting some secondary minerals along the fractures and with high birefringence. The crystals present a compositional zoning from the cores toward the rims (it wil be better demonstrated on Chapter 5). The zoning of olivine can be seen in Figure 32.

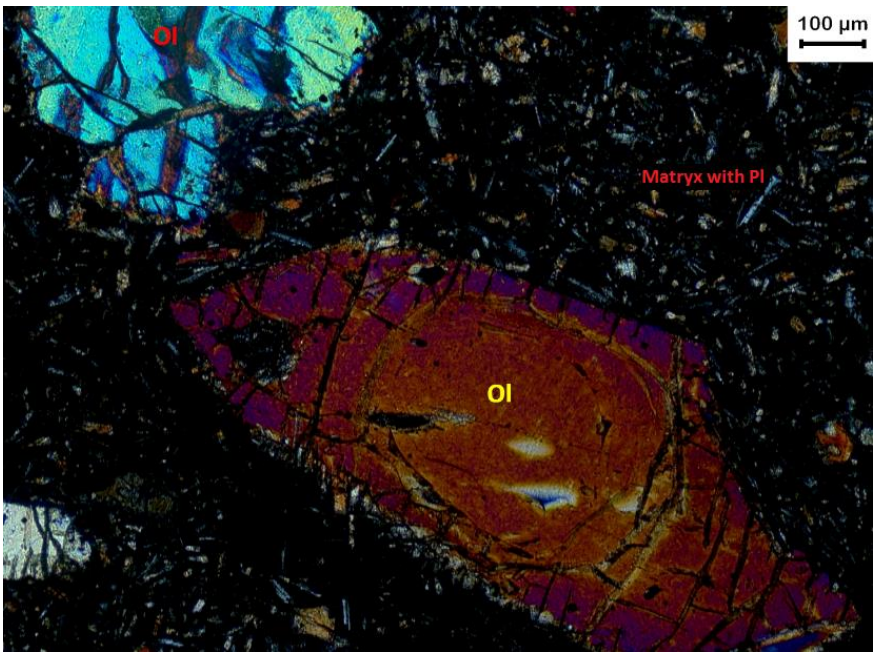

Figure 32 – Photomicrography of the Stolpen basalt (sample 68231) showing the zoning in phenocryst of olivine, with orange interference color in the core and purple color in the rim. 10x magnification and XPL.

Clinopyroxene is clustered into aggregates in the basalts (glomeroporphyritic texture), also the crystals fill amygdales (amygloidal texture) and present both low birefrigence and zoning from the core to the edges. The zoning in clinopyroxene is showed in Figure 33.

Opaques have anedric shapes and are widespread all over the matrix.

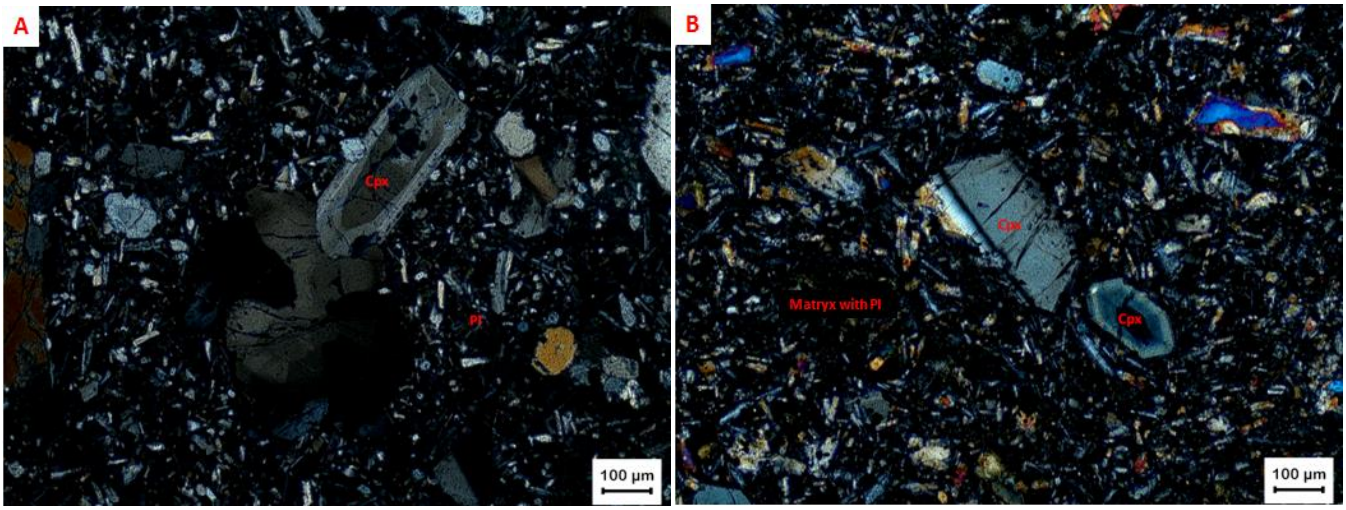

Figure 33– Photomicrographies of the Stolpen basaltshowing zoning in phenocrysts of clinopyroxene, with dark grey color in the core to light grey in the rims. 10x magnification and XPL. A) sample 68227 B) sample 68231.

Table 6 shows the average of modal composition for the Stolpen basalts.

Table 6 - Average composition for the Stolpen basalts according the thin sections analyses.

Minerals	% Average
Clinopyroxene	10,00
Plagioclase	60,00
Olivine	15,00
Opaque	15,00

4.1.2 Basalt boulders

The basalt boulders are found in southeast and northeast of Stolpen. They are distributed in the highest altitudes and up to 15 km distance from the main outcrop of the columnar basalts that belongs to the Castle of Stolpen. The Figure 34 present the distribution of the boulders associated with Stolpen town location. The boulders are distinguished by size and the black line is the topography profile that appears in Figure 35. The topography profile defines the standard distribution of the boulders, that present a main occurency associated with the highest as showed in Figure 36.

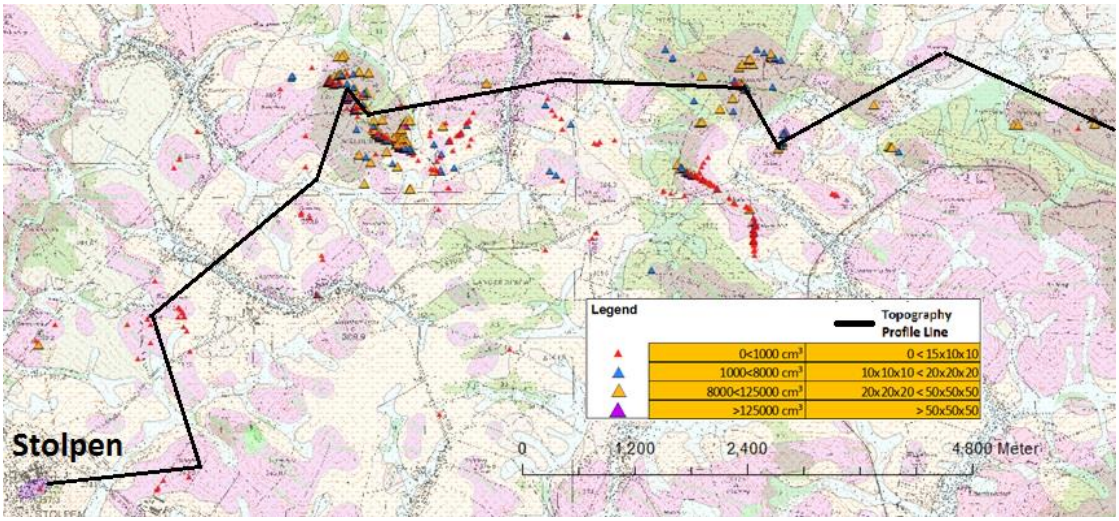

Figure 34– Geographic distribution of the boulders (distinguished by size). The black line refers to the topography.

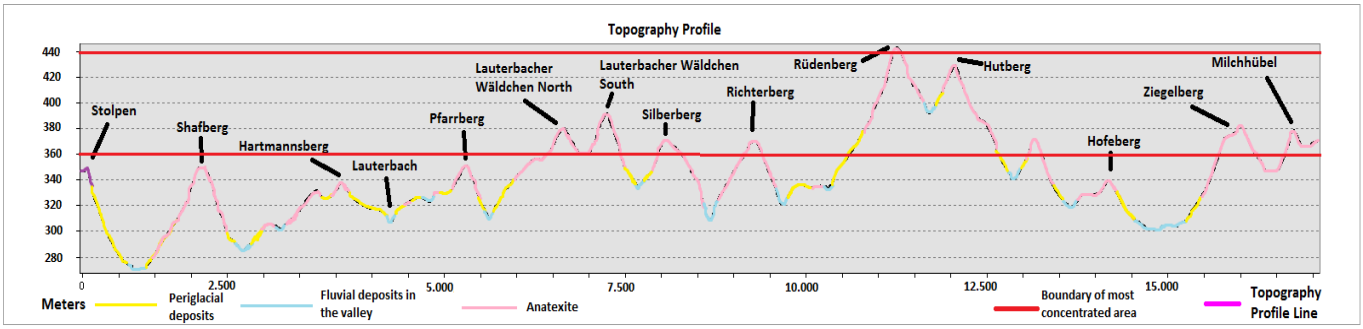

Figure 35 – Topographic profile of the studied area with respective litologies, name of the hills and a line showing where is the main occurency of the boulders.

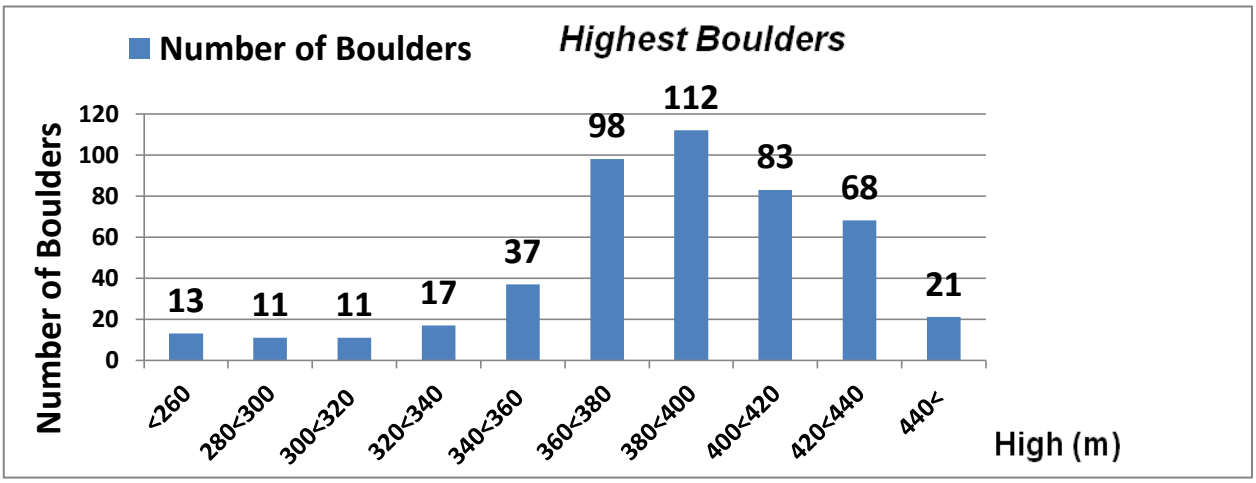

Figure 36 - Graphic correlating the number of the boulders *versus* altitude. This data shows were the boulders are concentrated.

The macroscopic features of the basalt boulders are very similar to the Stolpen basalts: aphanitic, bluish to greyish, presenting high hardness and high density (Figure 37).

Figure 37 – Macroscopic feature of the basalt boulder.

Under the microscope, the stone presents a subophitic texture, with phenocrysts of olivine, clinopyroxene and plagioclase and a matrix of feldspar (Figure 38). Carbonate occurs replacing feldspars.

The matrix presents bigger feldspar crystals in comparison to the Stolpen basalt. The feldspars occur generally in tabular euhedral shapes. Opaque minerals occur all over the matrix.

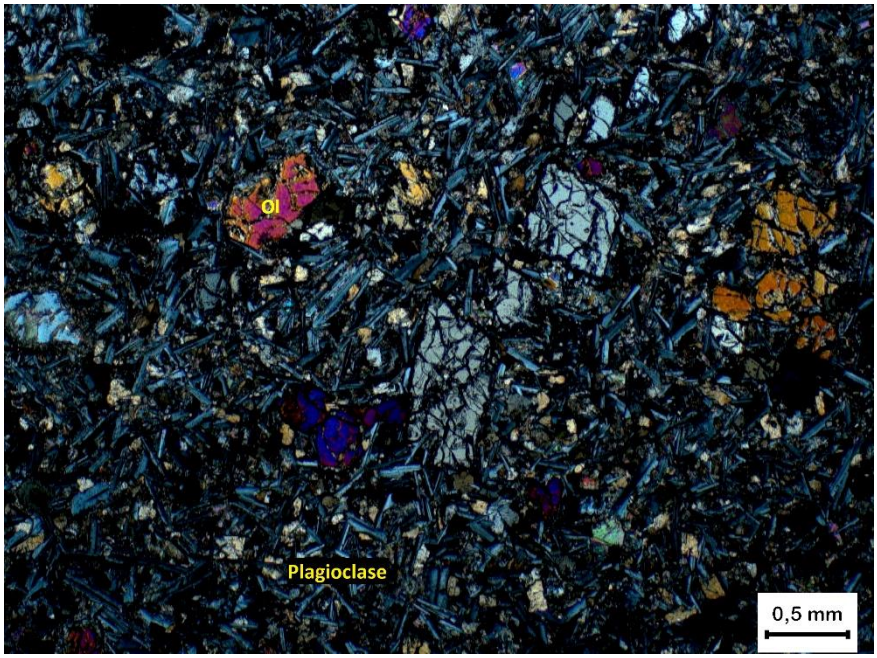

Figure 38 – Photomicrographies of the boulder (sample 69128). Subophitic texture with phenocrysts of olivine and clinopyroxene in a feldspar-rich matrix, with carbonate and opaque minerals. 2,5x magnification and XPL.

Olivine is generally fractured, with secondary minerals filling the fractures. The crystals are more homogenous (in terms of composition) if comparising with that of the Stolpen basalts. They have both high relief and birefringence (Figure 39A).

Clinopyroxene present low birefrigence, is subeuhedral and occurs in lower quantity than the olivine phenocrysts.

Plagioclase occurs in tabular shapes and present low birefringence. The crystals present compositional zoning (Figure 39B).

Carbonate occurs with two directions of cleavage, anomalous interference color and have relief pleochroism.

Table 7 shows the average modal composition of the basalt boulders.

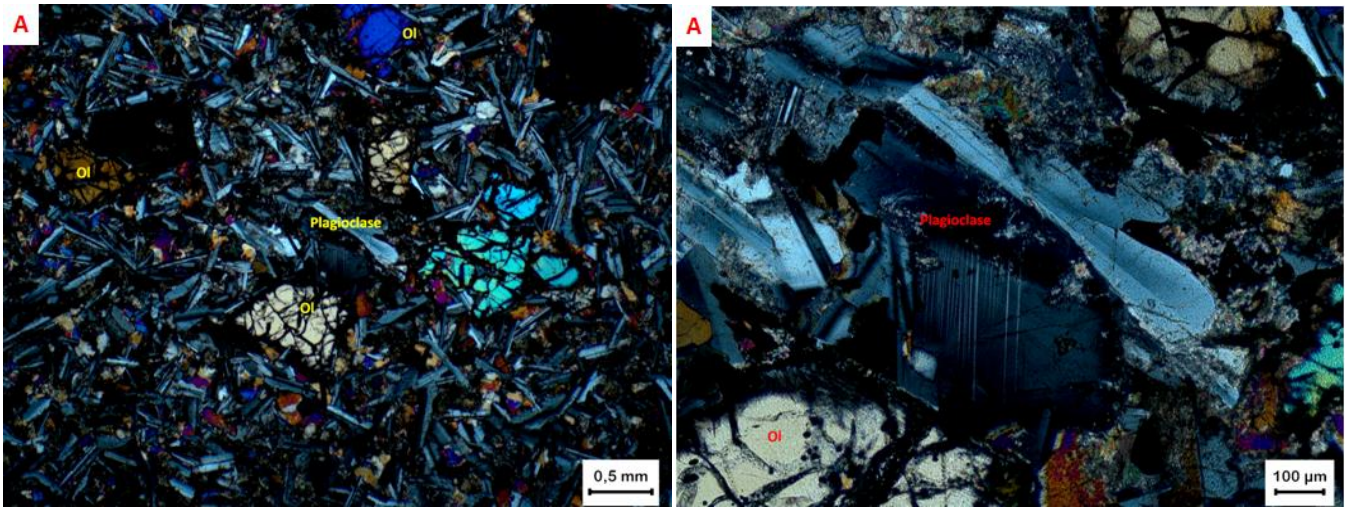

Figure 39 – Photomicrographies of the basalt boulder (sample 68230) A) Subophitic texture with phenocrysts of olivine and plagioclase in a feldspar-rich matrix. Magnification 2.5x, XPL B) Zoning in plagioclase, turning from white grey to dark grey interference colors. Magnification 10x, XPL.

Table 7- Average composition for the basalt boulders under thin sections.

Minerals	% Average
Carbonate	10,00
Clinopyroxene	5,00
Plagioclase	60.00
Olivine	10,00
Opaque	15,00

CHAPTER 5
MINERAL CHEMISTRY AND THERMOMETRY

The mineral chemistry studies were carried out in four samples (68227 and 68231 related to the Stolpen basalts and 68230 and 69128 from the bolders) in order to refining the petrographic characterization and to obtain chemical data for thermometry. The methodology is described on Chapter 1, item 1.5.4. Analyses were made in olivine, clinopyroxene and plagioclase crystals.

5.1 MINERAL CHEMISTRY

5.1.1 Stolpen basalts

The thin sections 68227 and 68231 were divided into different fields during the analyses as presented in Figure 40.

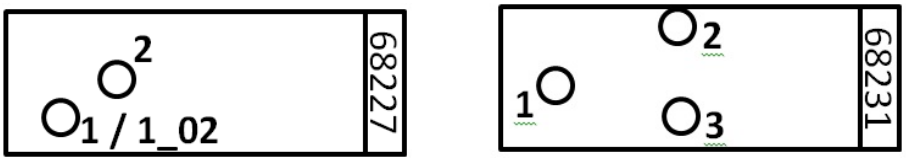

Figure 40 – Analyzed fields in the thin sections.

Table 8 shows the main analyzed minerals and respective analytical points.

Table 8– Relation of the fields, mineral and analyzed points (Cpx=Clinopyroxene; Ol=olivine:Pl=plagioclase).

68227	Mineral	Points
F1	Cpx	1 - 3
	Ol	4 - 7
	Cpx	8 - 10
F1_02	Pl	1 - 2
	Pl	3 - 4
	Pl	5 - 7
	Pl	8 - 9
F2	Cpx	1 - 11
	Pl	13
	Pl	14
	Pl	15 - 16
	Pl	17 - 18
	Pl	19 - 20

68231	Mineral	Points
F1	Ol	1 - 5
	Cpx	6 - 13
	Pl	14 - 15
	Pl	16 -17
	Pl	18 - 19
	Pl	20 - 21
	Pl	22 - 23
F2	Ol	24 - 28
	Ol	29 - 37
	Pl	38 - 43
	Pl	45
	Pl	46
	Pl	47
F3	Cpx	48 - 51
	Cpx	52 - 54
	Pl	55 - 56
	Pl	57 - 58
	Pl	59 - 60
	Pl	61 - 63

5.1.1.1 Olivine

Olivine was analyzed in three different fields: one in 68227 (F1) and two in 68231 (F1 and F2).

The analysis in sample 68227 obtained 4 points (Figure 41). The results are presented in Table 9.

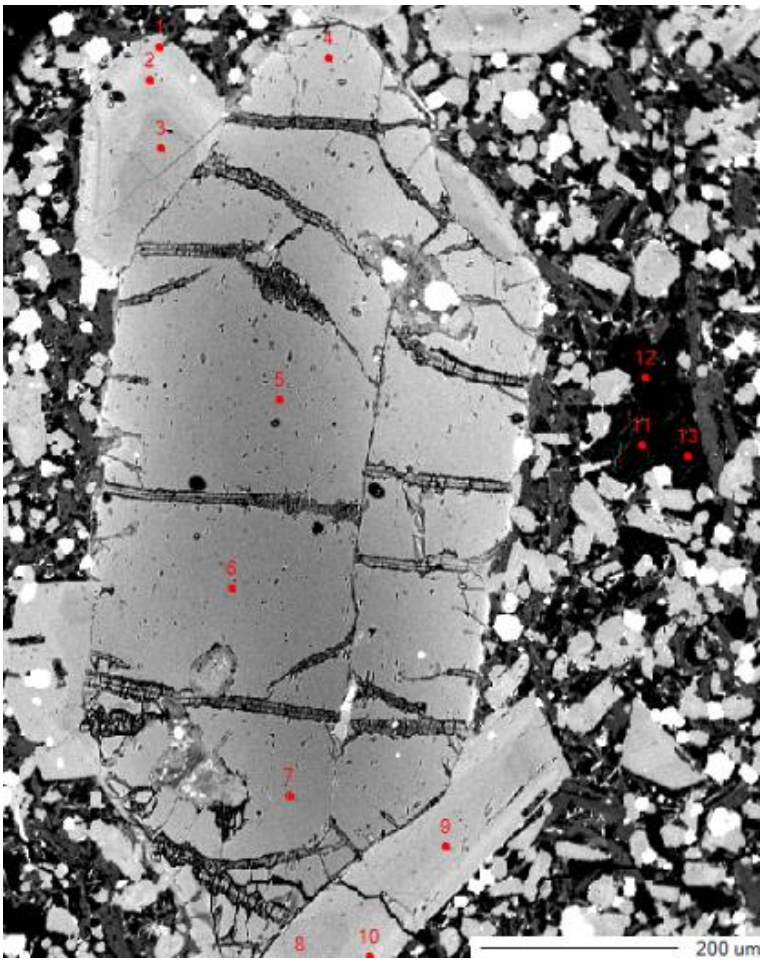

Figure 41 – Backscattered eletron image of an euhedral olivine from field 1 (sample 68227). Points 4 to 7.

Table 9 - Mineral chemistry analysis results for olivine from the sample 68227, field 1. Fa = fayalite; Fo = fosterite.

Sample	68227	68227	68227	68227	
Field	1	1	1	1	
Crystal	1	1	1	1	
Point	4	5	6	7	
Position	Rim	Core	Core	Interm.	
SiO2	38.816	39.756	39	38.933	Oxides (weight %)
TiO2	0.02	0.02	0.04	0.00	
Al2O3	0.023	0.032	0.038	0.056	
FeO	22.073	16.944	17.715	18.005	
MgO	39.35	44.41	43.48	43.02	
MnO	0.04	0.00	0.02	0.02	
CaO	0.408	0.228	0.231	0.268	
Na2O	0.013	0.021	0.009	0	
Cr2O3	0.03	0.01	0.03	0.05	
NiO	0.16	0.14	0.07	0.11	
K2O	0.012	0.003	0.001	0.007	
Total	**100.93**	**101.57**	**100.97**	**100.47**	
Si	1.00	0.99	0.99	0.99	Cations (4 oxigens)
Ti	0.00	0.00	0.00	0.00	
Al	0.00	0.00	0.00	0.00	
Fe	0.48	0.35	0.37	0.38	
Mg	1.51	1.65	1.63	1.63	
Mn	0.00	0.00	0.00	0.00	
Ca	0.01	0.01	0.01	0.01	
Na	0.00	0.00	0.00	0.00	
Cr	0.00	0.00	0.00	0.00	
Ni	0.00	0.00	0.00	0.00	
K	0.00	0.00	0.00	0.00	
Fo	0.7604	0.8236	0.8138	0.8097	End members
Fa	0.2396	0.1764	0.1862	0.1903	

The average formula unit for the olivine crystal in the sample 68227 is **($Mg_{1,60}$ $Fe_{0,40}$ $Ca_{0,01}$)SiO_4**, corresponding to *ca.* 80% of the fosterite endmember (Table 9). There is a slight increase of FeO and a decreasing of MgO contents from the core toward the rims (Figure 42; Table 9).

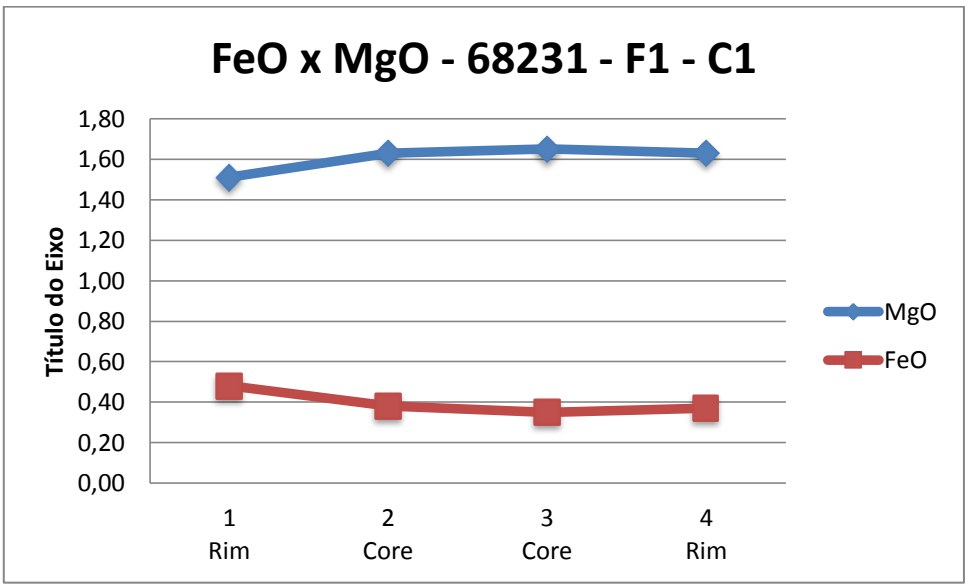

Figure 42 – Binary diagram presenting thedistribution of FeO and MgO along the olivine crystal (field 1, sample 68227).

The analysis in sample 68231 obtained 5 and 14 points in fields 1 and 2, respectively (Figures 43 and 44). The results are presented in Table 10.

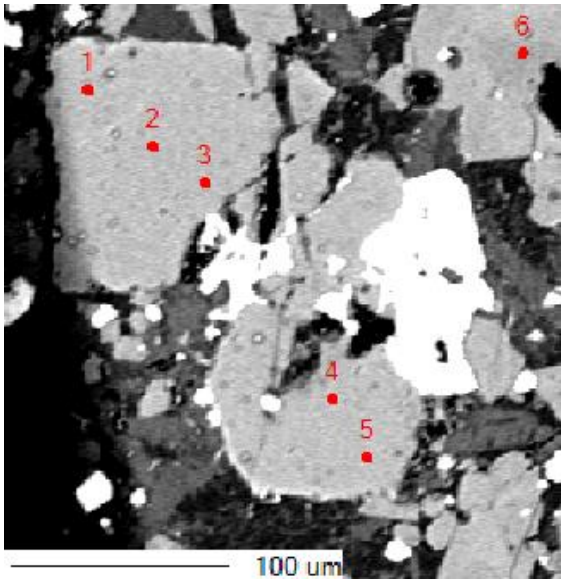

Figure 43 – Backscattered eletron image of two olivine crystals from field 1(sample 68231). Points 1 to 5 in C1.

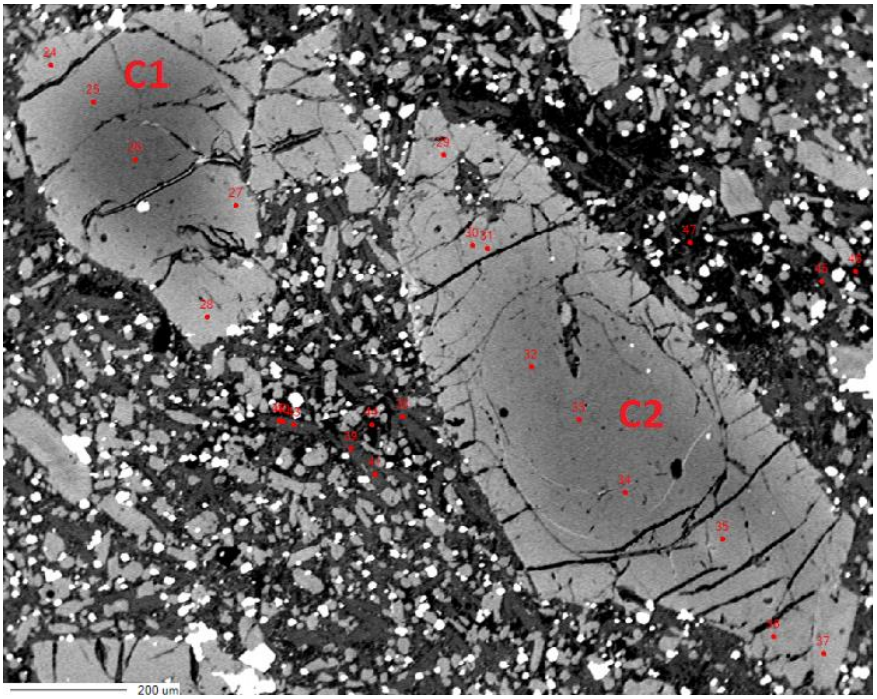

Figure 44 – Backscattered eletron image of two olivine crystals from field 2 (sample 68231). Points 24 to 28 and 29 to 37, in C1 and C2 respectively. Note the compositional zoning in the backscattered image.

Table 10 - Mineral chemistry analysis results for olivine from the sample 68231, fields 1 and 2. Fa = fayalite; Fo = fosterite.

Amostra	68231	68231	68231	68231	68231	68231	68231	68231	68231	68231	68231	68231	68231	
Campo	1	1	1	1	1	2	2	2	2	2	2	2	2	
Grão	1	1	1	2	2	1	1	1	1	1	2	2	2	
Ponto	1	2	3	4	5	24	25	26	27	28	29	30	31	
Posição	Borda	Núcleo	Borda	Núcleo	Borda	Borda	Núcleo	Núcleo	Borda	Borda	Borda	Interm.	Interm.	
SiO2	38.68	38.568	38.382	39	38.641	38.487	39.895	40.57	38.679	38.453	38.699	38.86	39.748	Oxides (weight %)
TiO2	0.00	0.00	0.00	0.01	0.04	0.00	0.03	0.01	0.00	0.03	0.02	0.01	0.00	
Al2O3	0.04	0.038	0.035	0.045	0.028	0.029	0.035	0.079	0.029	0.057	0.033	0.049	0.074	
FeO	23.40	23.57	23.689	23.78	23.715	22.918	15.853	12.311	21.821	23.669	23.391	21.294	16.702	
MgO	38.49	38.44	38.04	39.14	38.57	38.68	45.11	47.97	40.06	38.50	38.30	39.90	44.58	
MnO	0.07	0.03	0.00	0.02	0.02	0.01	0.00	0.02	0.03	0.04	0.00	0.01	0.00	
CaO	0.46	0.357	0.466	0.399	0.433	0.364	0.28	0.213	0.377	0.412	0.477	0.301	0.288	
Na2O	0.00	0.037	0.012	0.003	0	0.027	0	0	0	0.013	0.011	0.013	0.019	
Cr2O3	0.01	0.06	0.02	0.00	0.00	0.02	0.00	0.06	0.00	0.00	0.00	0.01	0.03	
NiO	0.05	0.06	0.04	0.09	0.10	0.10	0.15	0.25	0.04	0.00	0.11	0.12	0.35	
K2O	0.00	0	0.004	0	0	0	0.007	0.008	0.005	0.007	0.018	0.009	0.012	
Total	101.21	101.14	100.69	102.50	101.56	100.62	101.37	101.48	101.04	101.18	101.06	100.58	101.80	
Si	1.00	1.00	1.00	0.99	1.00	1.00	0.99	0.99	0.99	0.99	1.00	1.00	0.99	Cations (4 oxigens)
Ti	0.00	0.00	0.00	0.00	0.00	0.00	0.00	0.00	0.00	0.00	0.00	0.00	0.00	
Al	0.00	0.00	0.00	0.00	0.00	0.00	0.00	0.00	0.00	0.00	0.00	0.00	0.00	
Fe	0.51	0.51	0.52	0.51	0.51	0.50	0.33	0.25	0.47	0.51	0.51	0.46	0.35	
Mg	1.48	1.48	1.47	1.49	1.48	1.49	1.67	1.75	1.53	1.48	1.48	1.53	1.65	
Mn	0.00	0.00	0.00	0.00	0.00	0.00	0.00	0.00	0.00	0.00	0.00	0.00	0.00	
Ca	0.01	0.01	0.01	0.01	0.01	0.01	0.01	0.01	0.01	0.01	0.01	0.01	0.01	
Na	0.00	0.00	0.00	0.00	0.00	0.00	0.00	0.00	0.00	0.00	0.00	0.00	0.00	
Cr	0.00	0.00	0.00	0.00	0.00	0.00	0.00	0.00	0.00	0.00	0.00	0.00	0.00	
Ni	0.00	0.00	0.00	0.00	0.00	0.00	0.00	0.00	0.00	0.00	0.00	0.00	0.01	
K	0.00	0.00	0.00	0.00	0.00	0.00	0.00	0.00	0.00	0.00	0.00	0.00	0.00	
Fo	0.75	0.74	0.74	0.75	0.74	0.75	0.84	0.87	0.77	0.74	0.74	0.77	0.83	End members
Fa	0.25	0.26	0.26	0.25	0.26	0.25	0.16	0.13	0.23	0.26	0.26	0.23	0.17	

Table 10(continuation) -Mineral chemistry analysis results for olivine from the sample 68231, fields 1 and 2. Fa = fayalite; Fo = fosterite.

Amostra	68231	68231	68231	68231	68231	68231	
Campo	2	2	2	2	2	2	
Grão	2	2	2	2	2	2	
Ponto	32	33	34	35	36	37	
Posição	Núcleo	Núcleo	Núcleo	Interm.	Borda	Borda	
SiO2	39.456	40.091	39.608	38.908	38.876	43.336	Oxides (weight %)
TiO2	0.02	0.04	0.07	0.01	0.02	2.87	
Al2O3	0.052	0.033	0.035	0.046	0.041	9.911	
FeO	16.889	16.477	17.306	20.177	22.17	8.394	
MgO	43.77	44.71	44.57	40.97	39.40	11.04	
MnO	0.03	0.02	0.00	0.00	0.03	0.00	
CaO	0.271	0.281	0.201	0.318	0.35	22.635	
Na2O	0.004	0.013	0.009	0	0.01	0.508	
Cr2O3	0.04	0.00	0.00	0.03	0.00	0.01	
NiO	0.15	0.13	0.09	0.15	0.03	0.03	
K2O	0.011	0.01	0.002	0.008	0	0.005	
Total	100.68	101.80	101.89	100.62	100.92	98.74	
Si	0.99	1.00	0.99	1.00	1.00	1.11	Cations (4 oxigens)
Ti	0.00	0.00	0.00	0.00	0.00	0.05	
Al	0.00	0.00	0.00	0.00	0.00	0.30	
Fe	0.36	0.34	0.36	0.43	0.48	0.18	
Mg	1.64	1.65	1.65	1.56	1.51	0.42	
Mn	0.00	0.00	0.00	0.00	0.00	0.00	
Ca	0.01	0.01	0.01	0.01	0.01	0.62	
Na	0.00	0.00	0.00	0.00	0.00	0.03	
Cr	0.00	0.00	0.00	0.00	0.00	0.00	
Ni	0.00	0.00	0.00	0.00	0.00	0.00	
K	0.00	0.00	0.00	0.00	0.00	0.00	
Fo	0.82	0.83	0.82	0.78	0.76	0.70	End members
Fa	0.18	0.17	0.18	0.22	0.24	0.30	

Both olivine crystals from the field 1 are chemically homogeneous (Table 10). The average formula unit is **$(Mg_{1,48}\ Fe_{0,51}\ Ca_{0,01})SiO_4$**, corresponding to *ca.* 75% of the forsterite endmember (Table 10).

Both olivine crystals from the field 2 are clearly zoned showing an enrichment in FeO and a decreasing in MgO from the core to the rims (Figure 45, Table 10). The average formula unit was made for the core and rim from both crystals, as demonstrated below:

- C1, core: **$(Mg_{1,71}\ Fe_{0,29}\ Ca_{0,01})SiO_4$** (86% of the forsterite endmember)
- C1, rim: **$(Mg_{1,50}\ Fe_{0,49}\ Ca_{0,01})SiO_4$** (75% of the forsterite endmember)
- C2, core: **$(Mg_{1,63}\ Fe_{0,37}\ Ca_{0,01})SiO_4$** (81% of the forsterite endmember)
- C2, rim: **$(Mg_{1,51}\ Fe_{0,48}\ Ca_{0,01})SiO_4$** (76% of the forsterite endmember)

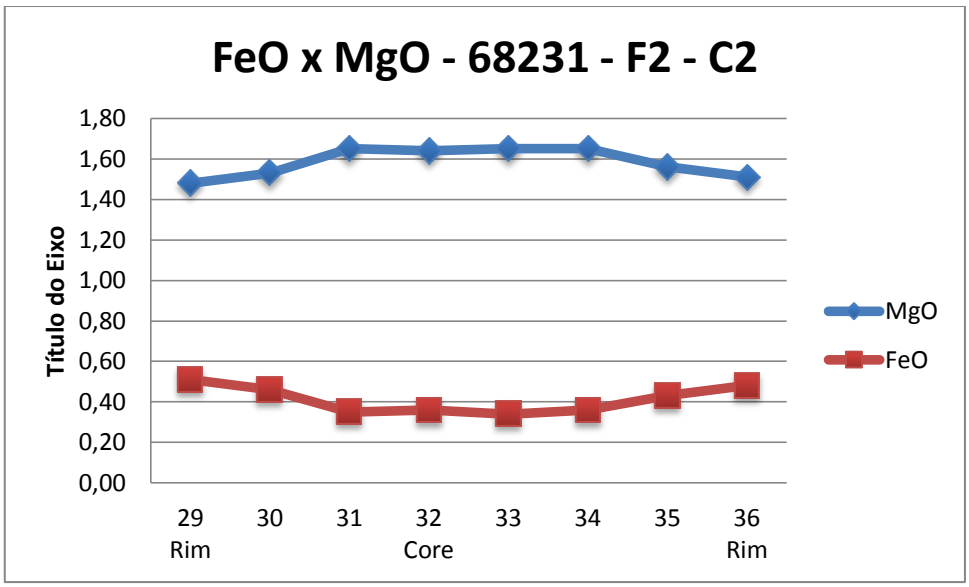

Figure 45- Binary diagram presenting the distribution of FeO and MgO along the crystal 2 (field 2, sample 68231).

The chemical maps obtained using the microprobe show these variations from the core toward the rims in both crystals from the sample 68231, as presented in Figures 46 and 47.

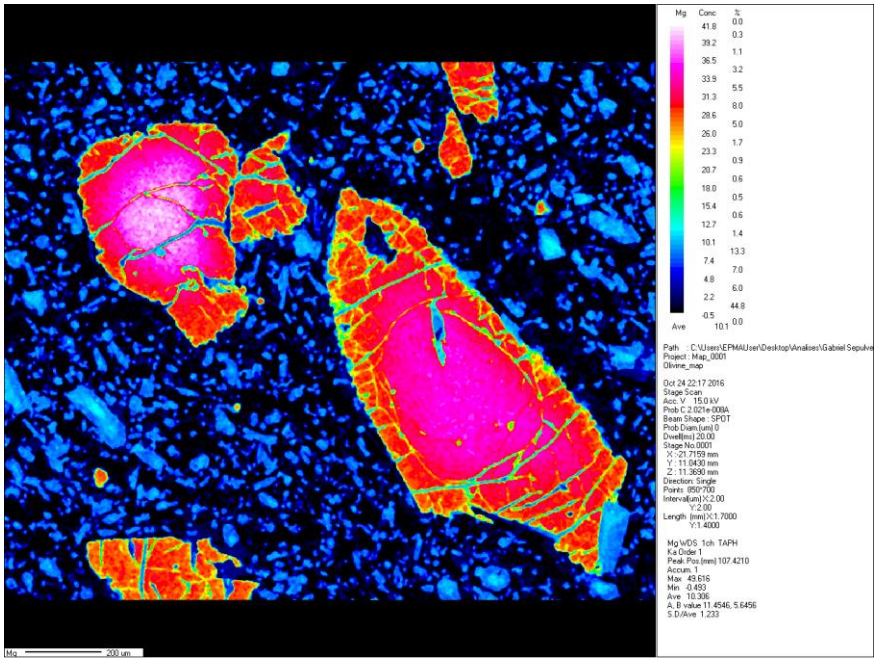

Figure 46–Chemical map presenting the variation of Mg content from the core (pink) to the rim (red).

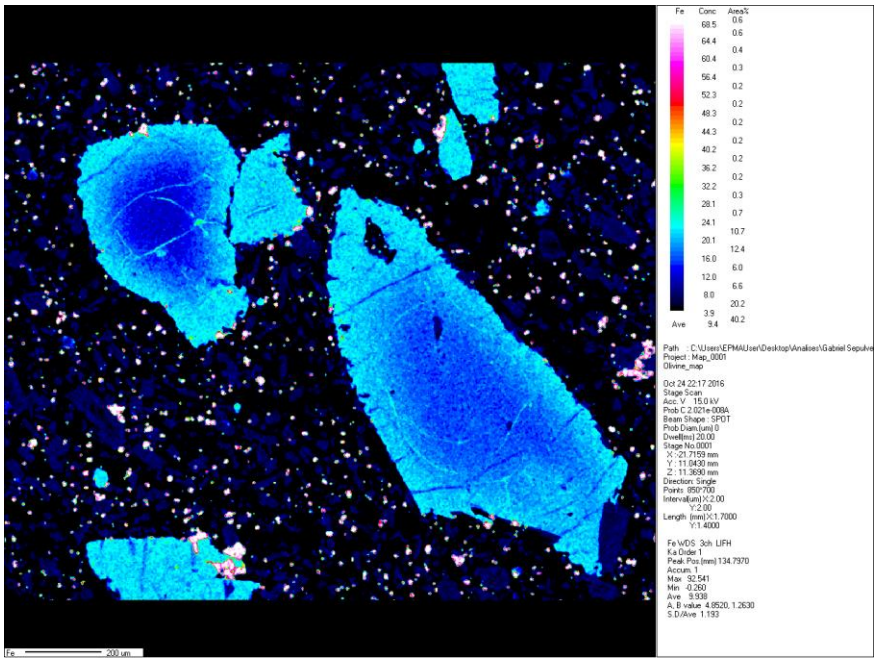

Figure 47 – Chemical map presenting the variation of Fe content from the core (dark blue) to the rim (light blue).

5.1.1.2 Pyroxene

Pyroxene was analyzed in five different fields: three in the sample 68227 (F1, F1_02 and F2) and two in the sample 68231 (F1 and F3).

The analysis in sample 68227 obtained 6 and 11 points in the fields 1 and 2, respectively (Figures 48 and 49). The results are presented in Table 11.

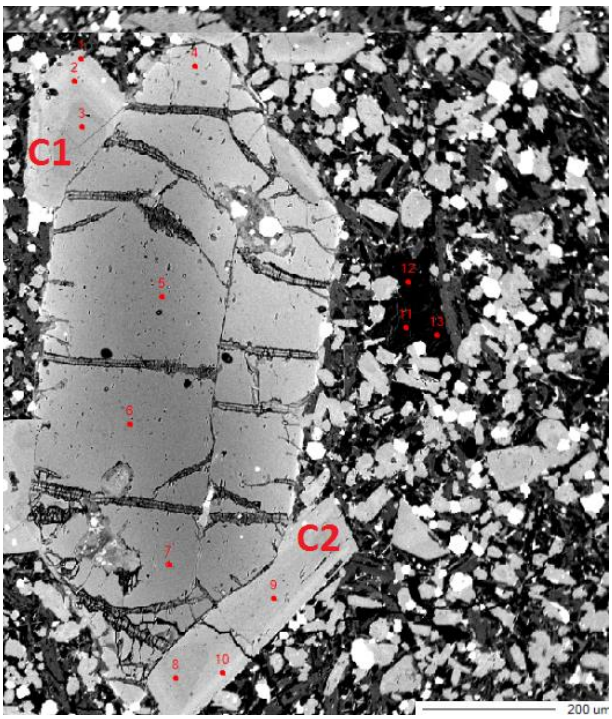

Figure 48 – Backscattered eletron image of two clinopyroxene crystals from field 1 (sample 68227). Points 1 to 3 and 8 to 10, in C1 and C2 respectively.

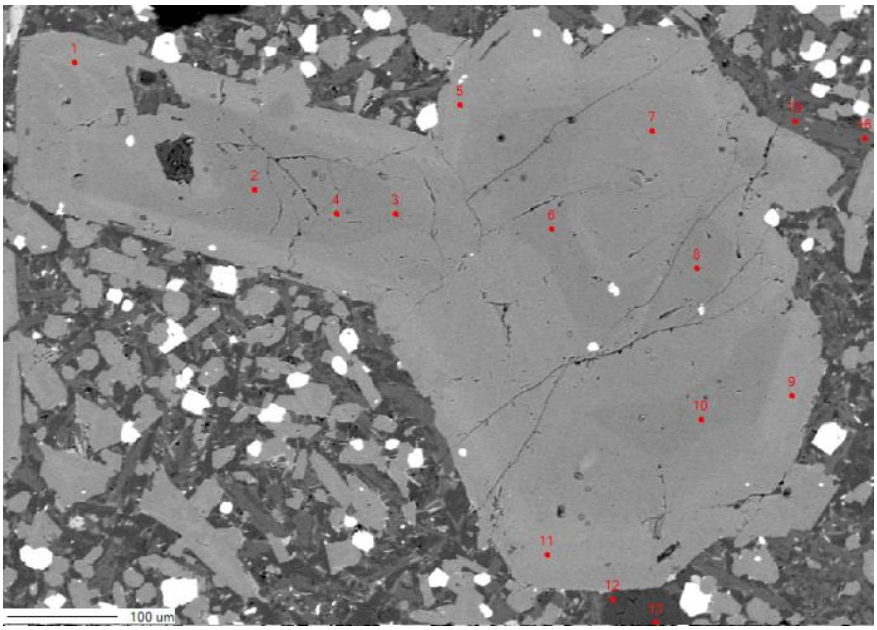

Figure 49 – Backscattered eletron image of a zoned clinopyroxene crystal from field 2 (sample 68227). Points 1 to 11.

Table 11 - Mineral chemistry analysis results for pyroxene from the sample 68227, fields 1 and 2. En = enstatite; Wo = wolastonite; Fs = ferrosilite.

Sample	68227	68227	68227	68227	68227	68227	68227	68227	68227	68227	68227	68227	
Field	1	1	1	1	1	1	2	2	2	2	2	2	
Crystal	1	1	1	2	2	2	1	1	1	1	1	1	
Point	1	2	3	8	9	10	1	2	3	4	5	6	
Position	Rim	Interm.	Rim	Interm.	Rim	Rim	Rim	Core	Core	Core	Rim	Core	
SiO2	45.68	46.37	50.45	50.08	46.56	43.01	42.98	50.80	50.54	50.84	45.05	51.12	Oxides (weight %)
TiO2	2.16	1.67	0.97	1.03	1.72	2.92	3.09	0.94	0.89	0.99	2.08	0.91	
Al2O3	8.59	7.81	4.41	4.59	7.62	10.18	10.33	4.32	3.94	3.98	9.06	3.70	
FeO	7.55	7.77	5.84	5.88	6.71	8.38	8.06	5.85	5.24	5.93	8.06	5.50	
MgO	11.72	12.50	14.67	14.81	12.84	10.91	10.73	15.09	15.06	15.21	11.57	15.40	
MnO	0.02	0.00	0.00	0.00	0.03	0.01	0.00	0.00	0.00	0.00	0.01	0.00	
CaO	22.78	23.09	23.04	23.17	23.11	22.94	22.68	22.81	22.91	22.64	22.73	22.68	
Na2O	0.54	0.44	0.32	0.36	0.42	0.48	0.50	0.37	0.37	0.32	0.43	0.37	
K2O	0.01	0.00	0.00	0.01	0.00	0.01	0.01	0.00	0.00	0.00	0.00	0.00	
Total	**99.05**	**99.66**	**99.70**	**99.92**	**99.00**	**98.85**	**98.37**	**100.16**	**98.94**	**99.91**	**98.99**	**99.68**	
Si	1.73	1.75	1.87	1.85	1.76	1.65	1.65	1.87	1.88	1.88	1.71	1.89	Cations (6 oxigens)
Ti	0.06	0.05	0.03	0.03	0.05	0.08	0.09	0.03	0.02	0.03	0.06	0.03	
Al	0.38	0.35	0.19	0.20	0.34	0.46	0.47	0.19	0.17	0.17	0.41	0.16	
Fe	0.24	0.24	0.18	0.18	0.21	0.27	0.26	0.18	0.16	0.18	0.26	0.17	
Mg	0.66	0.70	0.81	0.82	0.72	0.62	0.61	0.83	0.84	0.84	0.65	0.85	
Mn	0.00	0.00	0.00	0.00	0.00	0.00	0.00	0.00	0.00	0.00	0.00	0.00	
Ca	0.92	0.93	0.91	0.92	0.93	0.94	0.93	0.90	0.91	0.90	0.92	0.90	
Na	0.04	0.03	0.02	0.03	0.03	0.04	0.04	0.03	0.03	0.02	0.03	0.03	
K	0.00	0.00	0.00	0.00	0.00	0.00	0.00	0.00	0.00	0.00	0.00	0.00	
En	0.36	0.37	0.42	0.43	0.39	0.34	0.34	0.43	0.44	0.44	0.36	0.44	End members
Fs	0.13	0.13	0.10	0.10	0.11	0.15	0.14	0.09	0.09	0.10	0.14	0.09	
Wo	0.51	0.50	0.48	0.48	0.50	0.51	0.52	0.47	0.48	0.47	0.50	0.47	

Table 11 (continuation) - Mineral chemistry analysis results for pyroxene from the sample 68227, fields 1 and 2.En = enstatite; Wo = wolastonite; Fs ferrosilite.

Sample	68227	68227	68227	68227	68227	
Field	**2**	**2**	**2**	**2**	**2**	
Crystal	**1**	**1**	**1**	**1**	**1**	
Point	**7**	**8**	**9**	**10**	**11**	
Position	Interm	Core	Rim	Core	Rim	
SiO2	46.68	50.98	45.24	50.53	43.90	Oxides (weight %)
TiO2	1.83	0.99	2.92	1.08	2.55	
Al2O3	7.64	3.89	10.21	4.27	9.91	
FeO	6.67	5.53	8.12	5.74	8.04	
MgO	12.96	15.16	10.78	15.08	11.11	
MnO	0.00	0.01	0.01	0.00	0.00	
CaO	22.87	22.97	22.76	22.80	22.89	
Na2O	0.45	0.35	0.50	0.38	0.52	
K2O	0.01	0.00	0.01	0.01	0.01	
Total	**99.12**	**99.87**	**100.53**	**99.88**	**98.90**	
Si	1.76	1.88	1.69	1.87	1.67	Cations (6 oxigens)
Ti	0.05	0.03	0.08	0.03	0.07	
Al	0.34	0.17	0.45	0.19	0.45	
Fe	0.21	0.17	0.25	0.18	0.26	
Mg	0.73	0.83	0.60	0.83	0.63	
Mn	0.00	0.00	0.00	0.00	0.00	
Ca	0.92	0.91	0.91	0.90	0.93	
Na	0.03	0.03	0.04	0.03	0.04	
K	0.00	0.00	0.00	0.00	0.00	
En	0.39	0.44	0.34	0.43	0.35	End members
Fs	0.11	0.09	0.14	0.09	0.14	
Wo	0.50	0.47	0.52	0.47	0.51	

In both fields there is a compositional zoning in the pyroxene crystals (Figures 48 and 49). In the field 2, this zoning is better determined and thus we will use the crystal 1 (field 2) to describe its chemical main characteristics. The average formula unit for the core and rim of the crystal 1 is shown below:

- C1, core: **$(Ca_{0,90}\ Na_{0,03})\ (Mg_{0,84}\ Fe_{0,16}\ Al_{0,07}\ Ti_{0,04})\ (Si_{1,88}Al_{0,12})\ O_6$** (43,02% enstatite, 9,42% ferrosilite, 47,55% wolastonite)
- C1, rim: **$(Ca_{0,92}\ Na_{0,04})\ (Mg_{0,64}\ Fe_{0,25}\ Al_{0,12}\ Ti_{0,04})\ (Si_{1,70}Al_{0,30})\ O_6$** (34,58% enstatite, 14,19% ferrosilite, 51,24% wolastonite)

As demonstrated on Figure 50, there is an increase in FeO and a decreasing in MgO from the core to the rims (Table 10). The contents of Al_2O_3 and SiO_2 also vary, with an enrichment in Al_2O_3 and a decreasing in SiO_2 from the core toward the rims (Figure 51).

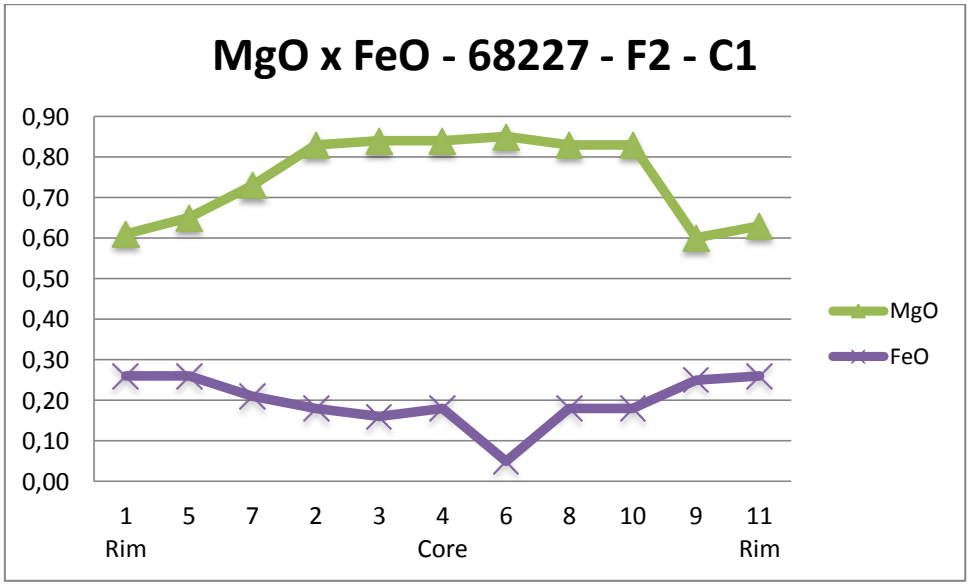

Figure 50 – Binary diagram showing the distribution of FeO and MgO along the crystal 1 (field 2, sample 68227).

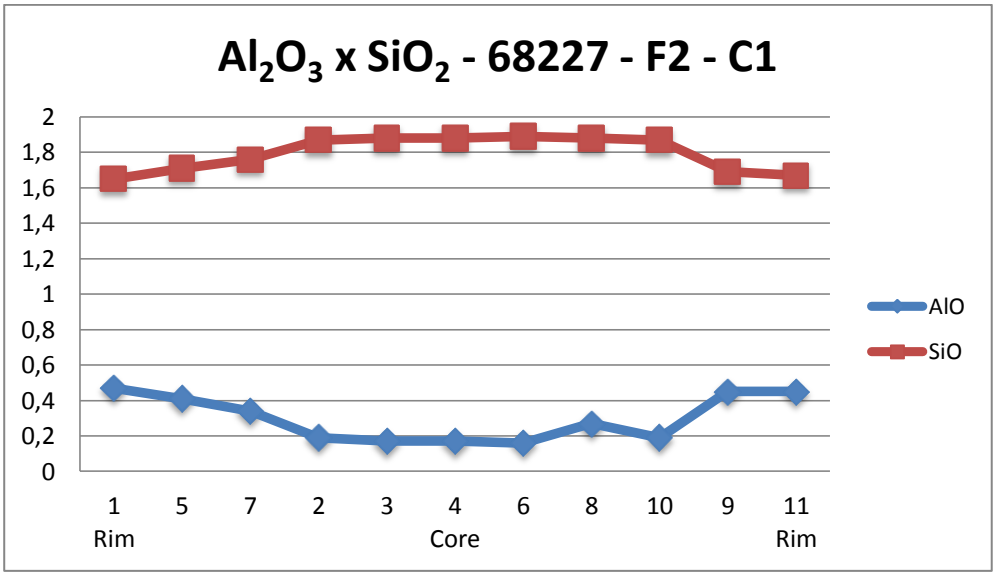

Figure 51– Binary diagram showing the distribution of Al_2O_3 and SiO_2 along the crystal 1 (field 2, sample 68227).

The chemical maps obtained using the microprobe (for Mg, Fe, Al and Si contents) show these zoning from the core toward the rims in the crystal 1, field 2, as presented in Figure 52.

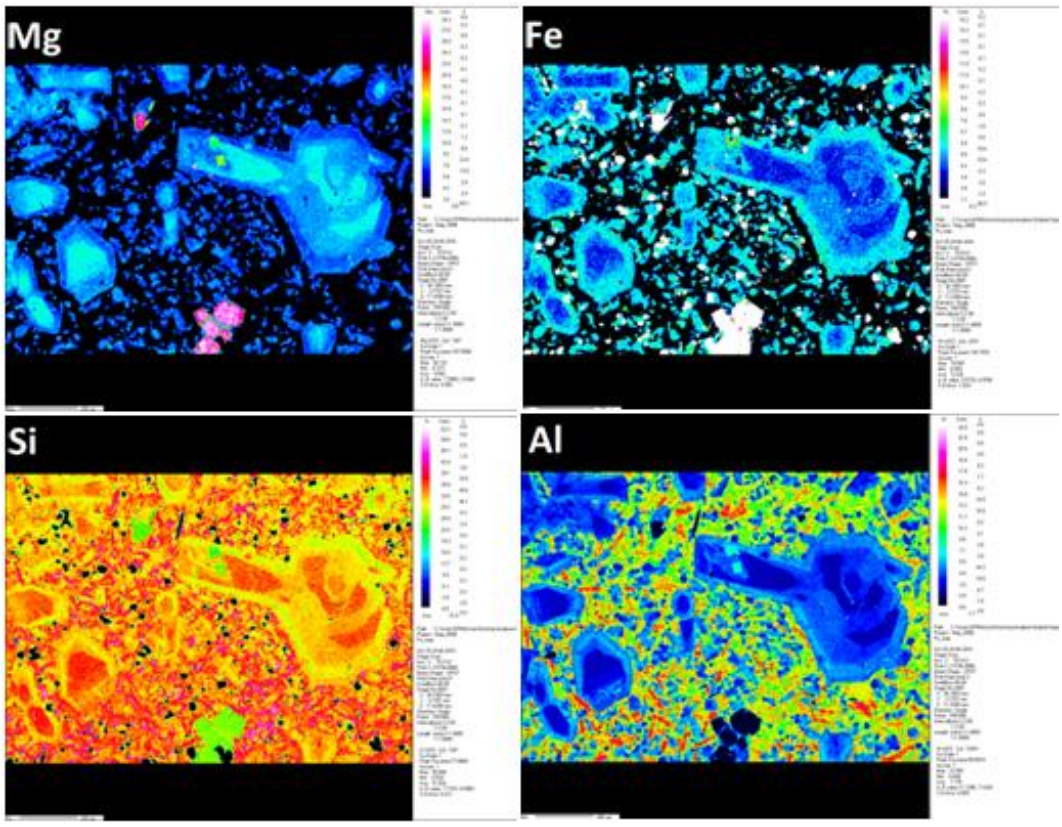

Figure 52 – Chemical maps obtained in the crystal 1, field 2, sample 68227.

Reproducing the chemical data of the crystal 1 (field 2, sample 68227), it is possible to determine not only its composition variation, but the difference in crystallization temperatures of the core and the rim (Figure 53).

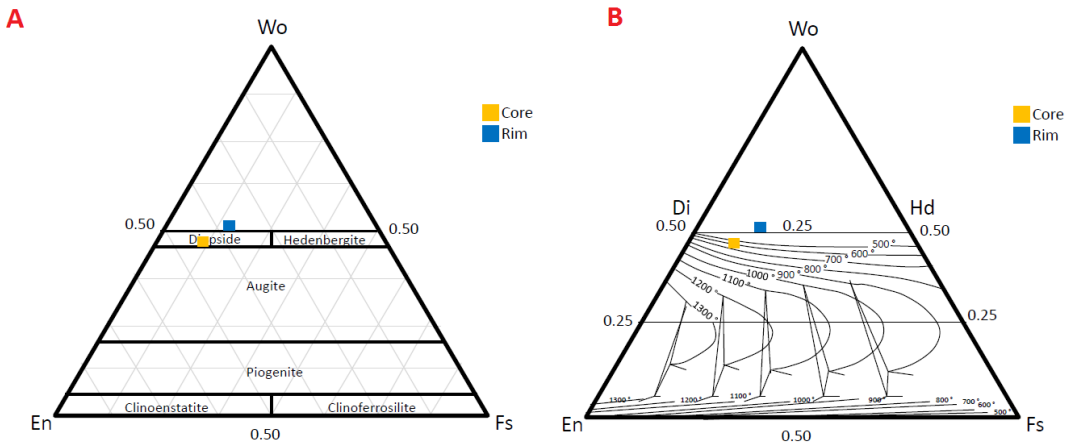

Figure 53 - Diagrams reproducing the chemical data of crystal 1, field 2 A) Composition and nomenclature of pyroxene according to Deer *et al.* (1992), B) Variation in crystallization temperatures for core and rim in a 5 kbar enviroment (Lindsley 1983).

The left diagram (Figure 53A) shows that the pyroxene is Ca-rich, with the core classified as diopside and the rim being more enriched in Ca, close to the wollastonite field. The right diagram (Figure 53B) presents the crystallization temperatures in a 5 kbar pressure enviroment (estimative due to the beggining of crystallization in a hyboabissal field) and shows that the core probably crystallizated around 750° C and the rim below 500 ° C, implying a cooling in magma during the formation of these rocks, which is indicated by the zoning in the Fe and Mg contents.

The analysis in sample 68231 obtained 8 and 7 points in the fields 1 and 3, respectively (Figures 54 and 55). The results are presented in Table 12.

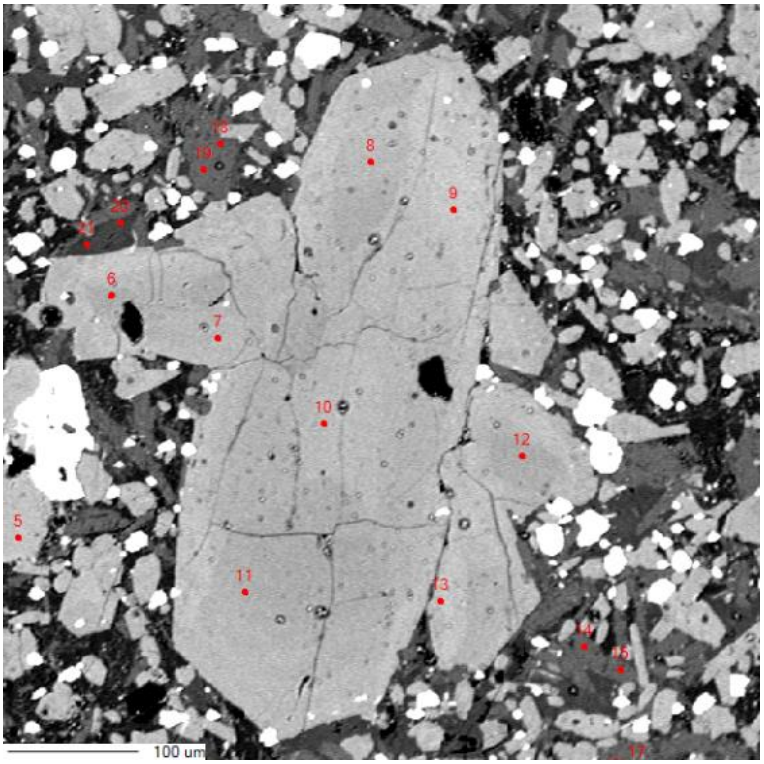

Figure 54– Backscattered eletron image of a clinopyroxene crystal from field 1 (sample 68231). Points 6 to 13.

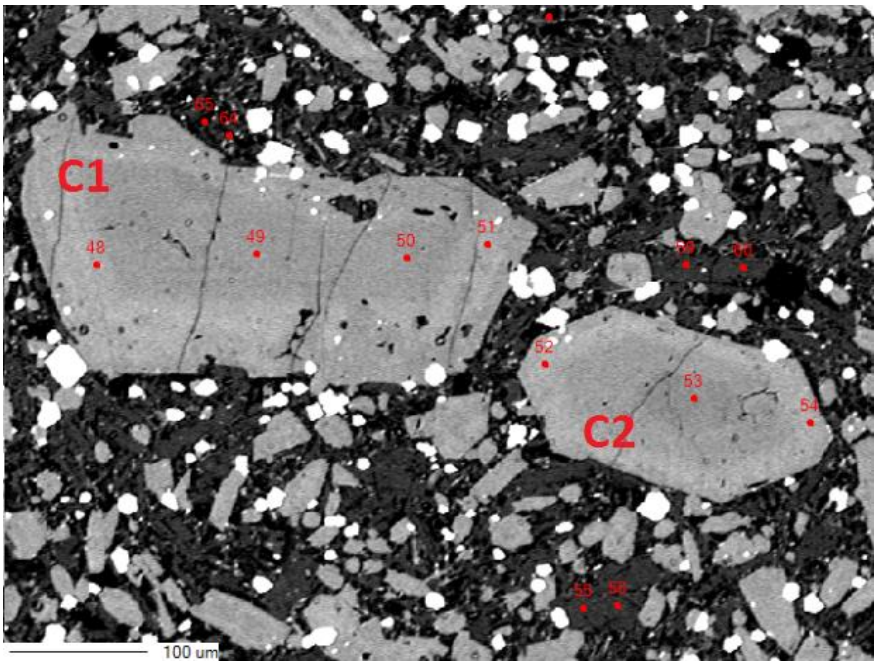

Figure 55 – Backscattered eletron image of two zoned clinopyroxene crystals from field 3 (sample 68231). Points 48 to 51 and 52 to 54, in C1 and C2 respectively.

As shown in the backscattered images (Figures 54 and 55), there is a compositional zoning in the pyroxene crystals from the sample 68231. In the field 3, the crystals present a better zoning that will be use to demonstrate the properties. The average formula unit for the core and rim of the crystals 1 and 2 is shown below:

- C1, core: **$(Ca_{0,92}\ Na_{0,03})\ (Mg_{0,70}\ Fe_{0,22}\ Al_{0,5}\ Ti_{0,06})\ (Si_{1,73}Al_{0,27})\ O_6$** (38,19% enstatite, 11,88% ferrosilite, 49,93% wolastonite)
- C1, rim: **$(Ca_{0,90}\ Na_{0,03})\ (Mg_{0,64}\ Fe_{0,27}\ Al_{0,11}\ Ti_{0,08})\ (Si_{1,67}Al_{0,33})\ O_6$** (34,50% enstatite, 14,50% ferrosilite, 51,00% wolastonite)
- C2, core: **$(Ca_{0,91}\ Na_{0,03})\ (Mg_{0,82}\ Fe_{0,18}\ Al_{0,06}\ Ti_{0,03})\ (Si_{1,88}Al_{0,12})\ O_6$** (43,01% enstatite, 9,35% ferrosilite, 47,64% wolastonite)
- C2, rim: **$(Ca_{0,94}\ Na_{0,04})\ (Mg_{0,64}\ Fe_{0,26}\ Al_{0,12}\ Ti_{0,08})\ (Si_{1,68}Al_{0,32})\ O_6$** (34,50% enstatite, 14,50% ferrosilite, 51% wolastonite)

For both crystals, there is an increase in FeO and a decreasing in MgO from the core to the rims (Figure 56, Table 12). The contents of Al_2O_3 and SiO_2 also vary, with a slight enrichment in Al_2O_3 and also a slight decreasing in SiO_2 from the core toward the rims (Figure 57).

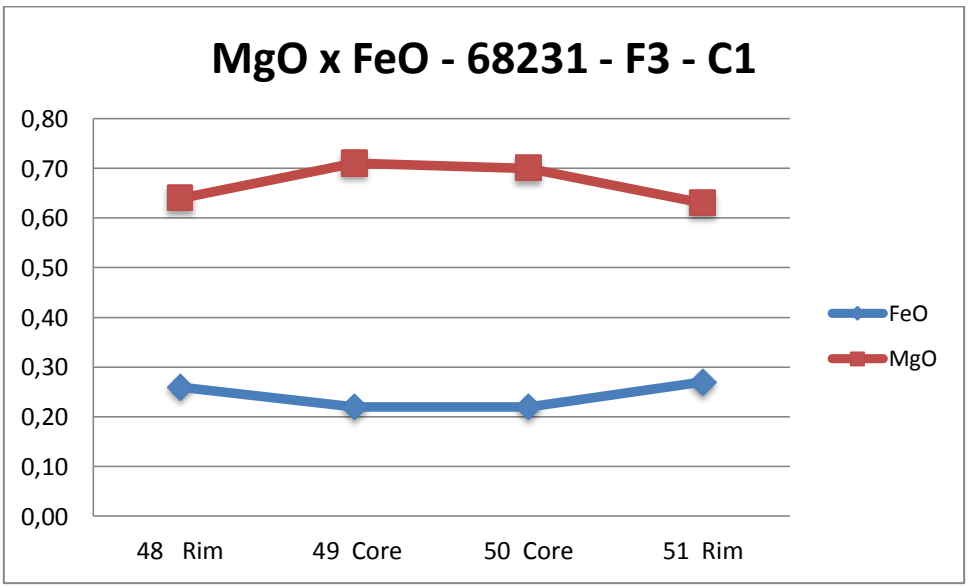

Figure 56 – Binary diagram showing the distribution of FeO and MgO along the crystal 1 (field 3, sample 68231).

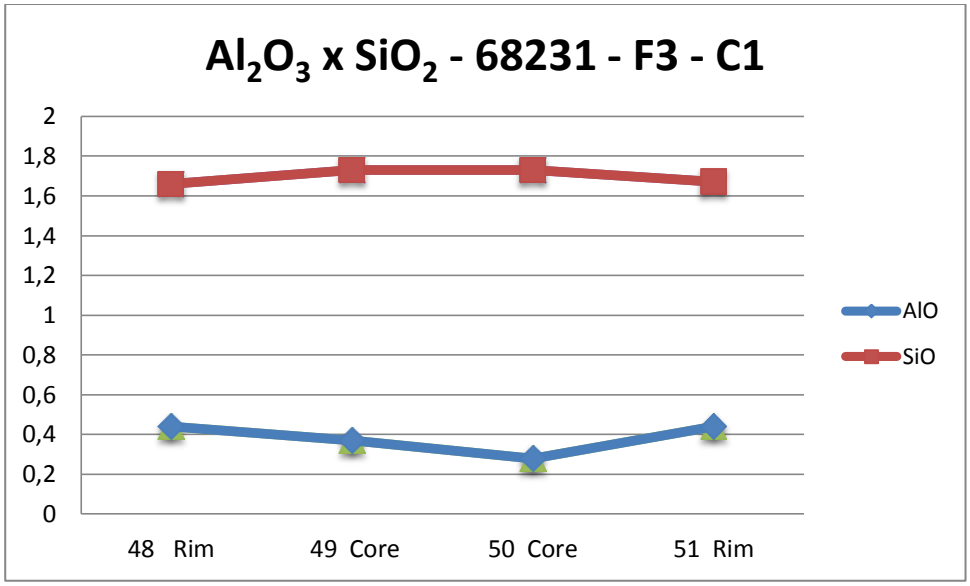

Figure 57 – Binary diagram showing the distribution of Al_2O_3 and SiO_2 along the crystal 1 (field 3, sample 68231).

Table 12- Mineral chemistry analysis results for pyroxene from the sample 68231, fields 1 and 3.En = enstatite; Wo = wolastonite; Fs = ferrosilite.

Sample	68231	68231	68231	68231	68231	68231	68231	68231	
Field	1	1	1	1	1	1	1	1	
Crystal	Px	Px	Px	Px	Px	Px	Px	Px	
Point	6	7	8	9	10	11	12	13	
Position	Rim	Interm.	Core	Interm.	Core	Core	Core	Rim	
SiO2	50.68	46.33	48.75	42.84	45.88	49.60	50.38	41.36	Oxides (weight %)
TiO2	0.91	1.87	1.53	2.79	2.29	1.22	1.08	3.34	
Al2O3	4.19	7.71	5.35	10.13	8.37	4.48	4.22	11.51	
FeO	5.81	6.64	7.18	8.37	6.99	6.33	5.94	8.87	
MgO	15.11	12.87	13.84	11.16	12.34	14.52	14.75	10.09	
MnO	0.01	0.03	0.00	0.01	0.03	0.00	0.00	0.00	
CaO	22.72	22.62	22.90	22.92	22.63	22.76	22.89	22.54	
Na2O	0.36	0.49	0.37	0.44	0.53	0.29	0.37	0.52	
K2O	0.01	0.00	0.01	0.00	0.00	0.00	0.01	0.01	
Total	**99.80**	**98.55**	**99.94**	**98.65**	**99.05**	**99.20**	**99.63**	**98.22**	
Si	1.87	1.75	1.82	1.64	1.73	1.85	1.87	1.60	Cations (6 oxigens)
Ti	0.03	0.05	0.04	0.08	0.06	0.03	0.03	0.10	
Al	0.18	0.34	0.24	0.46	0.37	0.20	0.18	0.52	
Fe	0.18	0.21	0.22	0.27	0.22	0.20	0.18	0.29	
Mg	0.83	0.73	0.77	0.64	0.69	0.81	0.82	0.58	
Mn	0.00	0.00	0.00	0.00	0.00	0.00	0.00	0.00	
Ca	0.90	0.92	0.92	0.94	0.91	0.91	0.91	0.93	
Na	0.03	0.04	0.03	0.03	0.04	0.02	0.03	0.04	
K	0.00	0.00	0.00	0.00	0.00	0.00	0.00	0.00	
En	0.44	0.39	0.40	0.35	0.38	0.42	0.43	0.32	End members
Fs	0.09	0.11	0.12	0.15	0.12	0.10	0.10	0.16	
Wo	0.47	0.49	0.48	0.51	0.50	0.48	0.48	0.52	

Table 12 (continuation) - Mineral chemistry analysis results for pyroxene from the sample 68231, fields 1 and 3.En = enstatite; Wo = wolastonite; Fs = ferrosilite.

Sample	68231	68231	68231	68231	68231	68231	68231	
Field	3	3	3	3	3	3	3	
Crystal	Px	Px	Px	Px	Px	Px	Px	
Point	48	49	50	51	52	53	54	
Position	Rim	Core	Interm.	Rim	Rim	Core	Rim	
SiO2	43.53	45.82	45.66	43.61	44.11	50.84	43.81	Oxides (weight %)
TiO2	2.79	2.07	2.01	2.75	2.72	1.02	2.72	
Al2O3	9.70	8.32	8.44	9.78	9.40	4.08	10.00	
FeO	8.02	6.88	6.97	8.39	8.07	5.78	8.30	
MgO	11.22	12.53	12.48	11.07	11.31	14.92	11.05	
MnO	0.04	0.00	0.00	0.02	0.00	0.03	0.00	
CaO	23.05	22.85	22.65	22.85	22.96	22.99	22.82	
Na2O	0.45	0.48	0.45	0.47	0.50	0.39	0.53	
K2O	0.00	0.00	0.01	0.01	0.02	0.00	0.02	
Total	**98.78**	**98.96**	**98.67**	**98.94**	**99.09**	**100.04**	**99.26**	
Si	1.66	1.73	1.73	1.67	1.68	1.88	1.67	Cations (6 oxigens)
Ti	0.08	0.06	0.06	0.08	0.08	0.03	0.08	
Al	0.44	0.37	0.38	0.44	0.42	0.18	0.45	
Fe	0.26	0.22	0.22	0.27	0.26	0.18	0.26	
Mg	0.64	0.71	0.70	0.63	0.64	0.82	0.63	
Mn	0.00	0.00	0.00	0.00	0.00	0.00	0.00	
Ca	0.94	0.92	0.92	0.93	0.94	0.91	0.93	
Na	0.03	0.04	0.03	0.03	0.04	0.03	0.04	
K	0.00	0.00	0.00	0.00	0.00	0.00	0.00	
En	0.35	0.38	0.38	0.34	0.35	0.43	0.34	End members
Fs	0.14	0.12	0.12	0.15	0.14	0.09	0.15	
Wo	0.51	0.50	0.50	0.51	0.51	0.48	0.51	

5.1.1.3 Plagioclase

Plagioclase was analyzed in five different fields: two in the sample 68227 (F1_02 and F2) and three in the sample 68231 (F1, F2 and F3).

The analysis in the sample 68227 obtained 9 and 7 points in F1_02 and F2, respectively (Figures 58 and 59). The results are presented in Table 13.

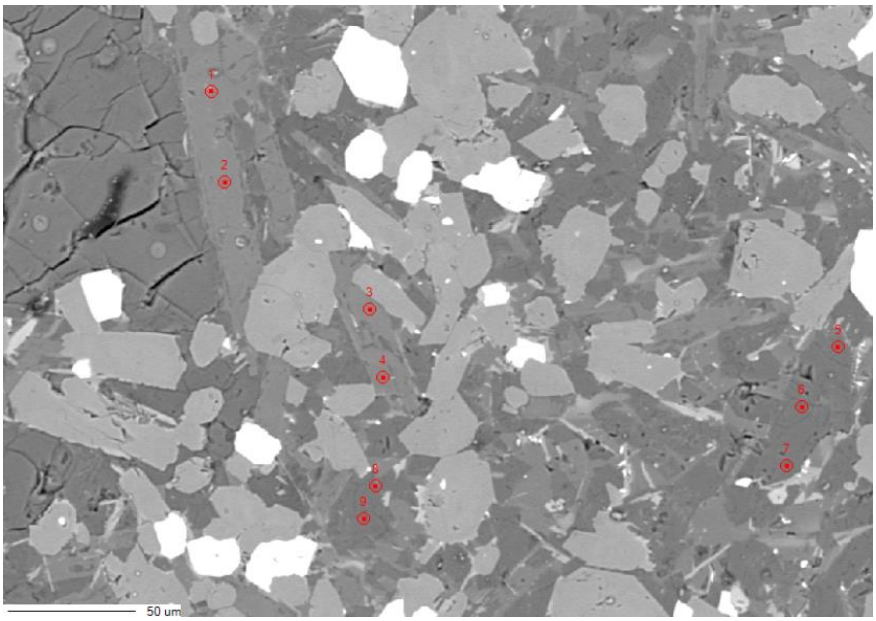

Figure 58 – Backscattered eletron image of four plagioclase crystals from field 1_02 (sample 68227). Points 1 to 2; 3 to 4; 5 to 7 and 8 to 9, in C1, C2, C3 and C4 respectively.

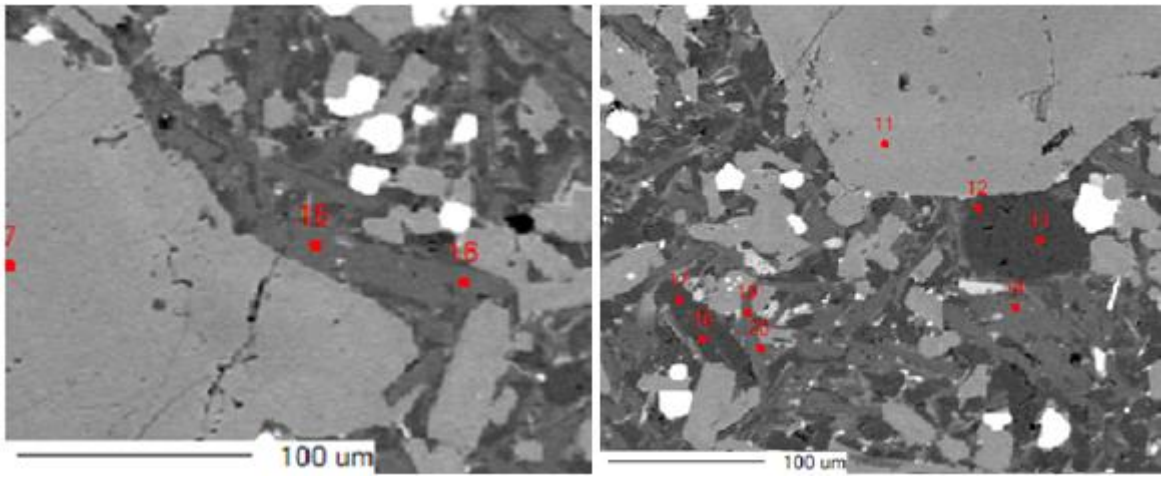

Figure 59– Backscattered eletron image of five plagioclase crystals from field 2 (sample 68227). Points 12 and 13; 14; 15 and 16; 17 and 18 and 19 to 20, in C1, C2, C3, C4 and C5 respectively.

Table 13 - Mineral chemistry analysis results for feldspar from the sample 68227, fields 1_02 and 2. Ano = anortite; Ab = albite; Or = oligoclase. In black color: Ca-feldspar; in blue color: Na-feldpar.

Sample	68227	68227	68227	68227	68227	68227	68227	68227	68227	68227	
Field	1_02	1_02	1_02	1_02	1_02	1_02	1_02	1_02	1_02	2	
Crystal	1	1	2	2	3	3	3	4	4	1	
Point	1	2	3	4	5	6	7	8	9	14	
Position	Core	Core	Core	Rim	Rim	Core	Rim	Rim	Core	Core	
SiO2	46.67	51.33	49.778	53	51.372	52.225	51.258	51.96	50.015	48.482	Oxides (weight %)
Al2O3	28.32	31.01	31.223	29.383	29.37	29.639	30.281	27.892	27.647	32.749	
FeO	3.15	0.47	0.612	0.445	0.631	0.603	0.556	0.637	0.569	0.472	
CaO	12.40	13.20	14.476	11.456	0.209	0.521	0.294	0.943	2.961	15.863	
Na2O	3.79	3.37	2.885	4.264	15.575	14.76	15.625	12.352	13.343	2.184	
K2O	2.01	0.26	0.174	0.419	2.559	2.315	2.733	5.128	4.94	0.16	
BaO	0.00	0.04	0.015	0.104	0	0	0	0	0.14	0.048	
total	**96.33**	**99.68**	**100.52**	**100.32**	**100.59**	**99.33**	**100.34**	**100.34**	**100.34**	**100.34**	
Si	2.27	2.34	2.29	2.43	2.39	2.41	2.36	2.44	2.37	2.22	Cations (8 oxigens)
Al	1.63	1.67	1.70	1.58	1.61	1.61	1.64	1.55	1.55	1.77	
Fe	0.13	0.02	0.02	0.02	0.02	0.02	0.02	0.03	0.02	0.02	
Ca	0.65	0.64	0.71	0.56	0.01	0.03	0.01	0.05	0.15	0.78	
Na	0.36	0.30	0.26	0.38	1.40	1.32	1.40	1.13	1.23	0.19	
K	0.13	0.02	0.01	0.02	0.15	0.14	0.16	0.31	0.30	0.01	
Ba	0.00	0.00	0.00	0.00	0.00	0.00	0.00	0.00	0.00	0.00	
Ano	57.25	67.31	72.73	58.24	0.66	1.74	0.92	3.21	8.98	79.29	End members
Ab	31.69	31.12	26.23	39.23	89.64	89.07	88.85	76.03	73.19	19.75	
Or	11.07	1.57	1.04	2.54	9.69	9.19	10.23	20.77	17.83	0.95	

Table 13 (continuation) - Mineral chemistry analysis results for feldspar from the sample 68227, fields 1_02 and 2. Ano = anortite; Ab = albite; Or = oligoclase. In black color: Ca-feldspar; in blue color: Na-feldpar.

Sample	68227	68227	68227	68227	68227	68227	
Field	2	2	2	2	2	2	
Crystal	2	2	3	3	4	4	
Point	15	16	17	18	19	20	
Position	Rim	Rim	Rim	Core	Interm.	Interm.	
SiO2	52.649	50.763	51.86	52.423	49.689	56.413	Oxides (weight %)
Al2O3	29.828	30.959	28.747	29.265	30.502	24.12	
FeO	0.587	0.533	0.592	0.575	0.521	0.392	
CaO	12.62	13.745	0.81	0.228	13.474	5.698	
Na2O	3.873	3.121	14.253	15.387	2.818	3.073	
K2O	0.335	0.258	2.57	2.284	0.879	7.21	
BaO	0.023	0.02	0	0	0.078	0.187	
total	**100.34**	**100.34**	**100.34**	**100.34**	**100.34**	**100.34**	
Si	2.39	2.33	2.42	2.41	2.32	2.66	Cations (8 oxigens)
Al	1.60	1.67	1.58	1.59	1.68	1.34	
Fe	0.02	0.02	0.02	0.02	0.02	0.02	
Ca	0.61	0.67	0.04	0.01	0.67	0.29	
Na	0.34	0.28	1.29	1.37	0.25	0.28	
K	0.02	0.02	0.15	0.13	0.05	0.43	
Ba	0.00	0.00	0.00	0.00	0.00	0.00	
Ano	63.01	69.77	2.73	0.74	68.68	28.71	End members
Ab	34.99	28.67	86.95	90.43	25.99	28.02	
Or	1.99	1.56	10.32	8.83	5.33	43.26	

As observed in Table 13, all the feldspar crystals are zoned and in general show NaO contents increasing toward the rims (it´s a igneous normal zoning). The average formula unit for Ca-feldspar (***crystal 2 in field 1_02 with core and rim***) and for Na-feldspar (***crystal 3 in field 1_02 with core and rim***) are demonstrated below:

- C2, F1_02, core: **$(Na_{0,26}Ca_{0,71}K_{0,01})$ $(Si_{0,29}Al_{0,70})AlSi_2O_8$** (72,4% anortite, 26,2% albite, 1,0% ortoclase)
- C2, F1_02, rim: **$(Na_{0,38}Ca_{0,56}K_{0,02})$ $(Si_{0,43}Al_{0,58})AlSi_2O_8$** (58,2% anortite, 39,2% albite, 2,5% ortoclase)
- C3, F1_02, core: **$(Na_{1,32}Ca_{0,03}K_{0,16})$ $(Si_{0,41}Al_{0,61})AlSi_2O_8$** (0,79% anortite, 89,25% albite, 9,96% ortoclase)
- C3, F1_02, rim: **$(Na_{1,40}Ca_{0,01}K_{0,15})$ $(Si_{0,38}Al_{0,63})AlSi_2O_8$** (1,74% anortite, 89,07% albite, 9,19% ortoclase)

The analysis in sample 68231 obtained 10, 10 and 9 points in the fields 1, 2 and 3, respectively (Figures 60, 61 and 62). The results are presented in Table 14.

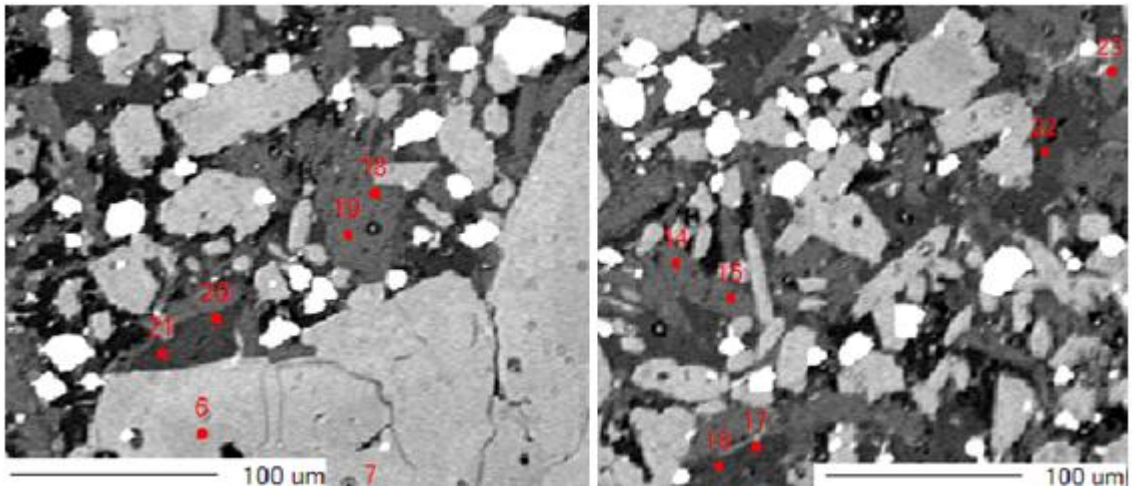

Figure 60– Backscattered eletron image of plagioclase crystals from field 1 (sample 68231). Points 12; 14 to 15; 16 to 17; 18 to 19 and 20 to 21; 22 and 23 in C1, C2, C3, C4, C5, C6 and C7 respectively.

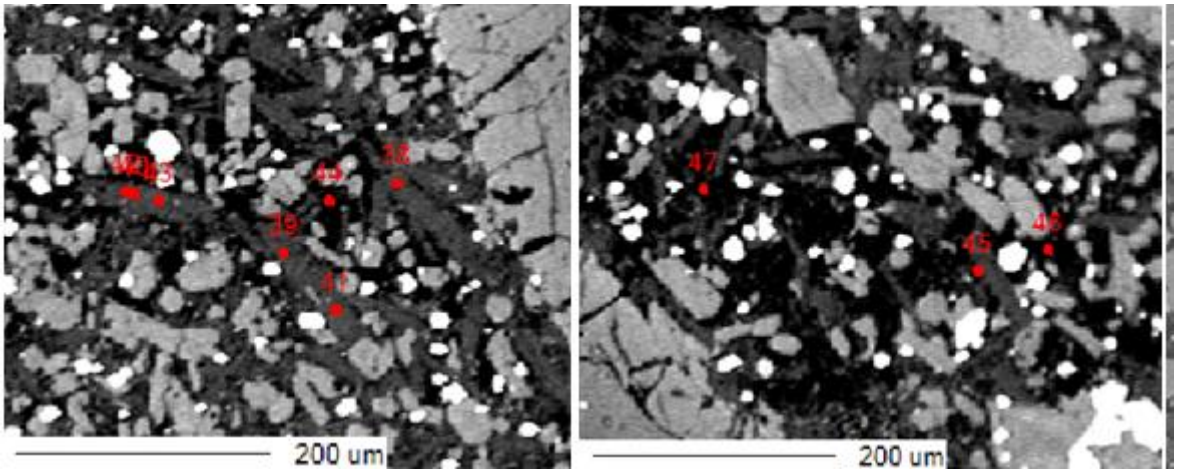

Figure 61 – Backscattered eletron image of plagioclase crystals from field 2 (sample 68231). Points 38 to 43; 45; 46 and 47 in C1, C2, C3 and C4 respectively.

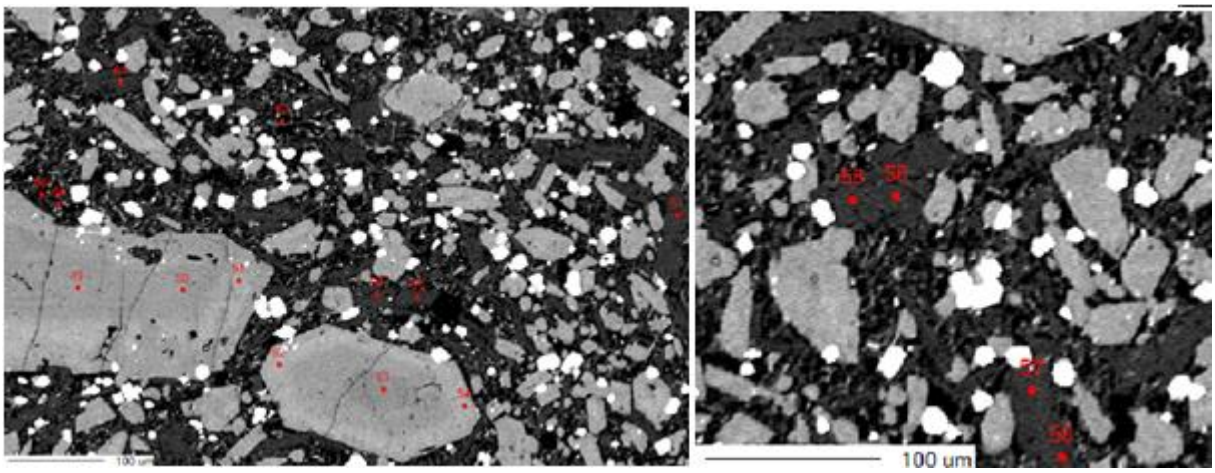

Figure 62– Backscattered eletron image of plagioclase crystals from field 3 (sample 68231). Points 55 to 56; 57 to 58; 59 to 60 and 61 to 63 in C1, C2, C3 and C4 respectively.

Table 14 - Mineral chemistry analysis results for feldspar from the sample 68231, fields 1, 2 and 3. Ano = anortite; Ab = albite; Or = oligoclase. In black color: Ca-feldspar; in blue color: Na-feldpar.

Sample	68231	68231	68231	68231	68231	68231	68231	68231	68231	68231
Field	1	1	1	1	1	1	1	1	1	1
Crystal	1	1	2	2	3	3	4	4	5	6
Point	14	15	16	17	18	19	20	21	22	23
Position	Core	Interm	Interm	Interm	Rim	Core	Rim	Core	Rim	Core
SiO2	53.33	53.64	44.39	49.43	54.22	53.25	46.33	46.70	44.69	51.98
Al2O3	28.51	28.84	32.99	30.16	28.09	29.46	31.83	31.80	33.12	29.22
FeO	0.71	0.71	0.76	0.54	0.58	0.60	0.68	0.79	0.70	0.78
CaO	10.95	11.55	1.24	0.69	10.55	11.73	0.68	0.81	1.03	12.08
Na2O	4.40	4.49	15.02	15.29	4.83	4.28	15.92	15.34	15.93	3.82
K2O	0.65	0.33	4.82	3.03	0.50	0.29	3.94	3.77	4.49	0.63
BaO	0.09	0.07	0.02	0.00	0.17	0.02	0.00	0.00	0.00	0.07
Total	98.63	100.54	100.52	100.32	100.59	99.33	100.34	100.34	100.34	100.34
Si	2.45	2.44	2.13	2.32	2.48	2.42	2.20	2.22	2.13	2.40
Al	1.54	1.55	1.87	1.67	1.51	1.58	1.78	1.78	1.86	1.59
Fe	0.03	0.03	0.03	0.02	0.02	0.02	0.03	0.03	0.03	0.03
Ca	0.54	0.56	0.06	0.03	0.52	0.57	0.03	0.04	0.05	0.60
Na	0.39	0.40	1.40	1.39	0.43	0.38	1.47	1.41	1.47	0.34
K	0.04	0.02	0.30	0.18	0.03	0.02	0.24	0.23	0.27	0.04
Ba	0.00	0.00	0.00	0.00	0.00	0.00	0.00	0.00	0.00	0.00
Ano	55.65	57.53	3.62	2.15	53.08	59.18	1.99	2.44	2.91	61.20
Ab	40.44	40.50	79.57	86.57	43.92	39.06	84.29	83.99	81.91	35.01
Or	3.91	1.97	16.80	11.28	2.99	1.77	13.73	13.57	15.18	3.79

Oxides (weight %)

Cations (8 oxigens)

End members

Table 14 (continuation) - Mineral chemistry analysis for feldspar from the sample 68231, fields 1, 2 and 3.Ano = anortite; Ab = albite; Or = oligoclase. In black color: Ca-feldspar; in blue color: Na-feldpar.

Sample	68231	68231	68231	68231	68231	
Field	2	2	2	2	2	
Crystal	1	2	2	3	3	
Point	38	39	41	42	43	
Position	Core	Core	Rim	Core	Core	
SiO2	52.59	51.97	52.97	52.83	52.76	Oxides (weight %)
Al2O3	29.40	28.61	29.29	28.98	28.59	
FeO	0.57	0.51	0.60	0.56	0.59	
CaO	11.98	11.43	11.74	11.82	11.08	
Na2O	4.01	3.74	4.31	4.13	4.22	
K2O	0.32	0.87	0.39	0.39	0.66	
BaO	0.10	0.05	0.07	0.08	0.06	
Total	100.34	100.34	100.34	100.34	100.34	
Si	2.41	2.43	2.42	2.42	2.44	Cations (8 oxigens)
Al	1.59	1.57	1.58	1.57	1.56	
Fe	0.02	0.02	0.02	0.02	0.02	
Ca	0.59	0.57	0.57	0.58	0.55	
Na	0.36	0.34	0.38	0.37	0.38	
K	0.02	0.05	0.02	0.02	0.04	
Ba	0.00	0.00	0.00	0.00	0.00	
Ano	61.07	59.43	58.71	59.82	56.80	End members
Ab	36.99	35.21	38.99	37.82	39.16	
Or	1.95	5.36	2.30	2.36	4.04	

Table 14 (continuation) -Mineral chemistry analysis results for feldspar from the sample 68231, fields 1, 2 and 3.Ano = anortite; Ab = albite; Or = oligoclase. In black color: Ca-feldspar; in blue color: Na-feldpar.

Sample	68231	68231	68231	68231	68231	68231	68231	68231	68231	
Field	3	3	3	3	3	3	3	3	3	
Crystal	1	1	2	2	3	3	4	5	6	
Point	55	56	57	58	59	60	61	62	63	
Position	Interm	Core	Rim	Interm	Core	Core	-	-	Core	
SiO2	52.88	52.76	52.59	52.61	52.03	52.11	53.26	51.65	53.03	Oxides (weight %)
Al2O3	29.12	29.08	29.07	29.37	29.71	29.33	29.09	28.14	29.06	
FeO	0.53	0.56	0.87	0.68	0.53	0.64	0.69	1.06	0.62	
CaO	11.67	11.73	11.40	11.87	12.34	12.20	11.43	0.73	11.87	
Na2O	4.20	4.18	4.50	4.17	3.88	4.10	4.22	13.96	4.19	
K2O	0.46	0.40	0.63	0.47	0.35	0.39	0.42	2.63	0.40	
BaO	0.08	0.08	0.04	0.06	0.07	0.05	0.06	0.00	0.10	
Total	**100.34**	**100.34**	**100.34**	**100.34**	**100.34**	**100.34**	**100.34**	**100.34**	**100.34**	
Si	2.42	2.42	2.41	2.41	2.39	2.40	2.43	2.43	2.42	Cations (8 oxigens)
Al	1.57	1.57	1.57	1.58	1.61	1.59	1.57	1.56	1.57	
Fe	0.02	0.02	0.03	0.03	0.02	0.02	0.03	0.04	0.02	
Ca	0.57	0.58	0.56	0.58	0.61	0.60	0.56	0.04	0.58	
Na	0.37	0.37	0.40	0.37	0.35	0.37	0.37	1.27	0.37	
K	0.03	0.02	0.04	0.03	0.02	0.02	0.02	0.16	0.02	
Ba	0.00	0.00	0.00	0.00	0.00	0.00	0.00	0.00	0.00	
Ano	58.93	59.31	56.18	59.46	62.39	60.76	58.41	2.49	59.55	End members
Ab	38.33	38.29	40.11	37.77	35.51	36.94	39.03	86.76	38.05	
Or	2.74	2.41	3.71	2.77	2.10	2.30	2.56	10.75	2.40	

Both Ca and Na-plagioclase are quite homogeneous, but NaO contents slight increase toward the rims (igneous normal zoning) (Table 14). The Ca-rich feldspar presents an average formula unit as **$(Na_{0,37}\ Ca_{0,57}\ K_{0,03})\ (Si_{0,42}\ Al_{0,57})AlSi_2O_8$** and the Na-feldpar as**$(Na_{1,40}\ Ca_{0,04}\ K_{0,21})\ (Si_{0,24}\ Al_{0,75})AlSi_2O_8$**. The Ca-rich feldspar is composed of 56-62% anortite, 35-43% albite and 2-4% orthoclase molecules, being classified as labradorite (Deer *et al.* 1992). The Na-rich feldspar is albite with K-feldspar exsolution (1-3% anortite, 79-86% albite, 10-16% orthoclase).

5.1.2 Basalt boulders

The thin sections 68230 and 69128 were divided into different fieldsin order to realize the microprobe campaing, as presented in Figure 63.

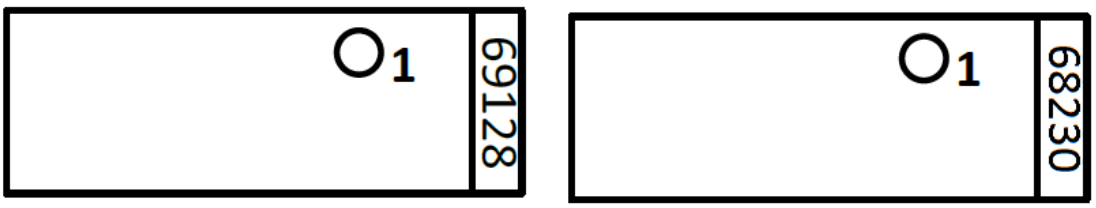

Figure 63 – Analyzed fields in the thin sections.

In the thin section 68230 and 69128 were analyzed 3 kinds of minerals in two fields, as presented in Table 15.

Table 15– Relation of the fields, mineral and analyzed points(Cpx=Clinopyroxene; Ol=olivine:Pl=plagioclase).

68230	Mineral	Points
1	Ol	2 - 4
	Ol	6 - 14
	Pl	15 - 23
	Cpx	24 - 29

69128	Mineral	Points
1	Ol	1 - 3
	Ol	4 - 5
	Ol	6 - 7
	Ol	9 - 10
	Ol	11 - 13
	Cpx	17 - 20
	Cpx	21 - 23
	Pl	24 - 26
	Pl	27 - 29
	Pl	31 - 32
	Pl	34 - 37

5.1.2.1 Olivine

Olivine was analyzed in two different fields: one in the sample 68230 and another one in the sample 69128.

The analysis in sample 68230 obtained 12 points in field 1 (Figure 64). The results are presented in Table 16.

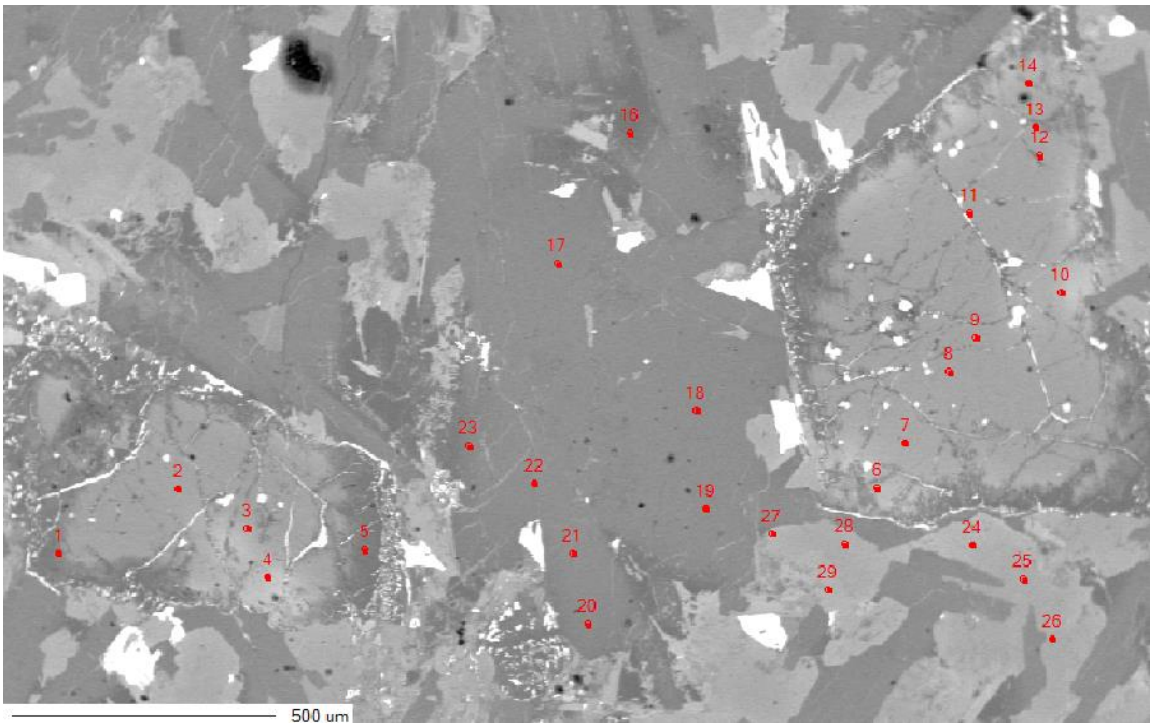

Figure 64 – Backscattered eletron image of olivine crystals from field 1 (sample 68230). Points 2 to 4 and 6 to 14 in C1 and C2, respectively.

Table 16– Mineral chemistry analysis results for olivine from the sample 68230, field 1. Fa = fayalite; Fo = fosterite.

Sample	68230	68230	68230	68230	68230	68230	68230	68230	68230	68230	68230	68230	
Field	1	1	1	1	1	1	1	1	1	1	1	1	
Crystal	1	1	1	2	2	2	2	2	2	2	2	2	
Point	2	3	4	6	7	8	9	10	11	12	13	14	
Position	Core	Core	Core	Rim	Interm.	Core	Core	Core	Rim	Interm	Rim	Rim	
SiO2	39.279	38.574	37	38.214	39.354	39.385	39.795	37.242	39.348	39.821	40.75	39.188	Oxides (weight %)
TiO2	0.02	0.04	0.03	0.00	0.01	0.01	0.00	0.05	0.02	0.00	0.00	0.03	
Al2O3	0.044	0.03	0.055	0	0.038	0	0.015	0.009	0.068	0.009	0.033	0.018	
FeO	18.871	24.378	30.157	27.786	20.818	18.446	18.462	30.487	18.594	19.477	16.881	23.199	
MgO	43.01	38.81	33.38	35.43	41.50	42.85	43.45	33.07	42.89	42.63	40.91	39.64	
MnO	0.01	0.02	0.02	0.00	0.00	0.01	0.01	0.00	0.00	0.00	0.03	0.00	
CaO	0.26	0.217	0.258	0.228	0.239	0.262	0.276	0.2	0.197	0.202	0.235	0.225	
Na2O	0	0	0.011	0	0	0	0.002	0	0.005	0.002	0	0	
Cr2O3	0.05	0.00	0.00	0.01	0.03	0.06	0.05	0.02	0.02	0.04	0.05	0.02	
NiO	0.20	0.16	0.13	0.19	0.19	0.20	0.24	0.11	0.15	0.20	0.19	0.20	
K2O	0.1	0.008	0.044	0	0.001	0.013	0.003	0.003	0.004	0	0.005	0.003	
Total	**101.84**	**102.23**	**101.35**	**101.86**	**102.17**	**101.23**	**102.30**	**101.18**	**101.29**	**102.38**	**99.08**	**102.52**	
Si	0.99	0.99	0.99	1.00	0.99	0.99	0.99	1.00	0.99	1.00	1.04	1.00	Cations (4 oxigens)
Ti	0.00	0.00	0.00	0.00	0.00	0.00	0.00	0.00	0.00	0.00	0.00	0.00	
Al	0.00	0.00	0.00	0.00	0.00	0.00	0.00	0.00	0.00	0.00	0.00	0.00	
Fe	0.40	0.52	0.67	0.61	0.44	0.39	0.39	0.68	0.39	0.41	0.36	0.49	
Mg	1.61	1.48	1.33	1.38	1.56	1.61	1.61	1.32	1.61	1.59	1.55	1.50	
Mn	0.00	0.00	0.00	0.00	0.00	0.00	0.00	0.00	0.00	0.00	0.00	0.00	
Ca	0.01	0.01	0.01	0.01	0.01	0.01	0.01	0.01	0.01	0.01	0.01	0.01	
Na	0.00	0.00	0.00	0.00	0.00	0.00	0.00	0.00	0.00	0.00	0.00	0.00	
Cr	0.00	0.00	0.00	0.00	0.00	0.00	0.00	0.00	0.00	0.00	0.00	0.00	
Ni	0.00	0.00	0.00	0.00	0.00	0.00	0.00	0.00	0.00	0.00	0.00	0.00	
K	0.00	0.00	0.00	0.00	0.00	0.00	0.00	0.00	0.00	0.00	0.00	0.00	
Fo	0.80	0.74	0.66	0.69	0.78	0.81	0.81	0.66	0.80	0.80	0.81	0.75	End members
Fa	0.20	0.26	0.34	0.31	0.22	0.19	0.19	0.34	0.20	0.20	0.19	0.25	

The olivine here is not compositionally homogeneous, presenting an enrichment in FeO and decreasing in MgO from the core to the rim (Table 16). The average formula unit was made for the core and rim from both crystals, as demonstrated below:

- C1, core: **$(Mg_{1,61}\,Fe_{0,40}\,Ca_{0,01})SiO_4$** (80,23% of the forsterite endmember)
- C1, rim: : **$(Mg_{1,40}\,Fe_{0,60}\,Ca_{0,01})SiO_4$** (70,13% of the forsterite endmember)
- C2, core: : **$(Mg_{1,54}\,Fe_{0,46}\,Ca_{0,01})SiO_4$** (76,90% of the forsterite endmember)
- C2, rim: **$(Mg_{1,48}\,Fe_{0,49}\,Ca_{0,01})SiO_4$** (75,29% of the forsterite endmember)

The analysis in sample 69128 obtained 13 points in field 1 (Figure 65). The results are presented in Table 17.

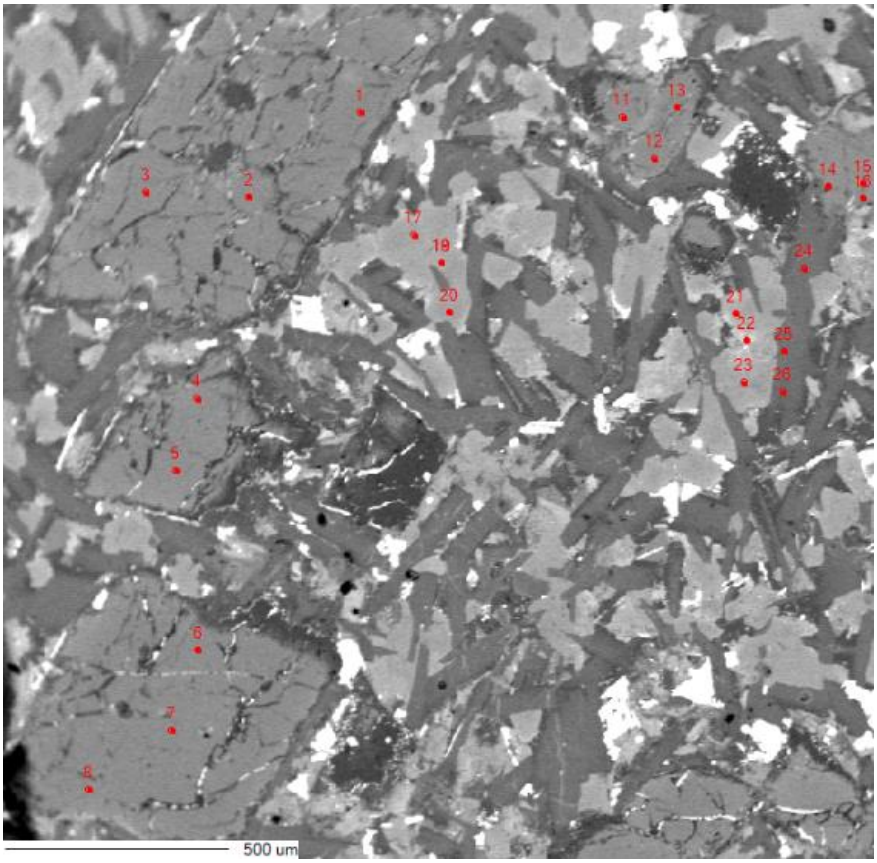

Figure 65 – Backscattered eletron image of olivine crystals from field 1 (sample 69128). Points 1 to 3;4 to 5; 6 to 8; 9 to 13.

Table 17 – Mineral chemistry analysis results for olivine from the sample 69128, field 1. Fa = fayalite; Fo = fosterite.

Sample	69128	69128	69128	69128	69128	69128	69128	69128	69128
Field	1	1	1	1	1	1	1	1	1
Crystal	1	1	1	2	2	3	3	4	5
Point	1	2	3	4	5	6	7	9	13
Position	Rim	Core	Interm.	Rim	Core	Rim	Core	Core	Interm.
SiO2	39.75	56.411	39.958	40	40.228	40.074	40.194	39.912	39.748
TiO2	0.00	0.03	0.02	0.00	0.02	0.01	0.02	0.04	0.00
Al2O3	0.11	1.537	0.039	0.044	0.069	0.01	0.019	0.088	0.074
FeO	15.99	7.194	15.402	17.033	14.939	15.584	15.566	15.533	16.702
MgO	44.18	31.06	45.45	44.62	44.98	45.41	45.43	45.20	44.58
MnO	0.00	0.05	0.01	0.00	0.00	0.01	0.00	0.00	0.00
CaO	0.25	0.076	0.267	0.273	0.263	0.322	0.244	0.287	0.288
Na2O	0.06	0.563	0.021	0	0.038	0.012	0.022	0	0.019
Cr2O3	0.03	0.03	0.05	0.03	0.05	0.03	0.06	0.06	0.03
NiO	0.35	0.15	0.33	0.30	0.36	0.34	0.26	0.29	0.35
K2O	0.00	0.048	0.06	0.01	0.012	0.018	0.009	0.015	0.012
Total	**100.71**	**97.14**	**101.61**	**102.67**	**100.96**	**101.82**	**101.82**	**101.42**	**101.80**
Si	1.00	1.34	0.99	1.00	1.00	0.99	0.99	0.99	0.99
Ti	0.00	0.00	0.00	0.00	0.00	0.00	0.00	0.00	0.00
Al	0.00	0.04	0.00	0.00	0.00	0.00	0.00	0.00	0.00
Fe	0.34	0.14	0.32	0.35	0.31	0.32	0.32	0.32	0.35
Mg	1.65	1.10	1.68	1.64	1.67	1.68	1.67	1.67	1.65
Mn	0.00	0.00	0.00	0.00	0.00	0.00	0.00	0.00	0.00
Ca	0.01	0.00	0.01	0.01	0.01	0.01	0.01	0.01	0.01
Na	0.00	0.03	0.00	0.00	0.00	0.00	0.00	0.00	0.00
Cr	0.00	0.00	0.00	0.00	0.00	0.00	0.00	0.00	0.00
Ni	0.01	0.00	0.01	0.01	0.01	0.01	0.01	0.01	0.01
K	0.00	0.00	0.00	0.00	0.00	0.00	0.00	0.00	0.00
Fo	0.83	0.88	0.84	0.82	0.84	0.84	0.84	0.84	0.83
Fa	0.17	0.12	0.16	0.18	0.16	0.16	0.16	0.16	0.17

Oxides (weight %)

Cations (4 oxigens)

End members

The olivine here is homogeneous, with low variance in the forsterite content (82-84% endmember) and presents the followaverage formula unit **$(Mg_{1,60}\ Fe_{0,31}\ Ca_{0,01})Si_{1,03}O_4$.**

5.1.2.2 Pyroxene

Pyroxene was analyzed in two different fields: one in the sample 68230 and another one in the sample 69128.

The analysis in sample 68230 obtained 6 points in F1 (Figure 66). The results are presented in Table 18.

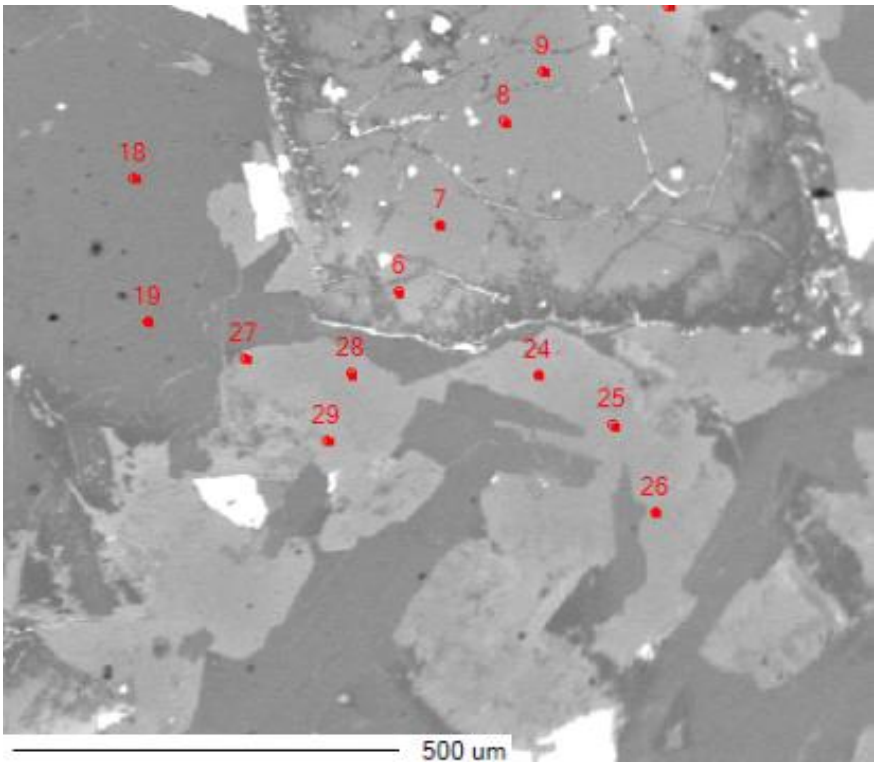

Figure 66 – Backscattered eletron image of clinopyroxene crystals from field 1 (sample 68230). Points 24 to 26 and 27 to 29.

The chemical distribution of the elements here is quite homogeneous (Table 18). The average formula unit is **$(Ca_{0,54}\ Na_{0,02})\ (Mg_{0,99}\ Fe_{0,41}\ Al_{0,04}\ Ti_{0,01})\ (Si_{1,93}Al_{0,07})O_6$.** The crystals are Mg-Ca-rich with 47-52% enstatite, 14-24% ferrosilite and 28-34% wolastonite (Table 18).

Table 18 - Mineral chemistry analysis results for pyroxene from the sample 68230, field 1. En = enstatite; Wo = wolastonite; Fs = ferrosilite.

Sample	68230	68230	68230	68230	68230	68230	
Field	1	1	1	1	1	1	
Crystal	Px	Px	Px	Px	Px	Px	
Point	24	25	26	27	28	29	
Position	Rim	Core	Interm.	Rim	Core	Core	
SiO2	51.80	52.03	51.30	53.54	52.08	51.91	Oxides (weight %)
TiO2	0.54	0.48	0.55	0.26	0.54	0.60	
Al2O3	2.92	2.80	4.16	0.95	2.67	2.27	
FeO	11.51	10.50	8.83	20.06	12.99	14.69	
MgO	16.55	16.80	17.07	22.38	18.12	16.53	
MnO	0.00	0.02	0.03	0.00	0.01	0.05	
CaO	16.50	16.93	17.04	3.74	13.55	14.27	
Na2O	0.30	0.30	0.31	0.09	0.27	0.26	
K2O	0.00	0.01	0.01	0.00	0.00	0.00	
Total	**100.11**	**99.87**	**99.29**	**101.02**	**100.23**	**100.57**	
Si	1.92	1.93	1.90	1.97	1.92	1.93	Cations (6 oxigens)
Ti	0.02	0.01	0.02	0.01	0.01	0.02	
Al	0.13	0.12	0.18	0.04	0.12	0.10	
Fe	0.36	0.33	0.27	0.62	0.40	0.46	
Mg	0.91	0.93	0.94	1.22	1.00	0.92	
Mn	0.00	0.00	0.00	0.00	0.00	0.00	
Ca	0.66	0.67	0.68	0.15	0.54	0.57	
Na	0.02	0.02	0.02	0.01	0.02	0.02	
K	0.00	0.00	0.00	0.00	0.00	0.00	
En	0.47	0.48	0.50	0.62	0.52	0.47	End members
Fs	0.19	0.17	0.14	0.31	0.21	0.24	
Wo	0.34	0.35	0.36	0.07	0.28	0.29	

The analysis in sample 69128 obtained 7 points in field 1 (Figure 67). The results are presented in Table 19.

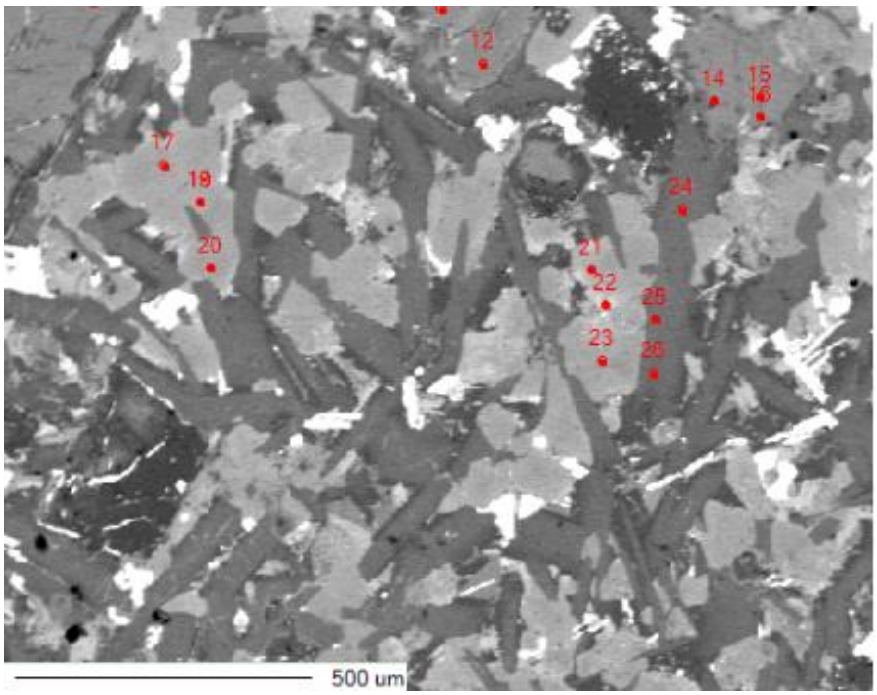

Figure 67 – Backscattered eletron image of clinopyroxene crystals from field 1 (sample 69128). Points 17 to 20 and 21 to 23.

The clinopyroxene here presents an average formula unit as follow **$(Ca_{0,57}Na_{0,21})(Mg_{0,52}\ Fe_{0,20}\ Al_{0,39}\ Ti_{0,02})\ (Si_{1,91}Al_{0,09})O_6$**. The crystals are Ca-rich with 40-47% enstatite, 14-18% ferrosilite and 34-46% wolastonite (Table 19).

Table 19 - Mineral chemistry analysis results for pyroxene from the sample 69128, field 1.En = enstatite; Wo = wolastonite; Fs = ferrosilite.

Sample	69128	69128	69128	69128	69128	69128	
Field	1	1	1	1	1	1	
Crystal	1	1	1	2	2	2	
Point	17	18	19	20	21	22	
Position	Rim	Core	Core	Rim	Rim	Core	
SiO2	63.14	47.35	47.35	47.19	63.20	50.63	Oxides (weight %)
TiO2	0.02	1.52	1.53	1.61	0.06	0.50	
Al2O3	22.72	7.26	7.30	7.34	23.05	3.04	
FeO	0.43	8.62	8.50	8.44	0.36	10.92	
MgO	0.00	13.43	13.59	13.10	0.00	15.70	
MnO	0.00	0.04	0.00	0.00	0.04	0.04	
CaO	4.29	19.75	20.05	20.81	4.34	15.97	
Na2O	8.81	0.48	0.46	0.49	8.77	0.32	
K2O	0.17	0.00	0.01	0.00	0.38	0.03	
Total	**99.57**	**98.43**	**98.78**	**98.99**	**100.19**	**97.15**	
Si	2.10	1.79	1.78	1.78	2.10	1.93	Cations (6 oxigens)
Ti	0.00	0.04	0.04	0.05	0.00	0.01	
Al	0.89	0.32	0.32	0.33	0.90	0.14	
Fe	0.01	0.27	0.27	0.27	0.01	0.35	
Mg	0.00	0.76	0.76	0.74	0.00	0.89	
Mn	0.00	0.00	0.00	0.00	0.00	0.00	
Ca	0.15	0.80	0.81	0.84	0.15	0.65	
Na	0.57	0.03	0.03	0.04	0.56	0.02	
K	0.01	0.00	0.00	0.00	0.02	0.00	
En	0.00	0.41	0.41	0.40	0.00	0.47	End members
Fs	0.07	0.15	0.15	0.14	0.06	0.18	
Wo	0.93	0.44	0.44	0.46	0.94	0.34	

5.1.2.3 Plagioclase

Plagioclase was analyzed in two different fields: one in the sample 68230 and another one in the sample 69128.

The analysis in sample 68230 obtained 9 points (Figure 68). The results are presented in Table 20.

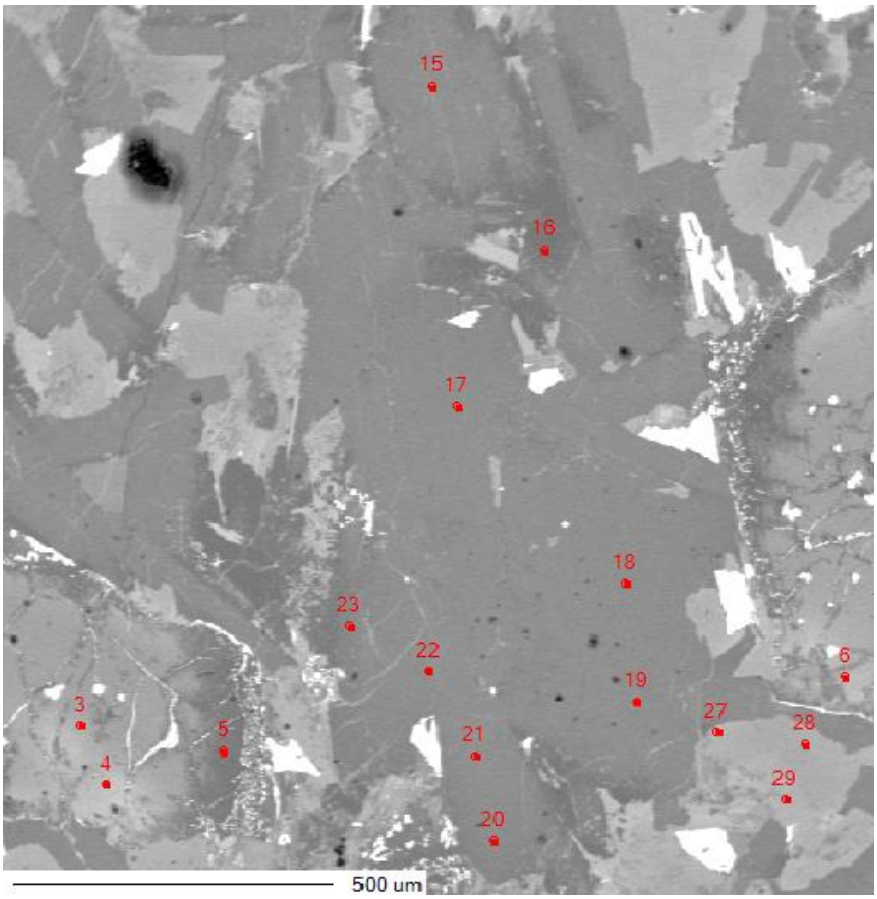

Figure 68 – Backscattered eletron image of plagioclase crystals from field 1 (sample 68230). Points 15; 17 a 19 and 20 to 23, in C1, C2 and C3, respectively.

The plagioclase in the sample 68230 presents an interesting normal zoning with an enrichment in NaO toward the rim (see the values for crystal 3 in Table 20). The average formula unit is **$(Na_{0,40}\ Ca_{0,55}\ K_{0,02})\ (Si_{0,47}\ Al_{0,51})AlSi_2O_8$**. The crystals are composed of 42-63% anortite, 29-40% albite and 1-4% orthoclase molecules, being classified as andesine to labradorite (Deer *et al.* 1992).

Table 20- Mineral chemistry analysis results for feldspar from the sample 68230, field 1. Ano = anortite; Ab = albite; Or = oligoclase.

Sample	68230	68230	68230	68230	68230	68230	68230	
Field	1	1	1	1	1	1	1	
Crystal	1	1	1	1	1	1	1	
Point	15	17	18	19	20	21	22	
Position	Core	Core	Interm	Rim	Rim	Interm	Interm	
SiO2	53.19	53.27	52.35	53.24	58.28	51.38	52.22	Oxides (weight %)
Al2O3	29.57	29.04	27.57	29.41	26.23	30.45	27.83	
FeO	0.60	0.63	1.50	0.56	0.48	0.60	2.95	
CaO	12.61	12.06	11.74	12.64	8.61	13.95	10.83	
Na2O	3.95	4.17	3.84	4.03	6.10	3.32	4.26	
K2O	0.21	0.20	0.25	0.20	0.46	0.13	0.50	
BaO	0.00	0.00	0.00	0.00	0.01	0.00	0.00	
Total	**100.13**	**99.36**	**97.25**	**100.08**	**100.16**	**99.83**	**98.59**	
Si	2.41	2.43	2.45	2.41	2.61	2.34	2.43	Cations (8 oxigens)
Al	1.58	1.56	1.52	1.57	1.38	1.64	1.52	
Fe	0.02	0.02	0.06	0.02	0.02	0.02	0.11	
Ca	0.61	0.59	0.59	0.61	0.41	0.68	0.54	
Na	0.35	0.37	0.35	0.35	0.53	0.29	0.38	
K	0.01	0.01	0.01	0.01	0.03	0.01	0.03	
Ba	0.00	0.00	0.00	0.00	0.00	0.00	0.00	
Ano	63.03	60.77	61.83	62.65	42.62	69.36	56.60	End members
Ab	35.73	38.02	36.61	36.17	54.67	29.89	40.29	
Or	1.24	1.21	1.55	1.19	2.71	0.76	3.11	

The analysis in sample 69128 obtained 12 points (Figure 69). The results are presented in Table 21.

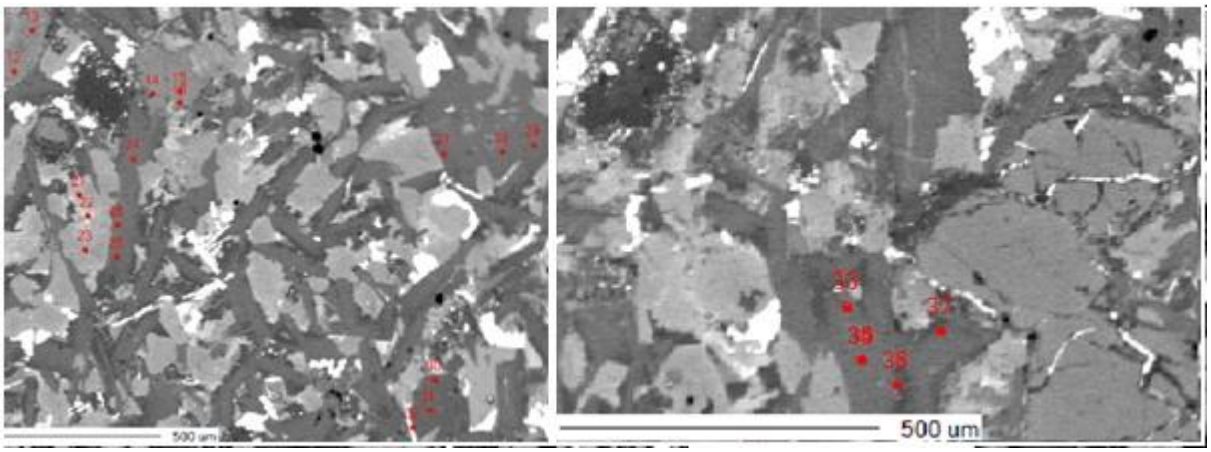

Figure 69 – Backscattered eletron image of plagioclase crystals from field 1 (sample 69128). Points 24 to 26; 27 to 29; 31 to 32 and 34 to 37.

The plagioclase here is quite homogeneous but presents NaO contents slight increasing toward the rims (igneous normal zoning) (Table 21). The average formula unit is **$(Na_{0,33}Ca_{0,59}K_{0,02})$ $(Si_{0,40}Al_{0,56})AlSi_2O_8$**. The crystals are composed of 42-63% anortite, 29-54% albite and 1-3% orthoclase molecules, being classified as labradorite (Deer *et al.* 1992).

Table 21 - Mineral chemistry analysis results for feldspar from the sample 69128, field 1. Ano = anortite; Ab = albite; Or = oligoclase.

Sample	69128	69128	69128	69128	69128	69128	69128	69128	
Field	1	1	1	1	1	1	1	1	
Crystal	1	1	1	2	2	2	4	4	
Point	24	25	26	27	28	29	34	35	
Position	Interm	Core	Rim	Rim	Core	Interm	Core	Core	
SiO2	53.184	50.865	53.607	51.908	45.287	52.639	51.9	52.901	Oxides (weight %)
Al2O3	29.418	26.895	28.646	29.773	24.63	29.409	29.04	29.391	
FeO	0.644	3.636	0.605	0.685	9.49	0.565	1.33	1.41	
CaO	12.574	11.244	11.979	13.281	9.014	12.663	12.064	11.893	
Na2O	3.942	3.657	4.202	3.692	2.486	3.994	3.98	3.337	
K2O	0.222	0.319	0.407	0.115	0.212	0.171	0.386	0.375	
BaO	0	0.009	0	0	0	0	0	0	
Total	**99.984**	**96.625**	**99.446**	**99.454**	**91.119**	**99.441**	**98.7**	**99.307**	
Si	2.41	2.42	2.44	2.37	2.35	2.40	2.40	2.42	Cations (8 oxigens)
Al	1.57	1.51	1.54	1.61	1.51	1.58	1.58	1.58	
Fe	0.02	0.14	0.02	0.03	0.41	0.02	0.05	0.05	
Ca	0.61	0.57	0.58	0.65	0.50	0.62	0.60	0.58	
Na	0.35	0.34	0.37	0.33	0.25	0.35	0.36	0.30	
K	0.01	0.02	0.02	0.01	0.01	0.01	0.02	0.02	
Ba	0.00	0.00	0.00	0.00	0.00	0.00	0.00	0.00	
Ano	62.96	61.64	59.69	66.08	65.49	63.02	61.16	64.71	End members
Ab	35.72	36.28	37.89	33.24	32.68	35.97	36.51	32.86	
Or	1.32	2.08	2.41	0.68	1.83	1.01	2.33	2.43	

5.2 PYROXENE AND FELDSPAR THERMOMETRY

This topic is dedicated to pyroxene and feldspar thermometry based on the principles of Lindsley (1983) and Deer *et al*. (1992), respectively.

5.2.1 Stolpen basalts

5.2.1.1 Pyroxene

The pyroxene here are zoned (see detailed interpretation on topic 5.1.1.2), being classified as diopside (Figure 70).

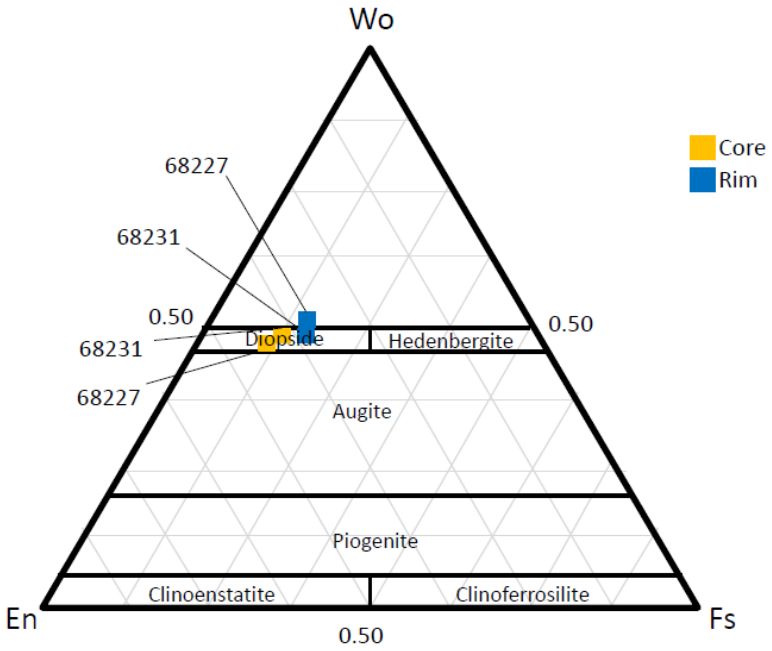

Figure 70 - Composition and nomenclature of pyroxene for the Stolpen basalts according to Deer *et al.* (1992).

According to this compositional zoning, we could determine the crystallization temperatures for the pyroxene phenochrysts in a 5 kbar pressure environment, as presented in Figure 71.

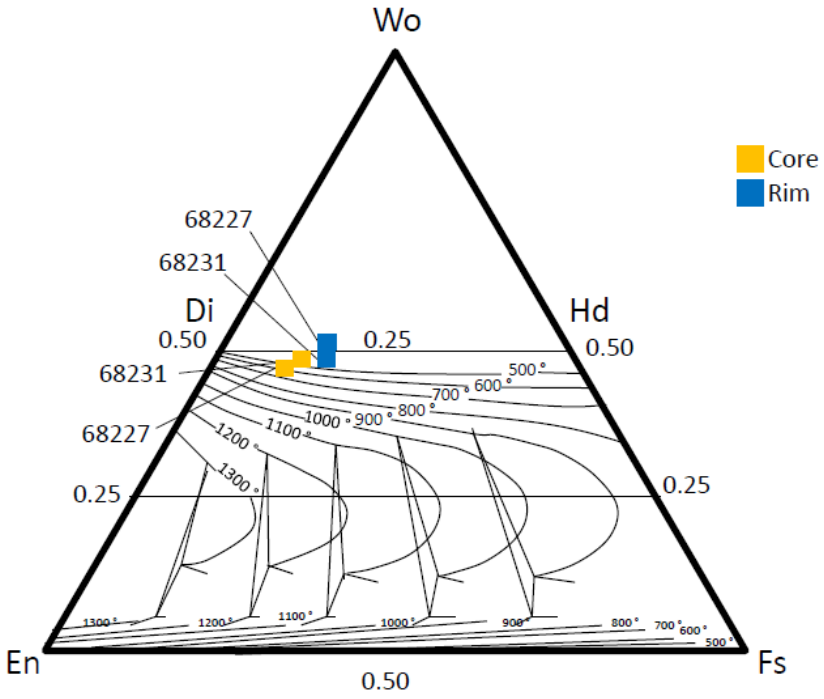

Figure 71 - Variation in crystallization temperatures for core and rim for the samples 68227 and 68231 in a 5 kbar enviroment (Lindsley 1983).

The rims crystallized at lower temperature (<500° C) than the core (>500° C), which indicates a cooling in magma during the formation of the rock. The pressure condition of 5 Kbars chosen due to the beginning of pyroxene phenocrysts crystallization in a hypoabissal field.

5.2.1.2 Plagioclase

The plagioclase could be divided into 2 different compositions: a Ca-rich feldspar and a Na-rich one. The Ca-rich plagioclase has a dominant anortitic composition (67,03% and 58,78% for 68227 and 68231, respectively) and the Na-rich one have a major albitic content (84,89% and 83,62% for 68227 and 68231, respectively). The ternary diagram of Figure 72 defines the Na-plagioclase as albite and the Ca-plagioclase as labradorite.

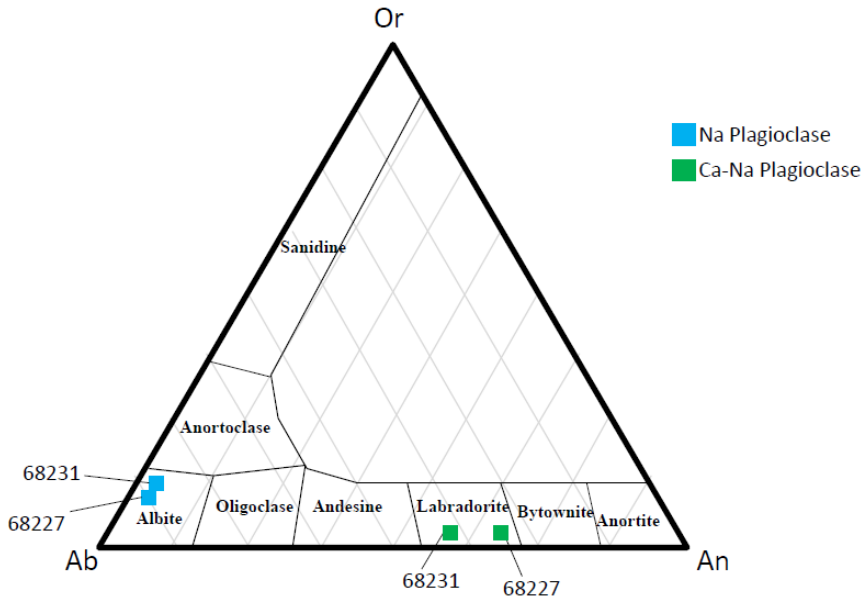

Figure 72 - Ternary ortoclase-anortite-albite diagram based on Deer *et al.* (1992).

The Figure 73 presents the projection of the analyzed plagioclases in a $NaAlSi_3O_8$-$KAlSi_3O_8$-$CaAl_2Si_2O_8$-H_2O system (Deer *et al.*1992). The diagram shows the crystallization temperatures for feldspars and corresponds to 5 kbar H_2O pressure conditions. The Ca-Na rich plagioclase crystallizes around 1150° C and the Na-rich plagioclase around 755° C.

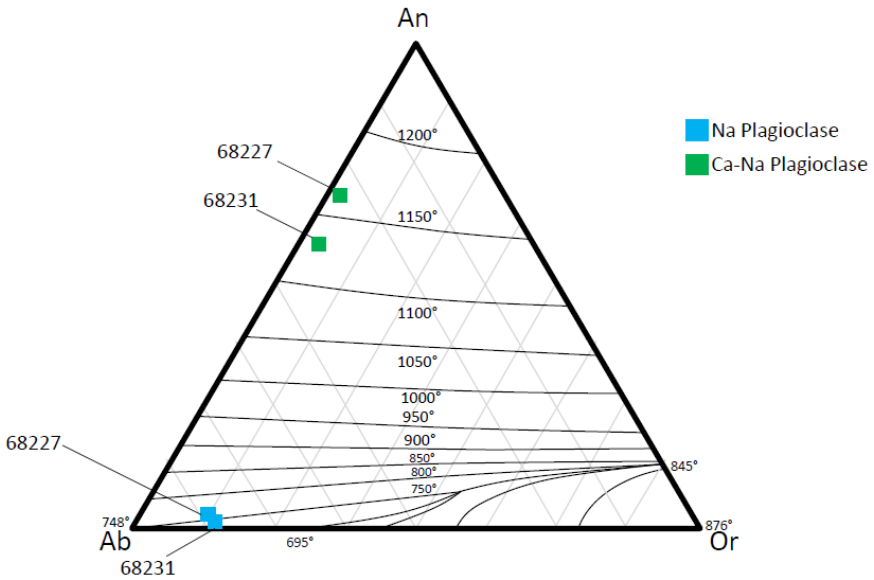

Figure 73–Estimated temperatures for different plagioclases (samples 68227 and 68231) based on the principle of Deer *et al.* (1992)

5.2.2 Basalt boulders

5.2.2.1 Pyroxene

The pyroxens phenocrysts from the boulders are quite homogeneous, as detailed on topic 5.1.2.2. Due to this, the analysis made on here in considered the average composition for the pyroxene in each sample. The pyroxenes could be classified as augite (Figure 74).

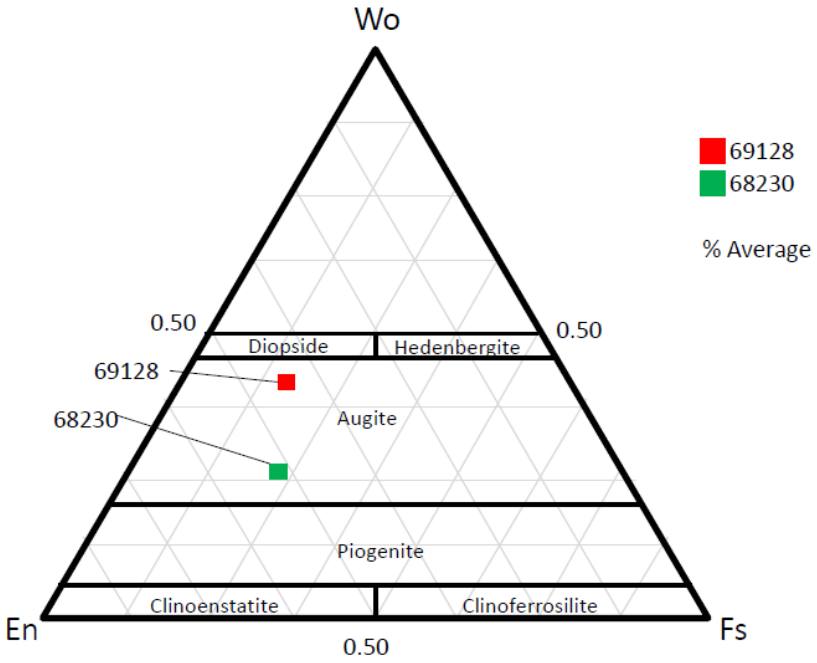

Figure 74 - Composition and nomenclature of pyroxene for the boulders according to Deer *et al.* (1992).

The estimated crystallization temperatures were 1250° C for the pyroxene phenochrystals of the sample 68230 and around 900° C for the pyroxene of the sample 69128 (Figure 75).

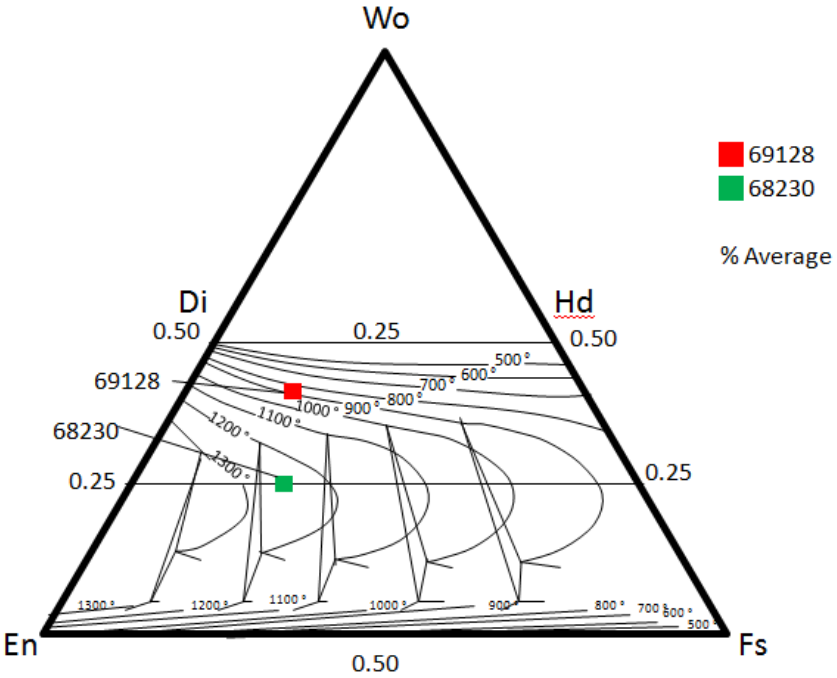

Figure 70 - Variation in crystallization temperatures for pyroxenes from the samples 68230 and 69128 in a 5 kbar enviroment (Lindsley 1983).

5.2.2.2 Plagioclase

The plagioclases from the sample 68230 are 56-69% anortite, 54-29% albite and 1-3% orthoclase molecules, being classified as labradorite (Deer *et al.* 1992) (Figure 76). The crystals from the sample 69128 are 59-66% anortite, 32-37% albite and 1-2% orthoclase molecules, being classified as labradorite (Figure 76).

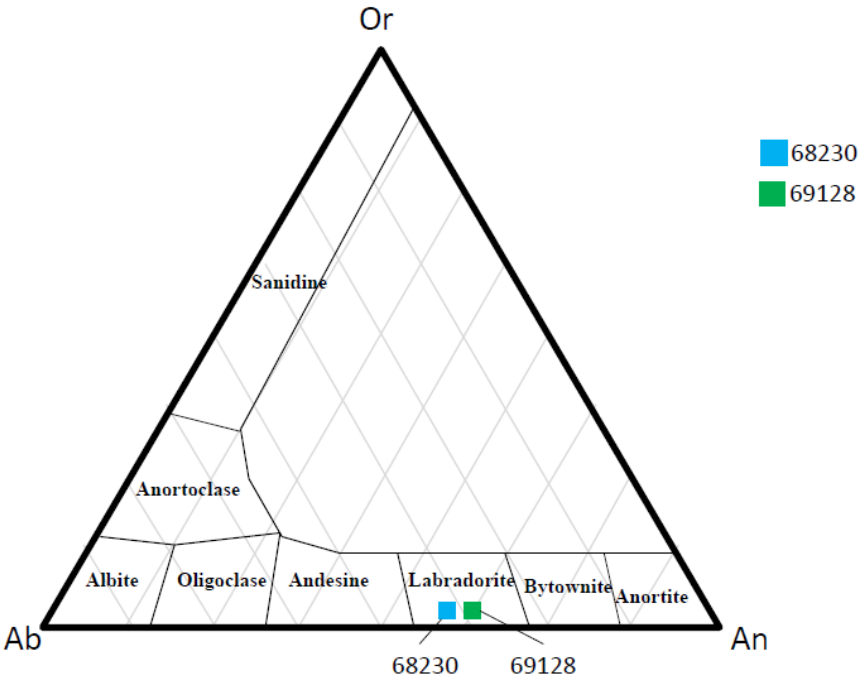

Figure 71 - Ternary ortoclase-anortite-albite diagram based on Deer *et al.* (1992).

The Figure 77 presents the projection of the analyzed plagioclases in the same system of the Figure 73. The plagioclases here crystallized at 1130 °C (sample 68230) and at 1150 °C (sample 69128).

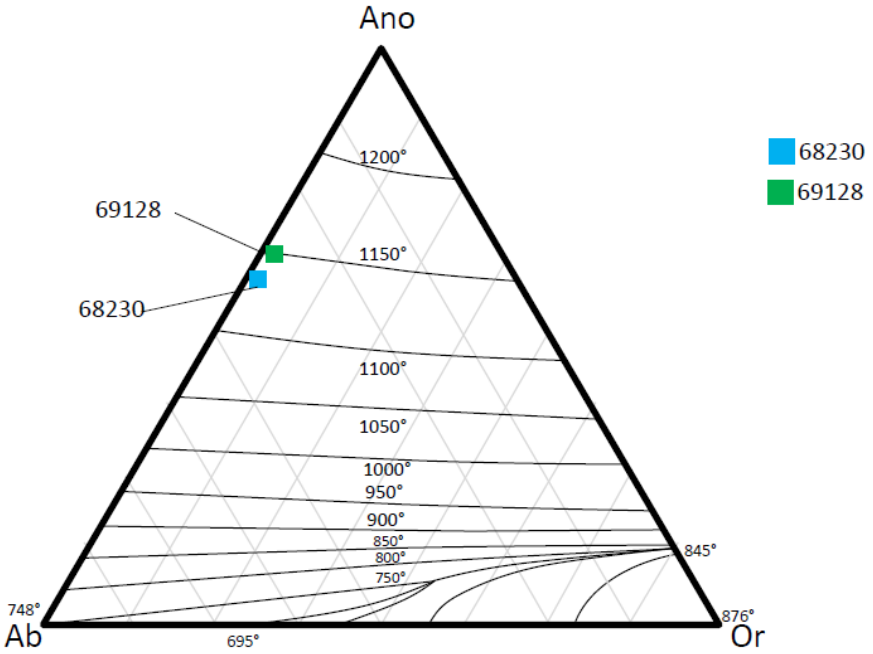

Figure 77- Estimated temperatures for different plagioclases (samples 68230 and 69128) based on the principle of Deer *et al*. (1992)

Table 22 summarizes the thermometric data. In Stolpen basalt analysis the crystallization temperature can be divided in core and rim for pyroxene and Na-Ca and Ca main content for plagioclase.. The crystallization temperature of Stolpen basalt is significantly lower than the boulders, up 600° C difference to pyroxene and 500° C to plagioclase.

Table 22 - Table presenting the pyroxene and feldspar themormetry for the samples based on the principles of Lindsley (1983) and Deer *et al*. (1992). Pl=plagioclase; Cpx=clinopyroxene.

Thermometry					
Rock	Sample	Mineral	Type	Thermometer Pl (Deer *et al.* 1989)	Thermother CPX (Lindsley 1983)
Stolpen	68227	CPX (Field 2)	Core	-	650° C
			Rim		< 500° C
		Pl	Na-Ca	755° C	-
			Ca	1170° C	
	68231	CPX	Core	-	500° C
			Rim		< 500° C
		Pl	Na-Ca	745° C	-
			Ca	1130° C	
Boulder	68230	CPX	Average	-	1250° C
		Pl	Average	1130° C	-
	69128	CPX	Average	-	900° C
		Pl	Average	1150° C	-

CHAPTER 6
DISCUSSION AND CONCLUSIONS

The basalt of Stolpen and boulders were characterized in detail by petrographic description and mineral chemistry analysis.

Petrographically the Stolpen basalt presents a glomeroporphyritic and amygdaloidal textures, with phenocrystals of olivine (forsterite) and clinopyroxene (diopside or Ca-augite) and a fine-grained matrix of thin plagioclase (labradorite and albite) laths and opaque minerals. Basalt boulders present an subophitic texture, with phenocrystals of olivine (forsterite) and clinopyroxene (augite), presence of carbonate replacing feldspars and a fine-grained matrix with laths of plagioclase relatively bigger than that of the Stolpen basalt and opaque minerals.

The mineral chemistry evidenced compositional zoning in olivines and pyroxene crystals in the Stolpen basalt. Olivines increases FeO and decreasing MgO from cores to the rims; pyroxene shows an increasing in FeO/SiO_2 and decreasing in MgO/Al_2O_3 from cores toward the rims. Microanalyses also presented that there are two types of plagioclase: albite and labradorite. In basalt boulders there is almost no zoning in the pyroxene phenocrysts, besides olivines show the same pattern of the Stolpen basalts. Zoning in plagioclase can not be distinguished, being defined as labradorite.

Based on the whole-rock geochemistry data (Figure 72) provided by Manuel Lapp, the Stolpen basalt is defined as basanite and the boulders as basalt (more SiO_2 and less $NaO + K_2O$ if comparing with basanites).

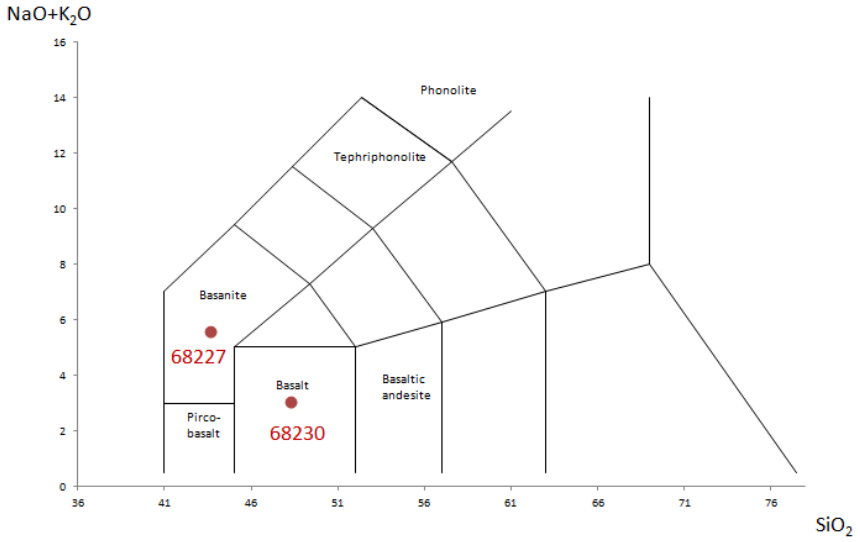

Figure 72 - TAS diagram showing the whole-rock chemistry classification for the Stolpen basalt (68227) and basalt boulder (68230) samples.

The main features of both rocks, showed during this TCC, can be summarized in Table 23.

Table 23 - Main features of the Stolpen basalt and boulders.

Characteristics		Stolpen	Boulders
Petrography	Texture	Zoning, glomeroporphyritic texture and amygdaloidal structure	Subophitic texture
	Mineralogy	Forsterite + Diopside + Albite + Labradorite + Opaque	Forsterite + Augite + Labradorite + Carbonate + Opaques
Cristallization Temperature	Clinopyroxene	500 to 650° C	900 to 1250° C
	Plagioclase	Na Plagioclase 745 to 755° C	Ca-Na Plagioclase 1130 to 1150° C
		Ca-Na Plagioclase 1130 to 1170° C	
Whole-rock chemisty (TAS Diagram according to Irvine & Baragar 1971)		Basanite	Basalt

The occurrence of chemical zoning in some minerals and the presence of different types of plagioclase (varying between calcic and sodic) indicates cooling during crystallization. These facts, associated with the thermometry, can be related to the *Bowen Reaction Series* (Figure 73), once plagioclase have continue series while pyroxene have a discontinue series. During the system cooling, first the calcic plagioclase and the pyroxene crystallize followed by the sodic plagioclase and the rims of the pyroxene. Our data confirmed that affirmation (see Table 23). So, the basalt boulders were crystallized in a higher temperature than the Stolpen basalt and, probably, in a slower system inferred here due the crystals size among others (in the matrix of the boulders the crystals are bigger than that present in the matrix of the Stolpen basalt).

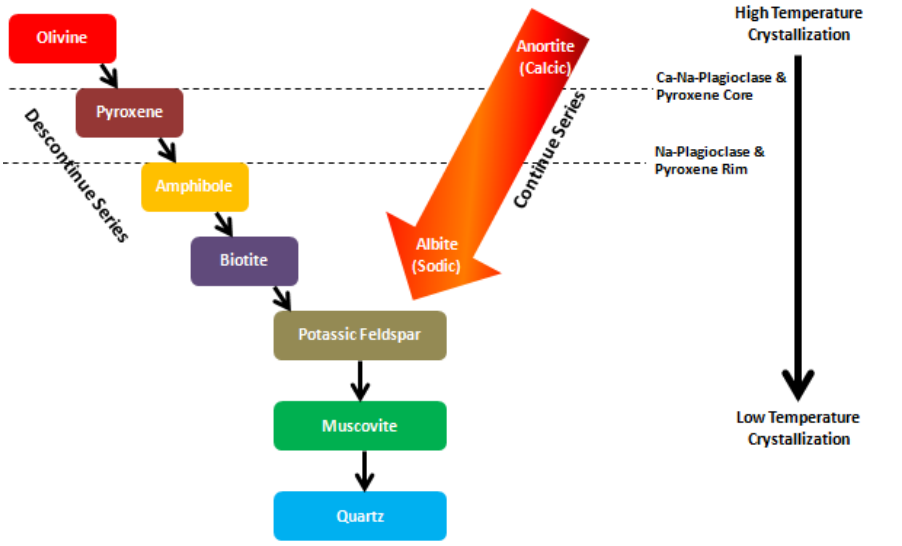

q

Figure 73 - Adapted Bowen Reaction Series for this work. The dash-lines present the temperature which plagioclase and pyroxene were crystallized.

The distinction between the two stones studied in this work gives the idea that the magma they are origined from have different affinities, so is possible to interpret from which system the stones are origined from. The crystallization sequence to Stolpen basalt is first the olivine, followed by the plagioclase and finally pyroxene. The sequence in the boulders is olivine followed by plagioclase and pyroxene simultaneously. As reviewed in chapter 3, the melting beneath ocean ridges produces basalt that contains around 50% SiO_2 and poor in K_2O and Na_2O, known as *tholeiitic* basalt. The first material that crystallizes in this melt it is the MgO olivine. In other hand, a typical crystallization sequence in Island Arc Basalts is olivine followed by Ca plagioclase, which have higher K_2O and Al_2O_3 contents.

Stolpen basalt have a relative higher content of alkalis as presented in TAS Diagram (Figure 72), wider calcic pyroxen content and occurence of Ca plagioclase, so it should be origined from a Island Arc Basalts. Thus, as the boulders have a lower alkali content due no presence of Na plagioclase and pyroxen with higher magnesium content, it can be interpreted from a Mid-ocean Ridge Basalts that produces tholeiitic basalt.

CHAPTER 7

REFERENCES

Bottinga Y., Weill D. F., 1970. Densities of liquid silicate systems calculated from partial molar volumes of oxide components. American Journal of Science, 269(2): 169-182.

Bottinga Y., Weill D.F., 1972. Viscosity of Magmatic Silicate Liquids;amodel for calculation. American Journal of Science, 272(5): 438-475.

Büchner J., Tietz O., Viereck L., Suhr P., Abratis M., 2015. Volcanology, geochemistry and age of the Lausitz Volcanic Field. International Journal of Earth Sciences, 104(8): 2057-2083.

Central Intelligence Agency, 2013. The World Factbook 2013-14 Washington, DC.

Chemale Jr., F., Dussin, I.A., Alkmim, F.F., Martins, M.S., Queiroga, G., Arsmtrong, R., Santos, M.N. 2012. Unravelling a Proterozoic basin history through detrital zircon geochronology: The case of the Espinhaço Supergroup, Minas Gerais, Brazil. GondwanaResearch, 22(1): 200-206.

Chula A.M.D., 1996. Caracterização geológica e geoquímica dos metamagmatitos e metassedimentos da região de Planalto de Minas, Município de Diamantina, MG. Dissertação de Mestrado, IGC/UFMG, 157

Deer W. A., Howie R. A., Zussman J., 1992. An introduction to the rock-forming minerals. London: Longman.

Kemnitz H., 1998 - Some remarks of the Neoproterozoic Lusatian greywackes, Germany, and their mafic intercalations. Acta Universitatis Carolinae. Geologica, 42(3-4): 443-446

Koch R.A., Pfeiffer L., Stammler L., Beeger D., 1983. Der Basalt von Stolpen in der Lausitz, Abhandlungen des Staatlinchen Museums für Mineralogie und Geologie zu Dresden Band 32, Leipzig: 75-77.

Kozdrój, W., Krentz O., Opletal M., 2001. Comments on the Geological Map Lausitz-Jizera-Karkonosze (without Cenozoic Sediments): 1: 100000. Sächsisches Landesamt für Umwelt und Geologie: 5-45.

Le Bas, M. J., Le Maitre, R. W., Streckeisen, A., Zanettin, B., 1986. A chemical classification of volcanic rocks based on the total alkali-silica diagram. Journal of petrology, 27(3): 745-750.

Lindesley, D. H., 1983. Pyroxene thermometry. American Mineralogist, 68(5-6): 477-493.

Mackenzie W. S., Donaldson C. H., Guilford C., 1982. Atlas of igneous rocks and their textures. London: Longman.

Philpotts A. R., 1989. Petrography of igneous and metamorphic rocks. Pearson College Div.

Press, F., Siever, R., Grotzinger, J., Jordan, T. H., 2006. Para entender a Terra. Bookman: 120-168.

Sgarbi G. N. C., 2007. Petrologia macroscópica das rochas ígneas, sedimentares e metamórficas. UFMG, 3: 135-230.

Sigurdsson, H., Houghton B., Mcnutt S., Rymer H., Stix J., 2015. The encyclopedia of volcanoes. Elsevier: 34-111.

Streckeisen A., Le Maitre R. W., 1978. A chemical approximation to the modal QAPF classification of the igneous rocks. Neues Jahrbuch für Mineralogie, Abhandlungen 136: 169–206.

Tietz O, Buchner J, Suhr P, Abratis M, Goth K (2011a) Die Geologiedes Baruther Schafberges und der Dubrauker Horken—Aufbauund Entwicklung eines kanozoischen Vulkankomplexes in Ostsachsen.Berichte der Naturforschenden Gesellschaft der Oberlausitz,Supplement 18:15–48.

Tietz O, Gartner A, Buchner J (2011b) The monogenetic Sonnenberg scoria cone—implications for volcanic development and landscape evolution in the Zittauer Gebirge Mountains since the Paleogene. Z Geol Wiss 39:311–334.

Whitmey D. L., Evans B. W., 2010. Abbreviations for names of rock-forming minerals. American mineralogist, 95(1): 185.